Master Thesis

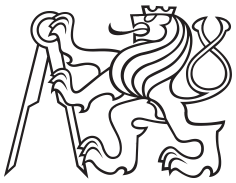

Czech Technical University in Prague

F3

Faculty of Electrical Engineering

Wireless Wooden Structure Sensor Design

Bc. David Žaitlík

Supervisor: Ing. Jan Včelák, Ph.D.
Field of study: Cybernetics and Robotics
Subfield: Cybernetics and Robotics
May 2019

Acknowledgements

I would like to thank my supervisor, Ing. Jan Včelák, Ph.D. for leading of this project.

I also want to thank Ing. Aleš Vodička for counseling the work with the PIC microcontroller and for design and 3D printing the enclosure for the sensor.

Declaration

Prohlašuji, že jsem předloženou práci vypracoval samostatně, a že jsem uvedl veškerou použitou literaturu.

I hereby declare that I have created this thesis independently and that I listed all the used literature.

In Prague, 21. May 2019

Abstract

This thesis deals with designing a battery-powered wood moisture sensor with wireless communication. The developed sensor is a part of the Moisture Guard platform developed at UCEEB CTU.

The main measurement method uses a wood resistance measurement; the secondary method uses wood cavity humidity and temperature measurement.

The sensor uses IQRF technology to communicate with an UniPi PLC, the central point of the sensor network.

The sensor hardware was developed within this thesis. The power consumption of the sensor parts was taken into account. The consumption was calculated for a different configurations of the frequency of measurement and transmission.

The microcontroller firmware of the sensor is not yet complete, but the low power abilities of the microcontroller, and how to used them, were described. Two applications for the UniPi PLC were developed using IQRF SDK. One for the IQRF network creation and second for the data acquisition.

Keywords: IoT, LPWAN, Wooden Structures, Sensor, Moisture

Supervisor: Ing. Jan Včelák, Ph.D.
UCEEB ČVUT,
Třinecká 1024,
Buštěhrad

Abstrakt

Tato práce se zabývá návrhem bateriově napájeného senzoru pro monitoring vlhkosti dřeva s bezdrátovou komunikací. Tento senzor je součástí systému Moisture Guard, který je vyvíjen na UCEEB ČVUT.

Hlavní metodou pro měření vlhkosti dřeva je odporová metoda, sekundární metodou je metoda měření vlhkosti vzduchu v kavitě dřeva.

Senzor využívá ke komunikaci s centrální jednotkou PLC UniPi technologii IQRF.

Hardware senzoru byl navrhnut. Hlavní důraz byl kladen na spotřebu energie jednotlivých součástí senzoru. Byla vypočítána odhadovaná spotřeba energie při různých konfiguracích frekvencí měření a odesílání dat.

Firmware mikrokontoleru není zcela hotov, avšak low-power vlastnosti použitého mikrokontroléru jsou popsány, včetně toho, jak je využít. Byly vyvinuty dvě aplikace pro UniPi PLC, které slouží k vztvoření IQRF sítě a získávání dat ze senzorů. K tomuto bylo využito IQRF SDK.

Klíčová slova: IoT, LPWAN, Dřevostavby, Senzor, Vlhkost

Překlad názvu: Návrh bezdrátového senzoru pro měření vlhkosti dřevěných konstrukcí

Contents

Figures

Tables

Chapter 1

Introduction

The Moisture Guard system, developed at UCEEB CTU, is a system for continuous wooden construction moisture monitoring. If a moisture in the construction is detected, the owner of the installation is warned.
An early warning can help to reduce the damage caused by the moisture, which decreases the price of a reconstruction of the building.
The first version of the Moisture Guard system was developed by Aleš Vodička in his master's thesis. Then the system was developed by him and his colleagues at UCEEB CTU.
At the beginning of writing this thesis, the system consists of a central unit, which is a PLC Tecomat Foxtrot, and several sensors communicating using RS485 connection to the central unit. There are two types of sensors:

- HT0x485 type, which measures temperature and a humidity of ambient air. This sensor communicates using the MODBUS RTU protocol over RS485.

Figure 1.1: Photo of the HT02485 sensor

- MHT0x485 type, which measures temperature and a humidity of ambient air, and air in a wooden cavity, using two SHT31 sensors. This sensor

also measures the moisture of a wooden sample using a resistive method. This sensor communicates using MODBUS RTU protocol over RS485.

Figure 1.2: Photo of the MHT03485 sensor

This system can be easily incorporated into a wooden building during its construction. However, this can not be said about already built buildings. To install Moisture Guard system to a building a wiring of the sensors is required, which is not a problem during the construction of the building, but to install this system to already built structure would require to dismantle some parts of the building, which is both costly and requires a lot of work. To satisfy customers with this need, a wireless version of this system is developed within this thesis. IQRF communication technology was specified in the thesis assignment. As a central unit an UniPi PLC was selected.
The development of a sensor unit and a central unit will be discussed in this thesis.
The developed sensor should have the same features as the MHT0x485 sensor, but IQRF wireless communication should be used instead of the RS485 communication.
The sensor should be battery powered, with a long lifetime, at least 10 years. There should be also an option to power up the sensor using an external power source, for example a PLC.

Chapter 2

Wood Moisture Measurement

2.1 Overview Of Wood Moisture Measurement Methods

With increasing moisture, the wood can decay, in addition to a change of its mechanical properties, so monitoring of its water content is very useful in order to prevent disasters.
The percentage of water contained in the wood is called moisture content of the wood MC, and can be calculated using the following equations:

$$MC = 100\frac{m_{water}}{m_{wood}}\,[\%] \tag{2.1}$$

$$MC = 100\frac{m_{wet} - m_{dry}}{m_{dry}}\,[\%] \tag{2.2}$$

The moisture content of the wood influences its properties and can pose risks to the wood. The types of risks are shown in figure 2.1. The construction wood should have the moisture content in range from 8 to 18%, in dependece on the use of the wood.[4]

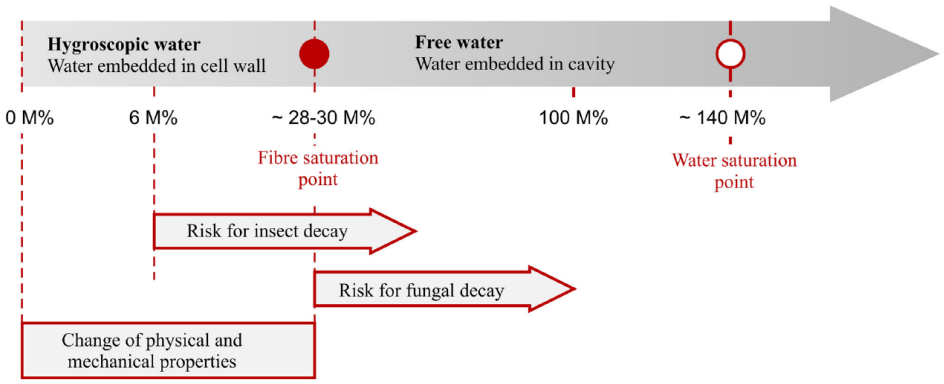

Figure 2.1: Wood moisture content and its influence on wood properties. Taken from [12].

To measure the moisture content of the wood, several methods can be used. A selection of direct and indirect methods is listed below:

- **Direct Methods**
  - **Oven-drying Method**
    A wood sample is extracted from the measured wood, and its weight is measured. Then the sample is dried at the temperature 103 $°C$ until its mass is constant. The moisture content is then determined using equation 2.2.
    This method is precise and is used for calibration.
  - **Distillation/Extraction Method**
    The measured wood is chipped to pieces of 20-50g and is placed to a heated flask while a solvent is added. The water contained in the wood evaporates and condenses in a cooler side of the flask. The weight of the dry wood and water is then measured and the moisture content is calculated using equation 2.1. This method is used if the wood contains preservatives, oils o terpenes.
- **Indirect Methods**
  - **Electrical Resistance Method**
    The electrical resistance is measured, usually using two electrodes inserted to the wood.
    The resistivity of wood decreases significantly with increasing moisture content in the wood. This method is $\pm$ 1% accurate for MC between 6% and the fibre saturation point of the wood. The accuracy decreases significantly above this point.
  - **Capacitive Method**
    The capacity of the wood is measured. Two electrodes are placed

on the surface of the measured wood, and the wood acts as a dielectricum of a capacitor.
The dielectric constant increases with increasing moisture content in the wood.
This method is accurate in the range from 2% of moisture content to the fibre saturation point of the wood. However, only moisture near the surface can be measured.

- **Microwave Method**
  This method is similar to the capacitive method but works on higher frequencies. The wood moisture content is determind from reflection and absorption of energy. The measurements are 0.5% accurate.
- **Colour Reaction Method**
  The MC of wood is determined using an indication paper inserted into a drilled hole in the measured wood. MC in the range from 6 to 20 % can be measured using this method. However, the ambient temperature between 15 to 25 $°C$ is required.

From the methods listed above, only the indirect ones are suitable for monitoring purposes, because the listed direct methods require the destruction of the wood sample. The capacitive method is suitable for monitoring of planks because it is capable of measurement of the moisture content maximally 35mm under the surface of the wood.
The microwave method presents great accuracy, but its price discourages of its usage.
Colour reaction method is limited to its narrow working temperature interval.[1, 12] However, this method can be done electrically, using an electrical relative humidity sensor inside the hole. The influence of the temperature can be negated by measuring the temperature and calculating the absolute humidity of the wood cavity.
The most used method is the Resistance Method, which was used in this thesis, accompanied by the measurement of wood cavity humidity.

2.2 Resistive Wood Moisture Measurement

The resistivity of wood is strongly dependent on its moisture content, making the resistance measurement a good mean to measure the wood moisture content.
The resistivity of wood is also dependent on temperature, with increasing temperature, the resistivity decreases.
The resistivity is also dependent on the species of the wood. The resistance of different species for different moisture contents can be seen in table 2.1.
It can be seen, that the resistance of almost dry wood reaches tens, or hundreds of $G\Omega$s, while the resistance drops to tens or hundreds of $M\Omega$s just after 6% of moisture content raise. The resistance of wet wood is lower than $1M\Omega$.
Even though the values of resistance of different species vary, the order of the resistance is moreover the same, and so is the logarithmic trend.
The logarithmic dependence of the wood resistance on the moisture content from equation 2.3 can be seen in figure 2.2, and also in table 2.1.
Furthermore, the resistivity of the wood is also dependent on the direction of measurement. The resistivity is lower in the parallel direction to the grain than in the perpendicular direction to the grain. [1, 12]

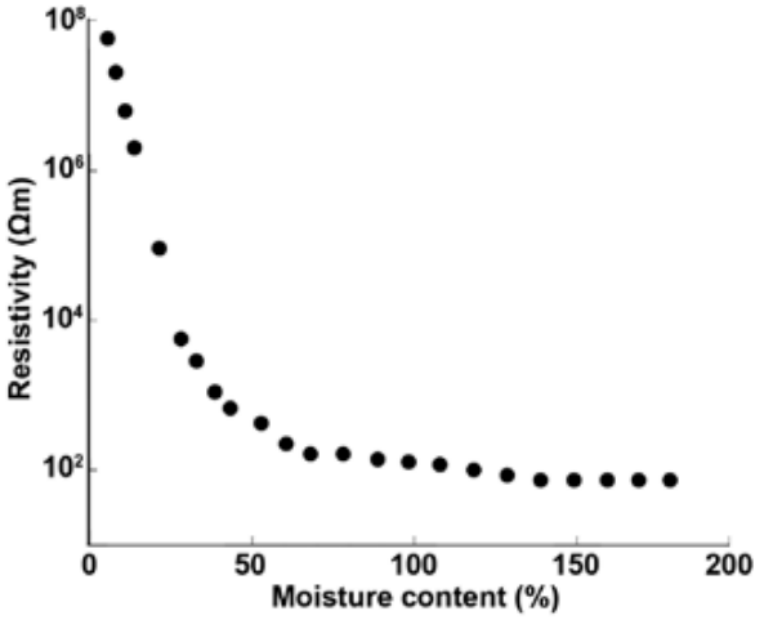

Figure 2.2: Resistance of slash pine in dependece on moisture content. Taken from [1].

Species of Wood	R[MΩ]			
	MC=7%	MC=13%	MC=19%	MC=25%
White Pine	20900	102	7.9	0.52
White Fir	57600	83	4.47	0.62
Black Spruce	700000	250	9.6	1
White Oak	17400	80	1.7	0.41
Birch	87000	96	5.13	0.7
Wallnut	51300	78	3.16	0.38

Table 2.1: Electrical resistance of selected wood species at different moisture content. [2]

The resistance is usually measured using two electrodes. These electrodes can be rammed into the wood (nail-type), screwed into the wood (screw-type) or glued into a pre-drilled cavity in the wood. Wood drying and corrosion can lead to a higher resistance value measured.
The corrosion of the electrodes can be avoided by using an electrode from non-corrosive material.
To negate the effects of contact loss by wood drying, the electrode can be additionally glued in using a conductive glue.
The electrodes can also be partially insulated, to measure only the inside of the wood, as seen in the figure 2.3.
An example of glued-in electrodes can be seen in the figure 2.4. [10, 11, 12]

The wood resistance can be calculated using the equation below, and is dependent on the measured wood species: [5]

$$logR = log\left(\frac{l}{S}\right) + b \cdot log\,(MC) + (a - 2b) \tag{2.3}$$

,where l is the distance between electrodes, S is the electrode-wood contact area, MC is moisture content, and a and b are constants at constant temperature. [5]
Constants a and b are dependent on the measured wood and used electrodes.

However, the resistance measurement accuracy can decrease over time, especially if the wood moisture content is above the fibre saturation point when the excitation voltage causes the molecules of wood to orient towards the generated electrical field. The wood becomes polarized, and it becomes electrically charged.
To mitigate this effect, a second measurement with an opposite polarity should be done after the end of the first measurement.

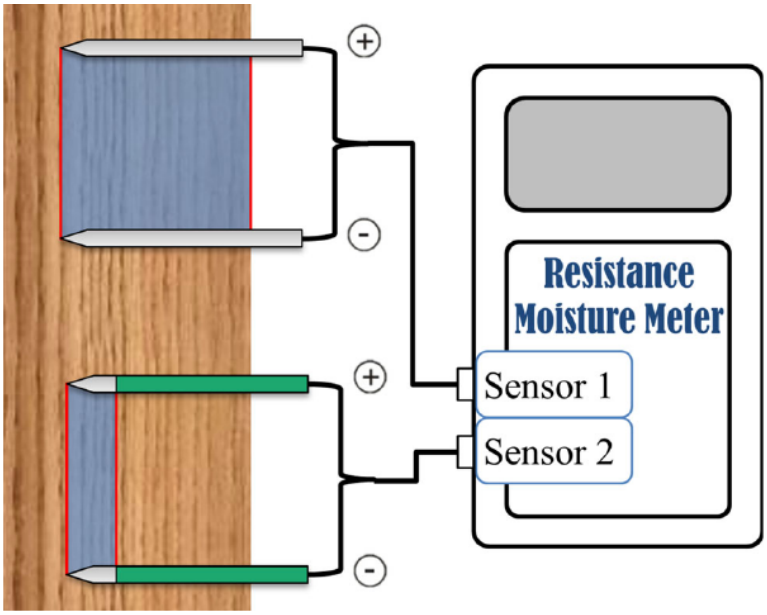

Figure 2.3: Comparison of measured areas using not insulated (Sensor 1) and insulated electrodes (Sensor 2). Taken from [12].

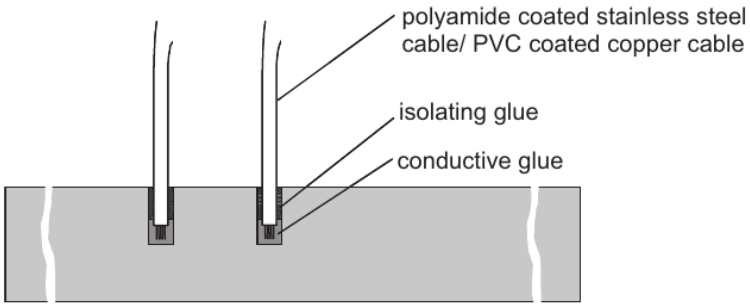

Figure 2.4: An example of glued-in electrodes. Taken from [11].

2.2.1 High Resistance Measurement

To measure resistances this high, two approaches are commonly used: a Wheatstone bridge or a current integrator.
To use a Wheatstone bridge, two of the resistors must be replaced by adjustable voltage sources. The schematic of this circuit can be seen in figure 2.5.
The resistor R_X is the measured resistor and the resistor R_S is a reference resistor.
Voltage reference V_2 has opposite polarity than voltage reference V_1, and is adjusted until the zero-cross detector detects a zero signal. Using this circuit,

excellent precisions, up to 0.1%, can be achieved. [8, 9]

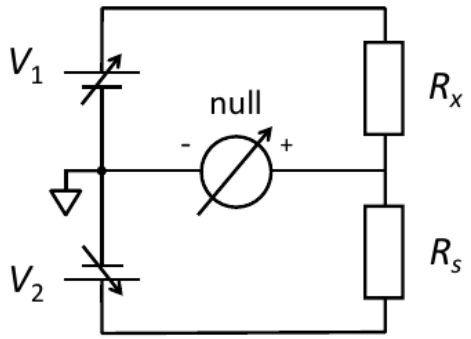

Figure 2.5: Schematic of the Wheatstone bridge circuit. Taken from [9].

The second approach is better for the purposes of this thesis because it does not need any adjustable voltage sources or nanovoltmeters as the Wheatstone bridge approach does. A simple schematic can be seen in the figure 2.6.
Its function is quite simple, an excitation voltage V_{test} is applied to the measured resistor R_x. The current flowing through the resistor R_x is then integrated using the integrator, whose output is a voltage ramp. Using a timer, the time to reach a set threshold voltage is measured.
The resistance can be calculated using the following equation:

$$R_x = \frac{V_{test} \cdot \Delta t}{C \cdot V_{tresh}} \tag{2.4}$$

Where Δt is the measured time when the comparator reached the comparator limit V_{tresh}. [8, 9]

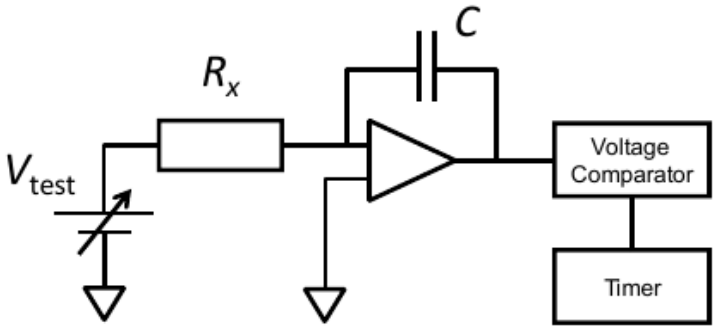

Figure 2.6: Schematic of current integration circuit. Taken from [9].

Chapter 3

Low Power Wide Area Networks

Because the developed sensor will be built-in a construction, a low-power and energy efficient communication method must be used.
Low Power Wide Area Networks (LPWANs) are the way to ensure both communication between the sensor and the UCEEB server, and long battery lifetime.
The long range of these network will not be most likely needed, because the sensor will be built in a building either with its own network, or with a nearby public network gateway.
However, these networks are very low power, with minimal energy consumption, enabling a battery powered device to last years.

3.1 Comparison of selected LPWANs

The list of selected wireless low power, long range networks (LPWANs) is in table 3.1.
It is clear from the table, that all of these networks have quite slow transfer speed, and are not usable for transfer of big ammount of data. Also, the packet size is usually small, which limits the amount of data even more. In general, these networks are designed for low power end devices which measure infrequently and are not continuously streaming data.
Another comparison can be seen in figure 3.1, which is a graphical represenation of ranges and data rates of selected network. Although IQRF network is not included in this comparison, it would be in the same spot as the ZigBee network.

The daily number of messages is also limited in some of the listed networks, this applies for example for LoRa and Sigfox networks, the IQRF network does not limit the daily number of messages, since the network is user-created, and there is no need for an operator, as in the case of the SigFox network.

Because these networks usually work in ISM bands, government regulations must be taken into consideration. For example, the transmitting power and duty cycle is strictly defined. Violation of these rules in the Czech Republic can be fined by Český Telekomunikační Úřad. However these regulations are usually already a part of specifications of these networks.
Some of the LPWAN operators require some sort of a certification done by certification authority, or by themselves, for example Sigfox network devices must be certified directly by Sigfox, LoRaWAN devices can be certified by LoRa Aliance, and this certification is recognised worldwide, or by České Radiokomunikace in the Czech Republic, but this type of certification is recognized only by České Radiokumunikace.
IQRF requires certification of the device only if the manufacturer wants this device to be listed on the IQRF Alliance website.
In all cases, using an already certified module speeds up and lowers the cost of the certification.

In this thesis I will focus mainly on IQRF and LoRa LPWANs, because LoRaWAN and IQRF communication technologies are used in the sensor developed within this diploma thesis.

Name	Frequency Band	Range	Transfer speed	Topology
LoRa	433/868 MHz	15-20km	250bps-50kbpsk	Star
Sigfox	433/868 MHz	15km	100bps	Star
IQRF	433/868 MHz	500m	19.2 kbps	Mesh
ZigBee	868MHz/2,4GHz	1km	100-250kbps	Mesh
DASH7	433/868 MHz	2km	9.6-167kbps	Tree

Table 3.1: Comparison of LPWANs

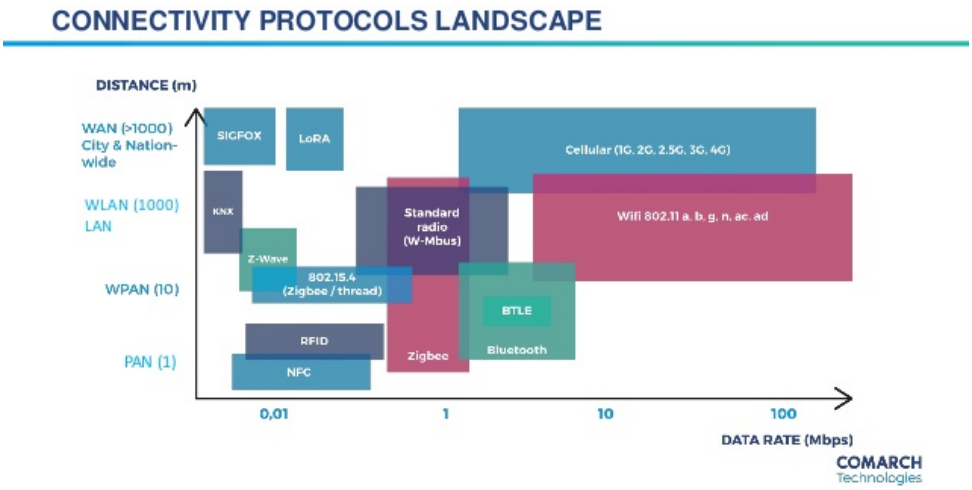

Figure 3.1: Comparison of range and datarate of LPWANs. [13]

3.2 IQRF

IQRF is a proprietary mesh LPWAN technology developed by the company Microrisc s.r.o. in 2004. At this time the technology is managed by the company IQRFTech s.r.o., which is a subsidiary company of the Microrisc s.r.o.

IQRF network uses 433Mhz, 868 MHz and 916MHz ISM bands and its bandwidth is 19.2kbps. To access the channel the IQRF uses Time Division Multiple Access (TDMA) method.
The transmitting power can be set in 8 steps (0-7) from 3.5mW to 12.5mW. The range of one hop in the network is typically tens of meters indoors, and hundreds of meters outdoors. This range is influenced by the transmitting power, used antenna, materials of walls, placement of the transmitter and many other factors.
There can be up to 240 devices in one network, each of these can be a member of two networks, which allows chaining of networks, the range of the network can be, in theory, tens of kilometers. One data packet can travel maximally 240 hops and can contain 64 bytes of payload data.

The IQRF network uses the mesh network topology by default, but it can be run as a star topology network or just a point-to-point network. In mesh topology, it is necessary to have one module as a coordinator. This coordinator works as the central point of the network, which collects the data from nodes or sends commands. The coordinator also assigns a logical address to nodes and creates a routing map of the network. To route messages in the network, the "Directional Flooding" protocol is used.

There are two steps to create an IQMESH network, Bonding, and Discovery. Bonding a node assigns a logical address to the node, and this node is added to a list of bonded nodes in the coordinator node. The coordinator is perfectly capable of sending messages to this node. The bonding should be done in a direct range of the coordinator.
To use features of IQMESH network topology, a Discovery must be run by the coordinator. If Discovery is not done, the routing is not available, which means the links between coordinator and nodes must be direct. Discovery is a process of finding routing paths in the network. Discovery uses a breadth-first search algorithm to search for the routing paths. At the start of the Discovery process, the coordinator sends a packet, and nodes within the direct connection to the coordinator respond to it. When the response is received by the coordinator, the address is assigned to the corresponding node by the coordinator. After this is done, the process is delegated by the coordinator

to the discovered nodes to discover their neighbors.

An example of a small IQRF network can be seen in figure 3.2. The coordinator is the green circle. Blue circles are end nodes. It takes just one hop from coordinator to an end node for nodes 1 to 4, and two hops to nodes 5 to 7. There are redundant links between most of the nodes, so if some links became noisy, for example, because some new obstruction on this link, the message can still reach affected nodes (unless all links are broken).

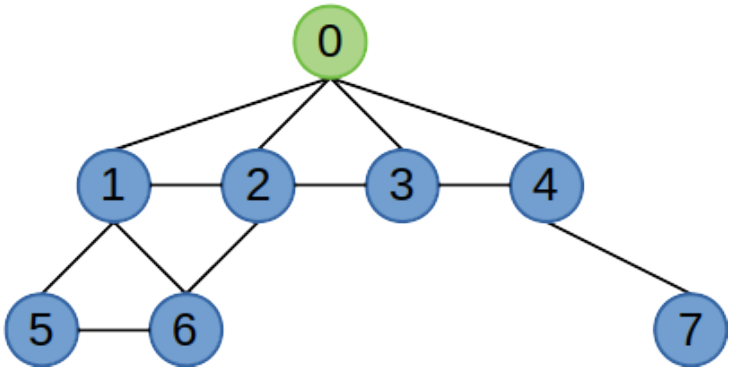

Figure 3.2: An example IQRF network.

To control the network, two approaches are available. These two approaches can be seen in figure 3.3. The user can use DPA (Direct Peripheral Access) Protocol, which doesn't require programming, or IQRF OS, which is more suitable for complex applications, but does not support the IQMESH network topology, only point-to-point or star topologies are possible to use. The DPA Protocol will be more discussed later in this thesis.

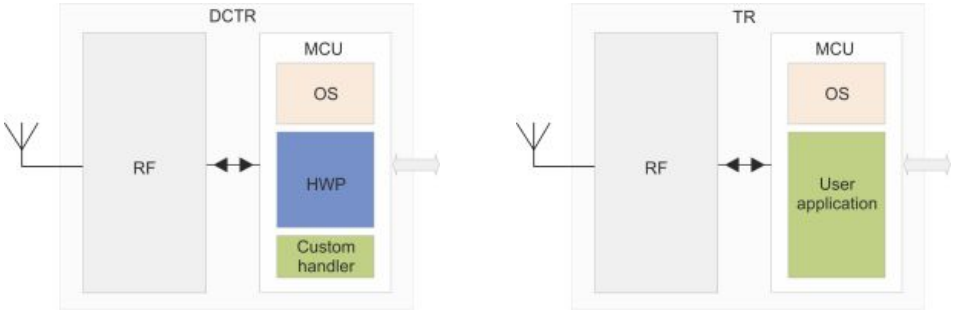

(a) : DPA **(b) :** OS

Figure 3.3: Two aplication approaches. Taken from [17].

To transfer a small amount of data, in counts of bits, the Fast Response Command (FRC) can be used. FRC greatly decrease the on-air time of a

packet. Fast Response Command will be discussed later in this thesis.
To incorporate IQRF connectivity to the device, various modules can be used.
These modules will be discussed in section 4.1.5.

3.2.1 DPA Protocol

The DPA is byte oriented protocol that uses messages to command end-nodes in the network. It is a higher level communication layer of the IQRF technology.
DPA enables a fast solution without programming IQRF modules, such as ADC readout, UART or SPI communication or interfacing with GPIOs. To control user interfaces, a DPA message is sent from the coordinator to an end node or nodes. End nodes need to have programmed so-called Hardware Profile, which processes a DPA message. Similarly, the coordinator node needs to have programmed a coordinator version of a Hardware Profile.
To add a custom functionality of a node, a Custom DPA handler must be implemented in the C language. However, this is unnecessary in most scenarios.

DPA can use RX STD and RX LP communication modes, but it is not possible to combine nodes with different modes in one network.

DPA Messages

The structure of a DPA message is displayed in the figure 3.4.

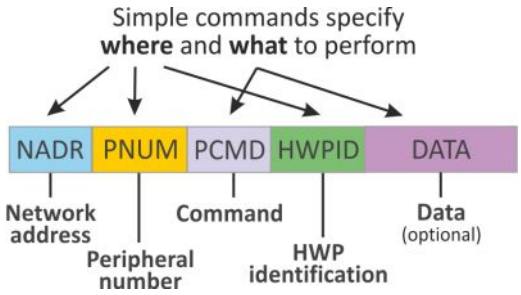

Figure 3.4: DPA protocol message format. Taken from [19].

Network Address NADR is a 2 byte number, but two byte addressing is not supported yet. Selected NADR values can be seen in the table 3.4.

NADR	Address
0x00	IQMESH Coordinator
0x01-0xEF	IQMESH Node
0xFF	IQMESH Broadcast

Table 3.2: NADR Values. Simplified, taken from [16].

PNUM and PCMD are 1 byte numbers. Peripheral Number PNUM specifies which peripheral is going to be controlled using the DPA message. Selected PNUM values can be seen in the table 3.3. Peripheral Comand Number PCMD varies depending on the selected peripheral and can be seen in [16].

HWPID	Address
0x00	Coordinator
0x01	Node
0x02	IQMESH Broadcast
0x03	EEPROM
0x04	EEEPROM
0x05	RAM
0x06	Red LED
0x07	Green LED
0x08	SPI
0x09	IO
0x0A	Thermometer
0x0C	UART
0x0D	FRC

Table 3.3: HWPID Values. Simplified, taken from [16].

Hardware Profile ID Number HWPID is a 2 byte number, and specifies the Hardware Profile the device should have. Only the device with the same HWPID will execute the request. If the 0xFFFF value is selected, any device with any HWPID will execute the request. A list of HWPID numbers can be seen in the table 3.4.

NADR	Address
0x0000	Default HW Profile
0x0001-0xXXXE	Certified HW Profiles
0xC05E	OTA Handler
0xXXXF	User HW Profiles
0xFFFF	Any HW Profile

Table 3.4: NADR Values. Simplified, taken from [16].

DATA field is optional, and its content depends on PNUM and PCMD. DATA field can contain up to 56 bytes. DATA field is used for example in UART DPA messages.

3.2.2 Fast Response Command - FRC

To transfer small data packets efficiently, the Fast Response Command (FRC) can be used. This mode of the communication is faster than the conventional way of sending packets in an IQRF network, where the coordinator is addressing nodes and sending the packet to each of them separately, this is called polling. While communicating using FRC is sent a packet with few bits sized slots, for each device one. These slots are then filled with data of the corresponding node. Bellow the formats of an FRC packet are listed:

- 2 bits from maximally 239 nodes
- 1 byte from maximally 63 nodes
- 2 bytes from maximally 31 nodes

It is clear now that the FRC is suitable just for applications with low data flow, such as binary states reading (or writing), or single value sensors (e.g., temperature sensors). The comparison of the speed of data reading by addressing each node separately and FRC data readout the in the figure 3.5. From the table in figure 3.5 it can be seen that the FRC is more than six times faster starting at 20 nodes network.
The FRC can be selective and unselective. As the name implies, the selective FRC allows selecting particular nodes of a network, whose data are required. Using the selective FRC, it is possible to make FRC requests with bigger data packets than it would normally be possible. For example, 1 byte packet in a network with 239 nodes, but only 63 of them are selected to respond to the FRC request.

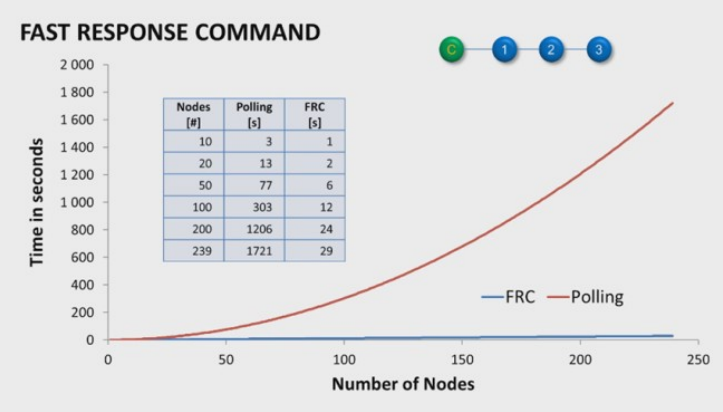

Figure 3.5: Data acquisition time comparison of polling and FRC. Taken from [18].

3.2.3 IQRF IDE

The software tool called IQRF IDE was used for programming the modules. The IDE presents an IQRF module configuration tool. Using this tool the user can set the TX power, network password, enable or disable user peripherals and many more.
This IQRF module configuration is then saved and uploaded to an IQRF module while programming.
The IQRF IDE has however more features, such as:

- Tool for a network map creation and graphical representation
- RE terminal
- Configurator, Analyzer, Tester and Scanner (CATS)

There are two ways to create a network within this IDE. The graphical one with prepared buttons for and dialog windows for bonding, unbonding, discovery and more network operations, this can be seen in the figure 3.6. This way is easy and fast to use, and it is the perfect way to learn about the IQRF network and its functions.
The other way is using DPA commands and RF terminal. This can be seen in the figure 3.7. The user can create DPA commands himself, using the DPA Framework Technical guide, or he can use prepared macros, which will create the DPA command for him. After sending a DPA command, the process can be seen in the RF terminal log, where DPA Request, Response, and Confirmations are distinguished by colors.
The parts of a DPA message are parsed, so the user can easily analyze the message.

To display the network, another graphical tool is prepared and can be seen in figure 3.8. Using this tool, the user can easily display the network. The nodes in a network can have different colors, to easily recognize their status: the coordinator is green, bonded but not discovered nodes are yellow, and bonded, and discovered nodes are blue. The links between nodes are displayed as well as the distance as the number of hops from the coordinator. This is displayed as layers under the coordinator node. Each layer means one hop.

Sadly, the IDE can be used only for computers with a Windows operating system and is not available for Linux computers.

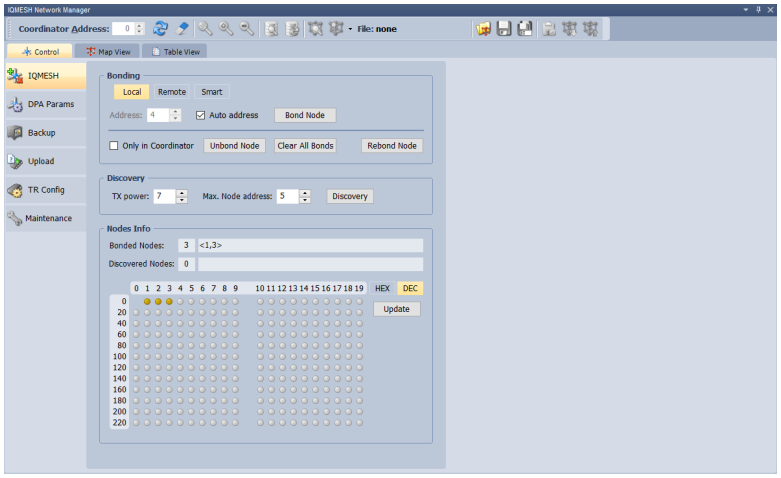

Figure 3.6: IQRF IDE - Network management window

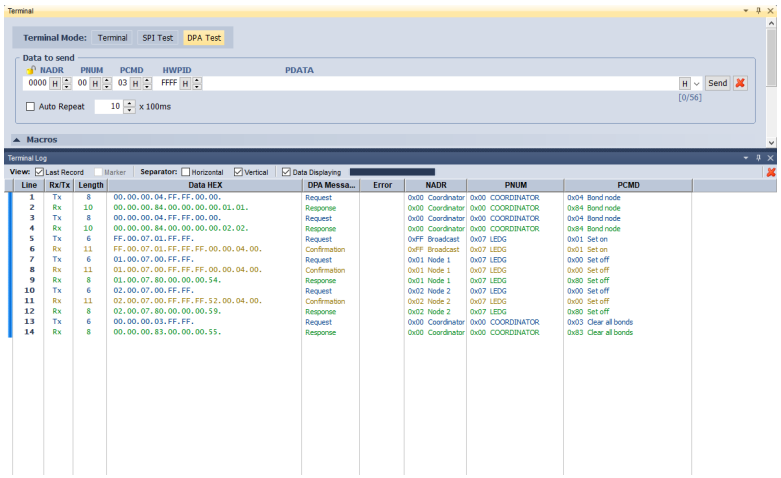

Figure 3.7: IQRF IDE - RF terminal window

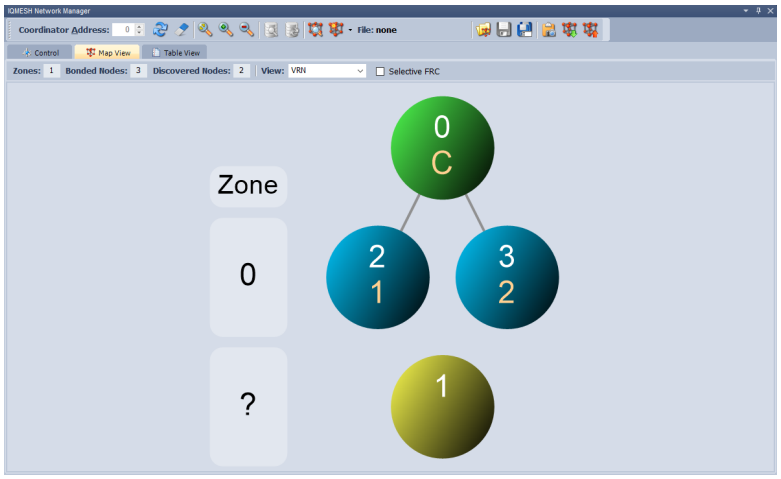

Figure 3.8: IQRF IDE - Network map window

3.2.4 IQRF SDK

The IQRF SDK is developed to add IQRF functionality to embedded devices, either with an operating system, such as Raspberry Pi or BeagleBone or without an operating system, for example, STM32 MCUs.
The IQRF SDK is open-source and can be found on IQRF Tech company's GitHub [20].
The IQRF SDK contains libraries written in C, C++, Python and Java programming languages.
For this thesis, the most interesting repositories are:

- clibdpa - C++ library for interfacing IQRF modules using SPI or CDC
- clibcdc - C++ library for interfacing IQRF modules using CDC
- clibspi - C library for interfacing IQRF modules using SPI
- pylibiqrf - Python library for interfacing IQRF modules using SPI or CDC

All of these libraries are suitable for use with an embedded Linux computer, such as Raspberry Pi.
However examples contained in these libraries could be better documented and show more functionality than simple node LED switching. For example, bonding of a new node is not shown in these examples, and all of these examples assume a node was already bonded.

3.2.5 Ways to reduce the power consumption of IQRF modules

To ensure low power consumption of the module, there are several operation modes the RF circuitry and the module itself.
Operation modes of the RF circuitry are:

- **STD RX**
  In this mode, a module is continuously receiving packed when `RFRXPacket` function is called. The average power consumption of the module in this mode is 12mA.
- **LP RX**
  When this mode is selected, receiving packets is periodically alternated with a sleep mode when `RFRXPacket` function is called. The approximate duration of a cycle is 47ms. In this mode, the average consumption of the module is 250μA.
- **XLP RX**
  This mode is similar to LP RX mode, but the duration of one cycle is 790ms, while the duration of packet receiving remains the same. The average consumption of the module is 18μA.

Sleep modes of the module are:

- **Sleep Mode**
  In the Sleep Mode the PIC microcontroller of the module is in a power saving mode, so are RF integrated circuit and peripherals. Switching this mode on and off is quick and doesn't require reinitialization of the RF integrated circuit.
- **Deep Sleep Mode**
  This mode is similar to the Sleep Mode, but RF integrated circuit is not in a power saving mode but is powered off. Switching this mode on and off requires more time and also reinitialization of the RF integrated circuit and corresponding settings.
- **RF Circuitry Sleep Mode**
  In this mode, the only part of the module in a power saving mode is the RF integrated circuit.

3.3 LoRa

LoRa is a LPWAN, and its name is an abbreviation of Long Range.
LoRa operates in the 868MHz ISM band in Europe with ten channels, 8 of them works as multispeed channels with transfer speed from 250pbs to 5.5kbps, one high-speed channel with the transfer speed of 11kbps, and one FSK channel with the transfer speed of 50kbps.
Chirp spread spectrum is used to transfer data, which ensures long range and high noise tolerance. Six chirp Spreading Factors, from Spreading Factor 7 to 12. The spreading factor influences the robustness of the transmission, with higher spreading factor, the reliability of the transmission is better, but each step also doubles the transmission time, which means lower data rate and higher consumption.
The maximum transmission power is 14dBm.

The consumption of a node can by optimized using Adaptive Data Rate, which enables the LoRa server to set the transmission power and the spreading factor of the node to reduce the airtime of a message, thus reducing its consumption.

The range of a transmission can be up to 5km in urban areas and up to 20km in rural areas.
One packet can contain payload up to 243B, but the size of the payload affects the transmit time, which implies more power consumption of the device.
The range of the network is up to 20km in rural areas, but this range drops to 5km in urban areas. The range is strongly dependent on the surrounding area and the node and the gateway location. More realistic ranges are 11km and 4km. [24]
The LoRaWAN coverage map of the Czech Republic, run by České Radiokomunikace, can be seen in figure 3.9.

To ensure a reliable coverage of the area, more gateways are placed within this area, so their ranges overlap. This means messages are received multiple times by different gateways. This is solved later, on LoRaWAN Server, which removes duplicate messages.
The simplified schematic of the LoRaWAN network can be seen in figure 3.10.
End nodes communicate with gateways using sub-GHz LoRa communication. Gateways communicate with a server using an internet connection, such as Ethernet or LTE.

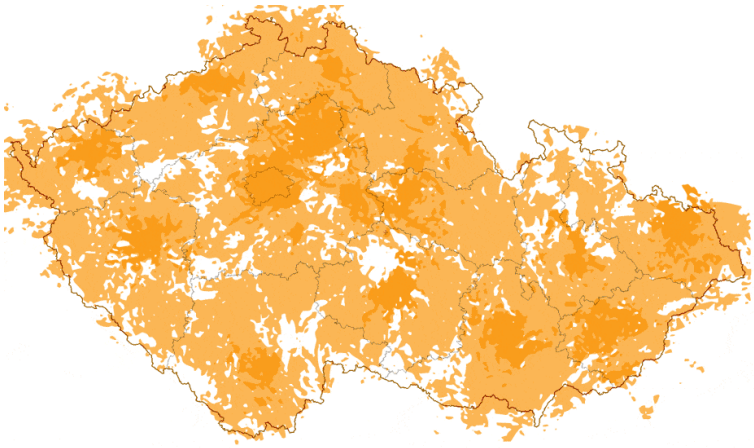

Figure 3.9: Map of LoRaWAN Coverage of the Czech Republic.[25]

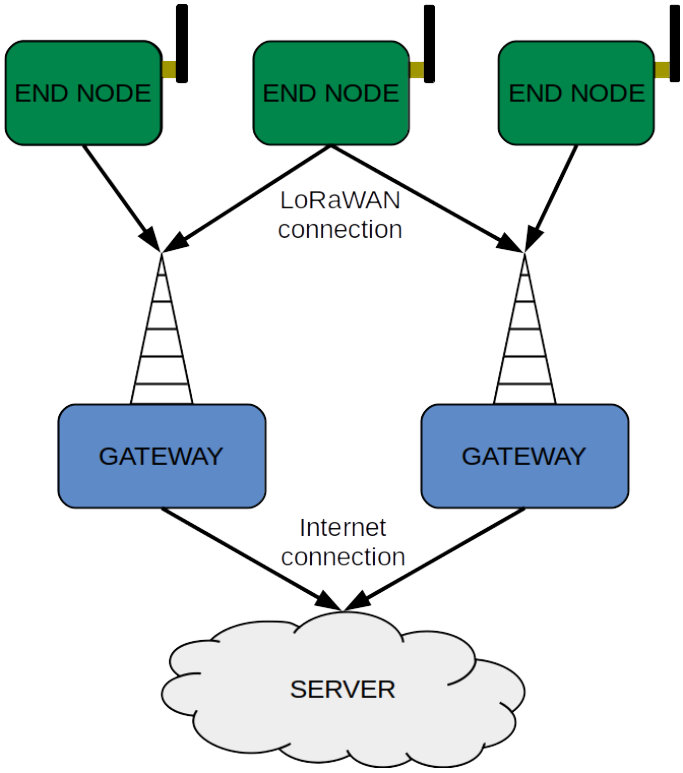

Figure 3.10: LoRaWan Network Architecture

LoRa is a bidirectional network, which means, that an end node can send messages to a gateway (uplink messages), and receive messages from the gateway (downlink messages). However the downlink messages can not be sent anytime to a device. The downlink messages are sent to nodes only during so-called downlink windows. The downlink windows are scheduled depending on the class of the device.

3.3.1 Device classes

The LORAWAN standard defines three device classes:

- **Class A: Bi-directional end-devices**
  This class of devices is allowed to communicate in both directions using two short downlink windows right after uplink communication. Transmissions are scheduled by an end-device using an ALOHA-type protocol. Downlink messages from a server to a node are scheduled to be sent in these windows, and wait for the next uplink.
  All LoRaWAN devices must implement features of the Class A specification.
- **Class B: Bi-directional end-devices with scheduled receive slots**
  Devices of class B have scheduled other downlink windows in addition to the regular ones class A devices have. These extra windows are scheduled on precise time. End-devices synchronize with a gateway using Beacon transmission.
- **Class C: Bi-directional end-devices with maximal receive slots**
  Class C devices have constantly opened downlink window, which closes just for transmission of an uplink message.

Most of the devices will be probably defined as Class A devices, because of the nature of LPWANs. Generally speaking, the device should last at least a decade on battery power, which implies it will probably be in some kind of power saving mode for the vast majority of its lifespan, so often communication and channel listening is undesirable.

Chapter 4

Sensor Design

4.1 Hardware design

The sensor consists of following parts:

- Power management
- Microcontroller
- Communication modules
- Temperature and humidity sensors SHT31
- Circuits for wood moisture measurement

The block diagram of the sensor can be seen in figure 4.1.
The sensor is designed to be primarily powered by a battery, however, in case of need, it can be powered using an external power source, using a cable. These options are exclusive to each other, it is not possible to use both power sources together.
If a battery is used as the power source, the output voltage of the battery is regulated using DC/DC step-up converter in a case of a drop of the battery voltage under 3.3V.
In the case of external power source use, the input voltage is regulated using DC/DC step-down converter to 3.3V.

The power supply voltage for the circuits and components of the sensor is $V_{CC} = 3.3V$. This voltage powers up the microcontroller, which, among others, controls P-MOSFET transistors to switch off all other devices and circuitry (excluding power management circuits) to save up energy.
The main task of the microcontroller is to communicate with SHT31 sensors using I^2C bus and measure the moisture of a wood, which employs another 5 GPIOs.
Last, but not least, the task of the microcontroller is to communicate with wireless network modules (IQRF or LoRa) using UART.

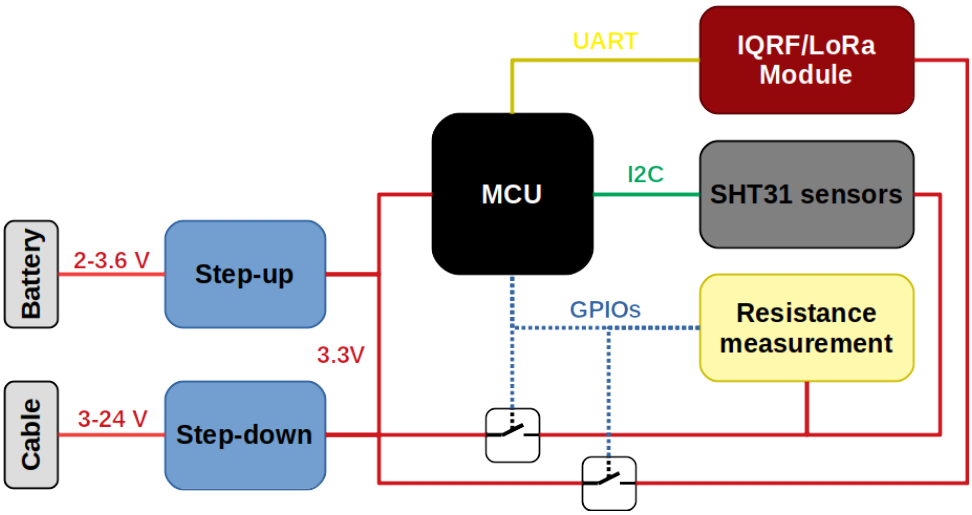

Figure 4.1: The block diagram of the sensor

4.1.1 Battery

The factors considered during the battery selections are listed below:

- Rechargeability
- Capacity
- Size
- Nominal voltage
- Discharge characteristic
- Self-discharge
- Safety
- Cost

Because the sensor will be built-in a construction, the battery can not be replaced, so the selected battery must be non-rechargeable.
The capacity of the battery must be sufficient enough, the size of the battery is a limitation. From the previous, wired variants of the sensor, the minimal width of the PCB was known to be about 40mm, so searching for a tiny battery would be useless, since an AA comparable size battery was perfectly adequate.
The nominal voltage of the selected battery must be in the range from 3V to 4V.
Self-discharge should be as low as possible. Otherwise, the effort to make the sensor low-power would be void.
The specifications above limited the selection to Lithium Thionyl Chloride ($LiSOCl_2$) batteries listed in the table 4.1.

Name	Q[mAh]	V_{nom}[V]	Self – discharge	Price [CZK]
T06/8AA9	2450	3.6	1%/year	330
LS14500	2600	3.6	1%/year	113
LS17500	3600	3.6	1%/year	163

Table 4.1: Comparison of selected batteries

All batteries listed in the table 4.1 are manufactured by SAFT and belong to the same LS series. The T06/8AA9 is double the price of the rest probably because of the mounting type. Its capacity was smaller with no advantage

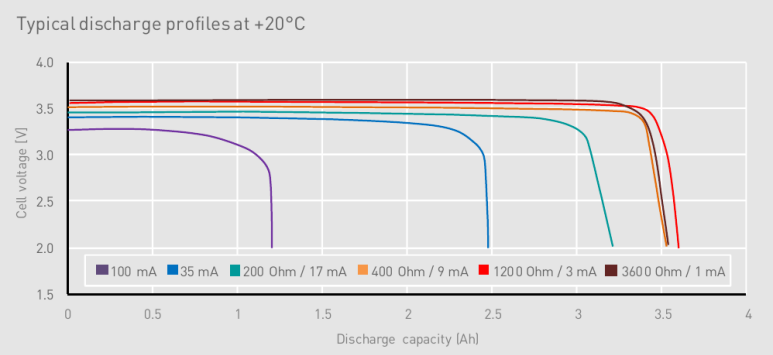

Figure 4.2: Discharge profiles of LS17500 battery. Taken from [29].

over the others, so it was excluded from the selection.

The LS14500 and LS17500 batteries have almost the same size, both are 50mm long, but their diameter is different, LS14500 having 14.55mm diameter and LS17500 17.13mm diameter.
Because the price is not so different and the LS17500 has the significantly bigger nominal capacity, the LS17500 was selected.
In case the consumption of the sensor allows it, the LS17500 can be easily replaced by LS14500, because they have the same footprint.

The discharge profiles of LS17500 can be seen in figure 4.2. The discharge profile is very flat so that the battery voltage will be $V_{bat} = 3.6V$ almost the whole time. The battery voltage starts to drop rapidly when the end of its life, so there is not a simple way how to determine its state of charge (SOC). This is, however, not needed for this application, a simple low battery voltage alert is sufficient. The LS17500 battery contains non-flammable electrolyte, which makes it safe for use in wooden constructions. Moreover the Battery Information Sheet [30] states, that the battery is not hazardous under normal operation conditions.

The battery voltage is measured using an analog-to-digital converter of the host microcontroller. Because the nominal voltage of the battery is $V_{BAT} \approx 3.6V$, which is over the supply voltage of the microcontroller $V_{CC} \approx 3.3V$, a voltage divider is necessary to measure safely and correctly. In order to minimize current flowing through the voltage divider, i used resistors of the value $R = R_1 = R_2 = 1M\Omega$. The output voltage of the voltage divider is then:

$$V_{ADC} = \frac{R_2}{R_1 + R_2} V_{BAT} = \frac{R}{2R} V_{BAT} = \frac{V_{BAT}}{2} \tag{4.1}$$

To prevent the voltage divider from consuming power while it's not needed, the ground pin of the voltage divider is connected to a GPIO pin of the microcontroller. This pin will be pulled high for most of the time, and it will be grounded just for the period of measurement.

4.1.2 Step-up DC/DC convertor for battery powered version of the sensor

This part of the sensors is used to ensure supply voltage $V_{CC} \geq 3.3V$ in case of too low battery voltage V_{bat}. Nominal voltage of the used $LiSOCL_2$ battery is $V_{bat} = 3.6V$.
The table 4.2 contains selection of DC/DC step up converters. The crucial factor for selection of the best converter was quiescent current I_Q and efficiency.

Name	Manufacturer	$I_Q[\mu A]$	Efficiency	Suitable
L6920	STMicroelectronics	9-15	95%	×
ST5R00	STMicroelectronics	16	83%	×
LM2621	Texas Instruments	80-110	87%	×
LT1300	Linear Technology	120-200	80%	×
LT1307	Linear Technology	50-90	80%	×
LT1615	Linear Technology	20-30	84%	×
MAX17222	Maxim integrated	0.3-0.6	95%	✓
MAX8815A	Maxim integrated	30	97%	×
AS1312	AMS	1	94%	✓
RT9263	RichTek	47	85%	×
TPS610982	Texas Instruments	0.3-0.8	93%	✓

Table 4.2: Comparison of DC/DC step-up converters

Considering mainly the quiescent current I_Q, the most suitable integrated circuits are the following:

- MAX17222 by Maxim integrated
- TPS610982 by Texas Instruments
- AS1312 by AMS

Unfortunately, the AS1312 IC had to be excluded from the selection because of unavailability from the suppliers. The rest of the selected ICs are compared in the table 4.3 below.

Name	$I_Q[\mu A]$	$I_{max}[mA]$	$V_{in}[V]$	Efficiency
MAX17222	0.3-0.6	500	0,95-5,5	95%
TPS610982	0.3-0.8	500	0,7-4,5	93%

Table 4.3: Comparison of the MAX17222 and the TPS610982. [31, 32]

From a quick look into the table 4.3 is clearly visible the similarity between attributes of both ICs.
To decide, efficiencies of the DC/DC step-up converters for load current $I_{LOAD} = 20mA$, which is the predicted load current of the sensor, were compared. One can see the plots of efficiencies in figure 4.3.
For both plots the output voltage is $V_{out} = 3.3V$. Comparing the efficiency for $V_{IN} = 2V$, which is the lowest predicted voltage plotted in graphs, it is clear, that the efficiency of both ICs, the MAX17222 and the TPS610982, is nearly equal.

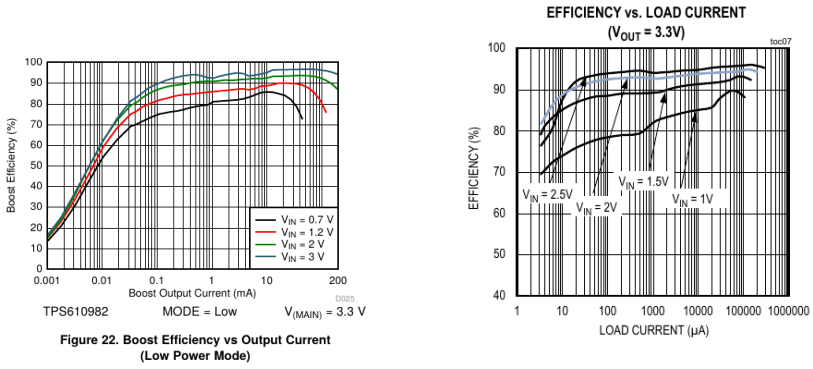

(a) : TPS610982 [31] **(b) :** MAX17222 [32]

Figure 4.3: Efficiency depencence on voltage and load current

The next step is to compare the price and complexity of the operating circuits of the ICs. Since the price is not a priority in this sensor, only the complexity of the operating circuits is compared, although the TPS610982 is slightly cheaper. Schematic for the TPS610982 can be seen in the figure 4.4a, and schematic for the MAX17222 can be seen in the figure 4.4b.
The advantage of the MAX17222 over the TPS610982 is the simplicity of the schematic and smaller count of passive parts used, which means smaller PCB footprint.

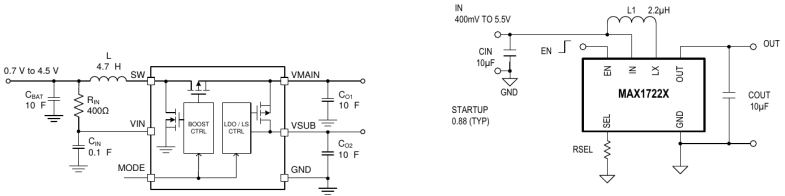

(a) : TPS610982 - Schematic. [31] **(b) :** MAX17222 - Schematic. [32]

Figure 4.4: Circuit schematic for TPS610982 and MAX17222

Another advantage of the MAX17222 is its behavior when the input voltage V_{in} is smaller than V_{out}. This behavior is best described using this pseudocode:

```
Vset = 3.3V ... setted output voltage
Vdiode = 0.2V ... diode voltage drop

if (Vin > Vset) then:
        if (Vin > (Vset + Vdiode)) then:
                Vout = Vin - Vdiode
        else if ((Vset + Vdiode) > Vin > Vset) then:
                behave as a buck DC/DC converter
else:
        behave as a step-up DC/DC converter
```

From the behavior described in the pseudocode above, the advantage of the MAX17222 over the TPS610982 for this specific application is clearly visible: The voltage of the battery should be $V_{bat} = 3.6V$ for the most of its lifespan (as described in the subsection 4.1.1). This means the voltage drop on the inner diode will be approximately $V_{Ddrop} \approx 0.2V$, meaning the output voltage of the converter will be $V_{out} \approx 3,4V$. Moreover, the converter will not be switching. Therefore the quiescent current I_Q will be small.
For these reasons, the MAX17222 DC/DC step-up converter was selected. However, one more pull-up resistor to the ENABLE pin of the MAX17222 was added.
Schematic used in the design can be seen in the figure4.5.

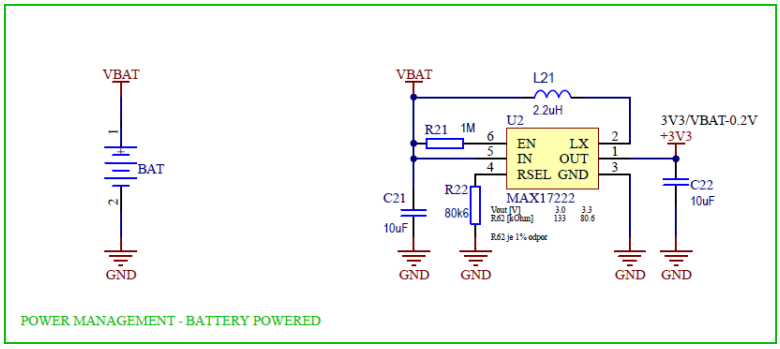

Figure 4.5: Schematic of the step-up DC/DC converter circuitry, designed in Altium Designer 16

4.1.3 Step-down DC/DC convertor for externaly powered version of the sensor

The maximal considered input voltage is $V_{in-max} = 24V$. To minimize heating of the sensor (which would render temperature measurement useless), it is vital to use a step-down DC/DC converter instead of a linear voltage regulator. For this task, the step-down DC/DC converter Richtek RT8299A was chosen. The decision was made on a price basis. The input voltage of this converter is $V_{in} = 3 \div 24V$, which is perfectly suitable for this application.[33]
A transil is used to protect the sensor circuitry from an electrostatic discharge. To protect the sensor from a voltage polarity switch (e.g., by a user) a serially connected diode was added.
The schematic can be seen in the figure 4.6.
Using the following equation from the datasheet of the RT8299A DC/DC step-down converter[33], the values of the resistors R73 and R74, which serve as a feedback voltage divider for the IC, were calculated:

$$V_{OUT} = V_{FB}\left(1 + \frac{R73}{R74}\right) \tag{4.2}$$

where $V_{FB} = 0.8V$, a $V_{OUT} = 3.3V$.
To ensure the automatical start-up of the converter, the ENABLE pin is connected to the input voltage line using a pull-up resistor.

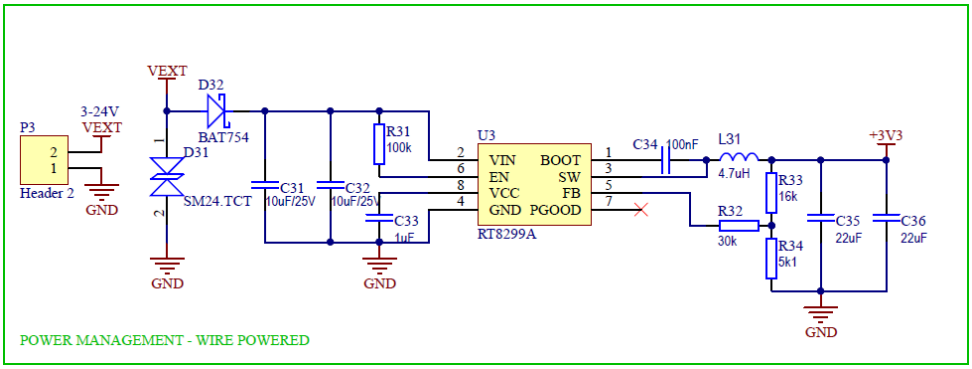

Figure 4.6: Schematic of the step-down DC/DC converter circuitry, designed in Altium Designer 16

4.1.4 Microcontroller

In the first design of this device, the IQRF module TR-76DA was used as the control unit. This module has on-board programmable PIC16LF1938 microcontroller. However programming of the module is limited, and not all of the features of embedded C language are available due to the custom compiler used by the IQRF OS. For example, time measurement, which is a very important feature for wood moisture measurement, is limited to the resolution of 10ms. Another bad feature of the IQRF OS is setting GPIO pins as high impedance during the Deep Sleep Mode, which is crucial to this application, because of used P-MOSFET transistors for powering off parts of the device, which was pulled down in the Deep Sleep Mode, instead of up, which caused powering on of these parts.

Another reason why it was decided not to use the TR76-DA module was the count of its GPIO pins, which is 11. This seriously limits the development of the device, for example, it would not be possible to add LoRa module to the device, and also options for another development would be restricted by this. Because of the reasons listed above a separate microcontroller was used as the control unit of the device.

The new design of the sensor was based on STM32L053C8 microcontroller from the low-power MCU family by ST Microelectronics, this microcontroller was however replaced by the PIC18F26K40 microcontroller manufactured by Microchip. This decision was made to ensure an easier development of the sensor in the future, because my colleagues are skilled in programming PIC microcontrollers, in contrary to the STM32 32-bit ARM microcontrollers.
The people who could support the development of the sensor based on a STM32 microcontroller are no longer working at UCEEB CTU, therefore this change had to be made.
Moreover, according to the table 4.4, this decision proved to be even more energy efficient, since the PIC18F26K40 microcontroller consumes less current than the STM32L053C8 microcontroller.

Mode	$\mathbf{I_{sup}}[\mu\mathbf{A}]$	
	STM32L053C8	**PIC18F36K40**
Run - 16MHz	3400	2600
Run - 4 MHz	280	650
LP Run - 32kHz	10	8
Sleep mode	1	0.9

Table 4.4: Comparison of current consumptions of STM32L053C8 and PIC18F26K40. [34, 35]

As said before, the PIC18F26K40 8-bit microcontroller was used in the final design of the sensor. This microcontroller is used in the wired version of the Moisture Guard sensor MHT03485, and has low power features, so the deciding process was quite straight-forward because it is suitable for a low power application and the firmware will be partially compatible with the MHT03485 sensor.
The 28-pin QFN package version of this microcontroller was used, to ensure the pin compatibility with the MHT03485 sensor.
This microcontroller has both UART and I^2C communications which are needed in this application, and also ADCs so that the battery voltage can be measured. The 28-pin QRF package enough GPIO pins to measure wood resistance, and control P-MOSFET transistors to enable and disable measurement and communication circuitry. The microcontroller has, of course, many other features, but these are not needed in this application.

The PIC microcontroller enables power for measurement and communication circuitry using two P channel MOSFET transistors T1 and T2, controlled by pins RA5 and RA4, respectively.
To prevent unnecessary current consumption on the voltage divider for the battery voltage measurement, the negative of the voltage divider is connected to the pin RA6. The output of the voltage divider is connected to the ADC on the pin RC0.
The communication module, either IQRF Module TR76D or LoRa Module RN2483, are connected to the microcontroller using UART on pins RC6 (`RX` signal) and RC7 (`TX` signal).
The SHT31 sensors are connected to the microcontroller using I^2C to the pins RC3 (`SCL` signal) and RC4 (`SDA` signal).
The control signals `DRIVE_LO` and `DRIVE_HI` of the resistance measurement excitation are connected to pins RB1 and RB2 and are driving transistors T11 and T12, respectively. By setting these pins to levels according to the table 4.5, the excitation voltage can be set to GND, low positive level (3.3V in this case), or negative level (-2.7V in this case). The signals must not be set to low logical level at the same time.
The control signal `SWITCH_CTR` of the P channel JFET transistor T8 is connected to the pin RA2. The output signals `COMP_NEG` and `COMP POS` of the comparators U10 and U9 are connected to pins RB4 and RB5, respectively.

DRIVE_HI	DRIVE_LO	**Excitation voltage level**
0	0	SHORT
0	1	POSITIVE
1	0	NEGATIVE
1	1	GND

Table 4.5: Excitation voltage level - logical table

The schematic implementation of the PIC microcontroller and its circuitry can be seen in the figure 4.7.

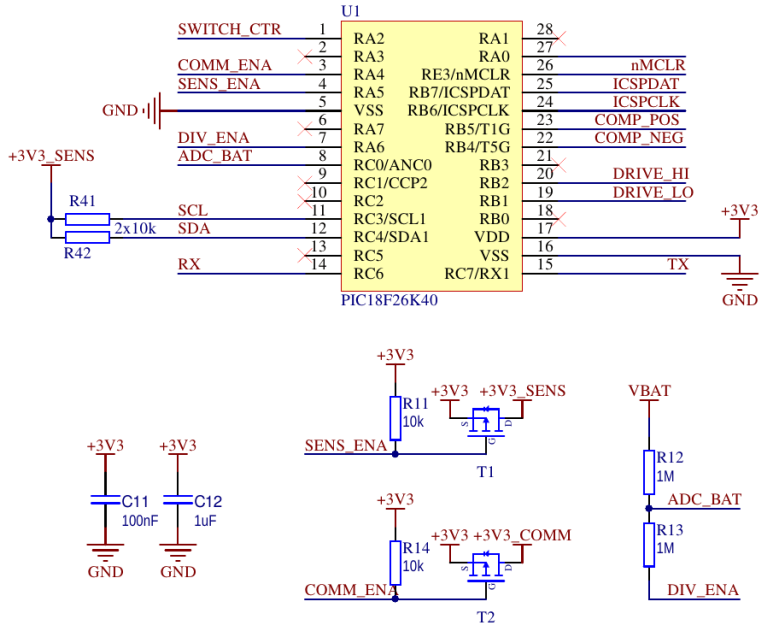

Figure 4.7: Schematic of the MCU circuitry, designed in Altium Designer 16

Current consumption and power saving features

The current consumption of the microcontroller is very important for this application because the microcontroller will always be powered on. The PIC18F26K40 microcontroller has several ways to reduce its power consumption, which are presented in this section.
The PIC18F26K40 has three power saving operation modes:

- Doze
- Idle
- Sleep

In the Doze mode, the CPU and program memory access runs on a lower clock rate than peripherals. The CPU executes one instruction cycle in every Nth instruction cycle. This ratio is set by `DOZE` bits from 1:2 to 1:256 in 8 steps.
In the Idle mode, the CPU and memory is halted, but the peripherals are still running.

The most interesting mode for this application is the Sleep mode because it is the mode with the least current consumption. There are several ways to wake up from the sleep mode, the most important for this application is Windowed Watchdog Timer (WWDT), because WWDT is used to wake up the microcontroller from the sleep mode.

The sleep mode can be optimized more and switched to Low Power sleep mode using `VREGCON` register. Waking up from the low power sleep mode is slower because some circuits can be switched off by the user. Therefore they need to return to the normal configuration. The low power sleep mode is more useful in application like this, where the sensors are in the sleep mode for a long period.

The current consumption of the PIC18F26K40 microcontroller is listed in the table 4.6. The consumption may vary in dependence of used peripherals. This table includes the current consumption of the low power modes, as well as the current consumption of high-performance modes, to demonstrate the ability of the microcontroller to dramatically decrease its power consumption. The figure 4.8 shows the current consumption dependence on the supply voltage for the system clock frequency of 32kHz.
By the closer inspection of this plot, one can see, that the supply current in the table matches the one shown in the plot.

Mode	$\mathbf{I_{sup}}[\mu A]$
Run - 64MHz	9400
Run - 16MHz	2600
Run - 4MHz	650
Run - 32kHz	8
Doze mode (16MHz - Doze ratio 16)	1200
Idle mode - 16MHz	1100
Sleep and Watchdog timer	0.9
ADC converting	250

Table 4.6: Current consumptions of the PIC18F26K40 microcontroller in different modes. [35]

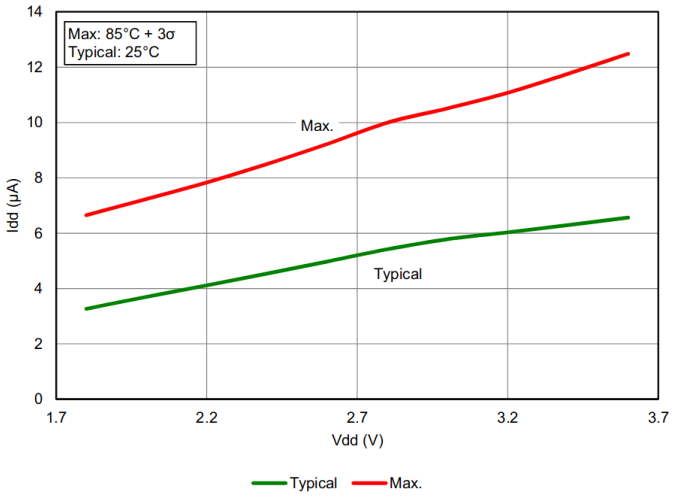

Figure 4.8: The dependency of the supply current I_{dd} on the supply voltage V_{dd}. System clock = 31kHz. Taken from [35].

Another useful feature is the Peripheral Module Disable ability, which allows to enable and disable selected peripherals, which helps to minimize the current consumptions of the microcontroller. To disable a peripheral, the `PMDx` registers are used. There are six `PMD` registers:

- `PMD0` register disables Peripheral Clock Network, Fixed Voltage Reference, CRC Engine, Clock Reference, and more.
- `PMD1` register disables timers.
- `PMD2` register disables ADC and DAC modules, Comparator module and Zero Cross Detection module.
- `PMD3` register disables PWM modules.

- `PMD4` register disables EUSART modules, MSSP (I^2C) modules and the Complementary Waveform Modulator module.
- `PMD5` register disables the Data Signal Modulator module.

Most of these modules are not needed and can be disabled all time, but some of them, such as ADC, EUSART or MSSP modules must be enabled for the correct operation of the sensor during taking the measurement or communication. However, these modules can be enabled and disabled at will.

4.1.5 Communication modules

In the thesis assignment, only IQRF communication is mentioned, but during the work on this thesis, it was decided to incorporate a LoRa module to add another possible communication channel. The reasons why it was decided so are described more in detail in section 4.2.
To transfer data from the device to a server two technologies can be used:

- IQRF Network
- LoRaWAN Network

Modules for both of these technologies exist, so the RF part of the sensor, but the antenna connection, didn't have to be designed.

IQRF module

Since there is not a wide selection of the IQRF modules, the selection was simple. From the selection of the IQRF modules, only TR-76 module can be soldered to a PCB at this time. This module is made in two versions, TR-76DA with on-board antenna, and TR-76D with pad for connecting the module to an external antenna. Because an external antenna was used, the TR-76D module was chosen. If it were decided not to use LoRa communication in the future, I would advise using TR-76DA IQRF module with an incorporated antenna.
Despite the module TR-76D is programmable, it was not used as the central unit of the sensor, as explained earlier in the section 4.1.4.
However, it was still necessary to programme this module to communicate with the control microcontroller using UART.
The module contains PIC microcontroller PIC16LF1938, manufactured by Microchip, external EEPROM memory, manufactured by Microchip, and RF circuitry with IC SPIRIT1, manufactured by ST Microelectronics.
TR76-D contains 11 input/output GPIOs and one input GPIO. These GPIOs can be used to communicate using UART, SPI, or I^2C, generate PWM, or use them as Digital-to-Analog or Analog-to-Digital converters. Description of the GPIOs, and their functions, is described in the datasheet of the TR-76 module ([38]).
Supply voltage of the module is $V_{CC} = 3 \div 3.6V$
The block diagram of the module is in figure 4.10. More detailed diagram of

the module can be seen in figure 4.11, this diagram shows how the pins of the module are connected to the pins of the microcontroller.
One of the important features of the module is to influence its power consumption. This means the module can adjust a transmitting power, change a receiving mode, or enable a power saving mode. Receiving modes and sleep modes are discussed in section 3.2.5
Power consumption of the module can be seen in figure 4.12. The power consumptions of various transmitting power level are marked with a green arrow with "TX 8 levels" text. The current consumption of the module is 19mA, when the highest transmitting power is set, and 8.3mA, when the lowest transmitting power is set. Transmitting power can be set in range 0-7. In the same picture is also plotted the power consumption of various receiving modes. In the RX STD mode, which means that the module is constantly listening for incoming messages, is the average current consumption of the module 12.3mA. If the mode RX LP is set, the average current consumption drops to 233μA. RX LP mode means the module is listening for messages in short periodic pulses. The RX XLP mode is very similar to the RX LP mode, but the period of the pulses is bigger. The current consumption of the module in the RX XLP mode is 12μA.
The third way how to adjust the power consumption of the module is to use sleep modes. There are three sleep modes of the module, all can be seen in the figure 4.12. When there is no need to receive or send messages, RF circuitry can be switched off, which saves 1.4mA of the current consumption. The module can also set itself to the Sleep Mode and the Deep Sleep Mode, the current consumption of the module in these modes is 1μA and 100nA, respectively.
For modules with integrated on-board antenna (TR-72DA, TR-76DA), its radiation pattern is plotted in the figure 4.13.

The implementation of the connection of the module to the MCU can be seen in figure 4.14.

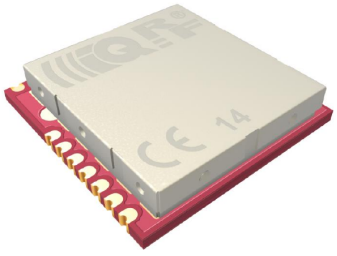

Figure 4.9: A picture of the IQRF module TR-76D. Taken from [38]

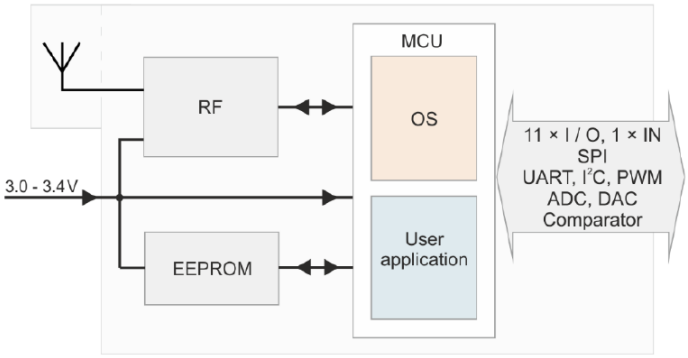

Figure 4.10: Block diagram of the IQRF module TR-76D. Taken from [38]

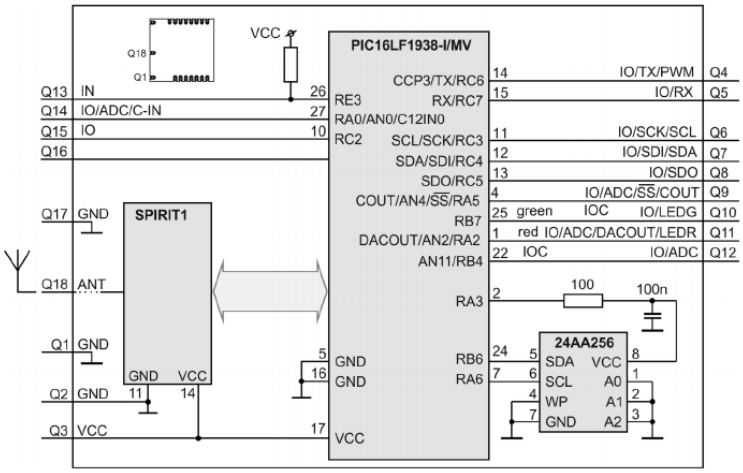

Figure 4.11: Simplified schematic of the IQRF module TR-76D. Taken from [38]

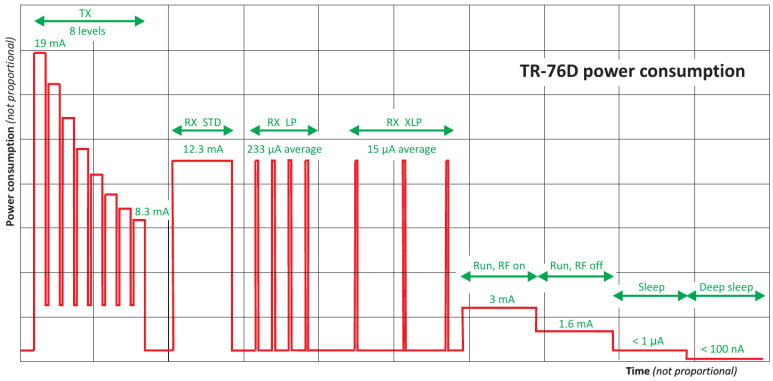

Figure 4.12: Graph of the current consumption of the IQRF module TR-76D. Taken from [39]

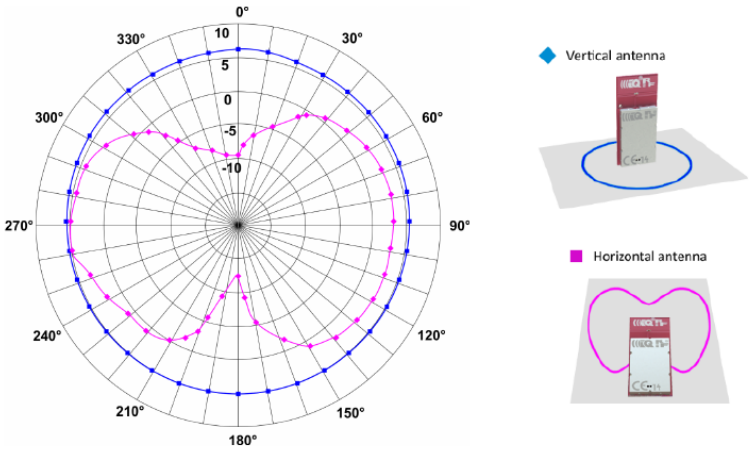

Figure 4.13: Radiation pattern of the on-board antenna of the TR-76DA module. Taken from [38]

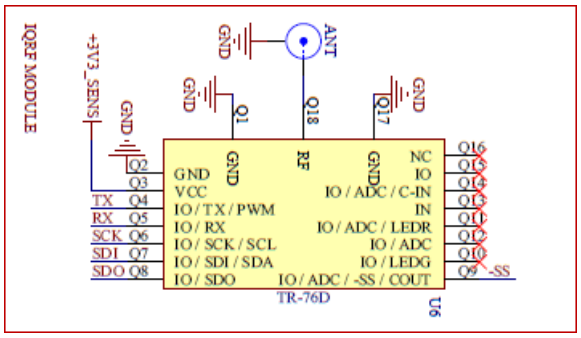

Figure 4.14: Schematic of the IQRF module circuitry, designed in Altium Designer 16

LoRa module

There are several modules for implementing the LoRa network to the device. They are based on Semtech SX1272 or SX1276 RF transceivers. While developing devices communicating using LoRa at UCEEB CTU, I encountered the following LoRa Modules:

- Microchip RN2483
- HopeRF RFM95W
- Semtech SX1276MB1xAS
- Nemeus MM002

From the modules listed above, it was decided to use the Microchip RN2483 LoRa Module. HopeRF RFM95W and Semtech SX1276MB1xAS require to have the complete LoRa stack implemented on a host microcontroller because they do not have their own microcontroller with the LoRa stack, these modules consist of SX1272 or SX1276 RF transceiver by Semtech and necessary RF circuitry, such as balun and antenna matching.
The fact the LoRa stack is not implemented on these modules adds an unnecessary amount of development to the application, and more powerful microcontroller would be needed to implement the LoRa stack.
Because of this issue ordered two modules were ordered: Nemeus MM002 and Microchip RN2483, with a host microcontroller with LoRa stack implemented. Both of them use UART to communicate with a host microcontroller and the communication is quite straightforward using ASCII commands.
The dimensions of these modules are similar, the RN2483 module is slightly bigger, as seen in the figure 4.16, so the size of the module is not the decisive factor.
By quick look to the table 4.7, one can see that the current consumption of the modules while transmitting is similar, in idle mode module RN2483 is doing slightly better, however this is not an issue, since the module will be switched off using a transistor switch for the most of the device lifespan. The same goes for the sleep current consumption, where the module MM002 has lower current consumption.
The main decisive factor is the price and availability from vendors. The price of the Nemeus MM002 module is 15€ and is not available from any of the usual suppliers of electronic parts, UCEEB CTU buys from, which disqualifies this module. However its great advantage versus the RN2483 module is availability to use it for Sigfox network connection, so if this module is better available in the future, it could be worth to incorporate this module to the new designs.

The RN2483 module costs 10€ and is available from most of the usual suppliers, which is the reason this module was used.

Mode	Current consumption	
	RN2483	**MM002**
Sleep	$16\mu A$	$< 2\mu A$
Idle	$2.8mA$	$11.7mA$
TX 7dBm	$28.8mA$	$20mA$
TX 13dBm	$36.5mA$	$33mA$
TX 14dBm	$38mA$	$39.5mA$

Table 4.7: Comparison of LoRa modules power consumption

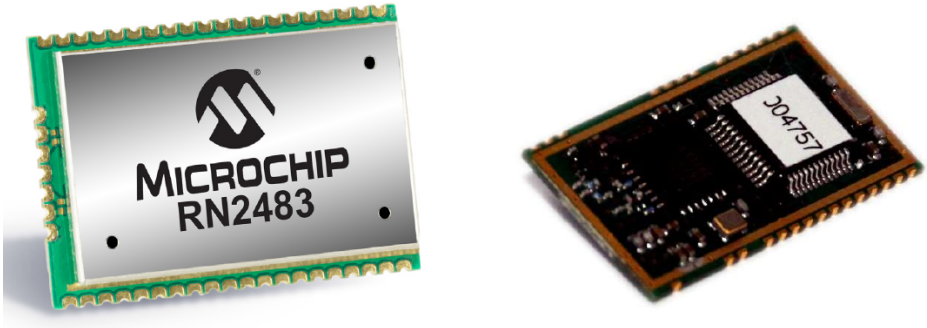

(a) : RN2483. Taken from [41]. **(b) :** MM002. Taken from [42].

Figure 4.15: Pictures of LoRa modules

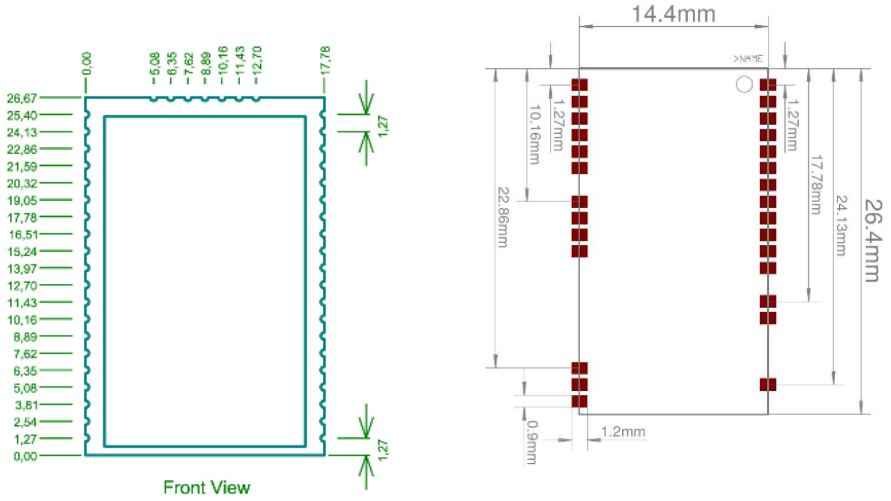

(a) : RN2483. Taken from [41].

(b) : MM002. Taken from [42].

Figure 4.16: Dimensions of LoRa modules

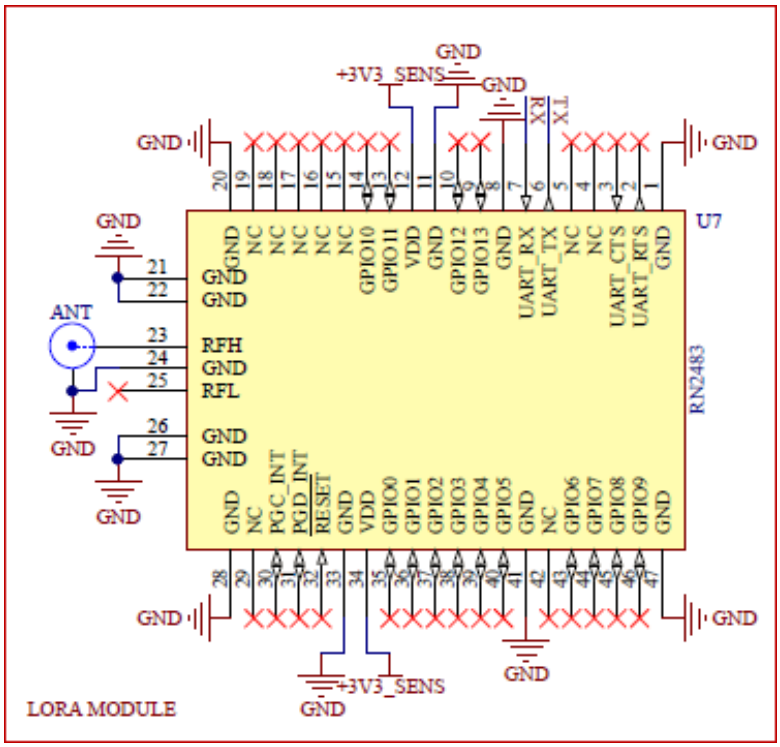

Figure 4.17: Schematic of the LoRa module circuitry, designed in Altium Designer 16

4.1.6 Sensors for the temperature and humidity measurement SHT31

There are two sensors for measurement of the temperature and humidity on the device. One sensor is placed on the top side of the device PCB and is dedicated to measure the ambient temperature and humidity. The second sensor is placed on the bottom side of the device and will be placed in a wood cavity to measure the temperature and humidity of this cavity. The connection between the sensor PCB and the cavity should be airtight so the cavity humidity would not be affected by the ambient humidity. Also, there should be no vias or holes in the area of the cavity.
The SHT31 sensors from Sensirion company were selected for the simple reason of using their predecessors SHT21 at UCEEB for a long time. Hence these sensors are proved precise and stable. The advantage of SHT31 over SHT21 is, among the others, the option to select the last bit of the I^2C address by connecting ADDR pin to the ground or supply voltage.
The accuracy of the sensor SHT31 can be seen in the figure 4.18, in the normal operating conditions of the temperature around 20°C and the relative humidity below 90% is the temperature accuracy better than 0.5% and the relative humidity accuracy is better than 2.5%.
The SHT31 also has built-in heater which can be turned on and off using I^2C command.
There are two major versions of the SHT31 sensor, SHT31-DIS, and SHT31-ARP. SHT31-DIS sensor communicates using digital I^2C protocol, whereas SHT31-ARP employs two DAC converters to communicate with a host MCU. In this sensor design, the digital version SHT31-DIS is used. The typical supply voltage is $V_{CC} = 3.3V$. Its maximal supply current in an idle state is $I_{sup-idle} = 2\mu A$ and its maximal supply current during a measurement is $I_{sup-measure} = 1.5mA$, while the measurement lasts maximally for 15ms. It is clear that this sensor is suitable for low-power application design. The idle supply current is typically lower, $I_{sup-idle_0} = 0.2\mu A$ according to the datasheet, but by simple calculation, its approximate electric charge consumption during a day if the sensor will measure once per day can be found using the formula below:

$$Q_{day} = \frac{(I_{sup-measure} \cdot t_{meas} + I_{sup-idle} \cdot (t_{day} - t_{meas})}{3.6 \cdot 10^9} [mAh] \qquad (4.3)$$

, where $I_{sup-measure}$ and $I_{sup-idle}$ are supply currents described above in microamperes, t_{day} is the duration of a day in milliseconds and t_{meas} is the duration of one measurement in milliseconds. The denominator of the fraction above converts the result from μAms to mAh. By applying this formula I calculated that electrical charge consumed over ten years is from $Q_{10y-min} \approx 17.75mAh$ to $Q_{10y-max} \approx 175mAh$. Please note, that this value is just for a single sensor. Therefore the considered value is double. The lower estimated value isn't much, but the maximal value is a concern because that's

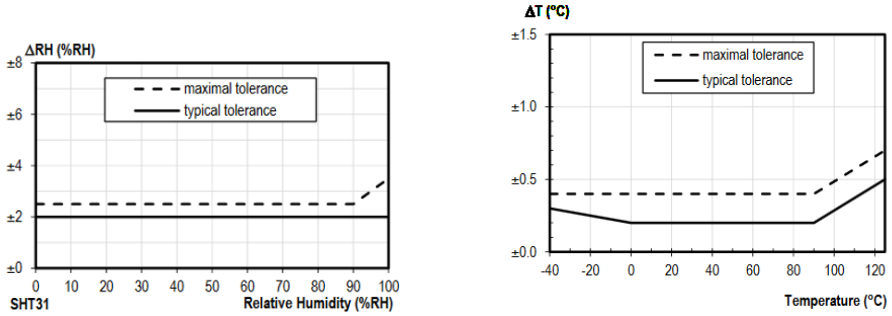

(a) : Relative humidity accuracy **(b) :** Temperature accuracy

Figure 4.18: Relative humidity and temperature accuracy of the SHT31 sensor dependent on the measured value

a significant bit of the charge of the battery, so it was decided to switch off these sensors using a P-MOSFET transistor with the rest of the circuitry. Three versions of the sensor SHT31-DIS are available with just a slight difference: [44]

- **SHT31-DIS-B** - the basic version of the sensor.
- **SHT31-DIS-F** - comes with a filter membrane, which protects the sensor according to the IP67 specification.[45]
- **SHT31-DIS-P** - comes with a protective cover, which protects the sensor during an assembly process. This cover should be removed after the assembly.[46]

In this sensor, the basic version of SHT31-DIS-B is used so far. There is no reason to use the SHT31-DIS-F version of the sensor, since the device will not be IP67 certified, however the use of the SHT31-DIS-P version could be useful in the future to ensure the quality of the device, it would, however, required another process of removing the cover, hence the cost of the device would increase.

The schematic implementation of this solution can be seen in figure 4.21. The sensor on the top layer of the PCB, with the designator U4, has its ADDR pin connected to the ground, and the sensor on the bottom layer of the PCB, with the designator U5, has its ADDR pin connected to the supply voltage. The I^2C addresses of the sensors are 0x44 and 0x45, respectively.

Figure 4.19: The picture of the SHT31-DIS-X sensor. Taken from [43]

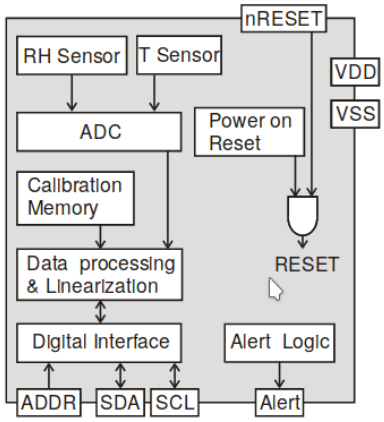

Figure 4.20: The block diagram of the SHT31-DIS-X sensor. Taken from [43]

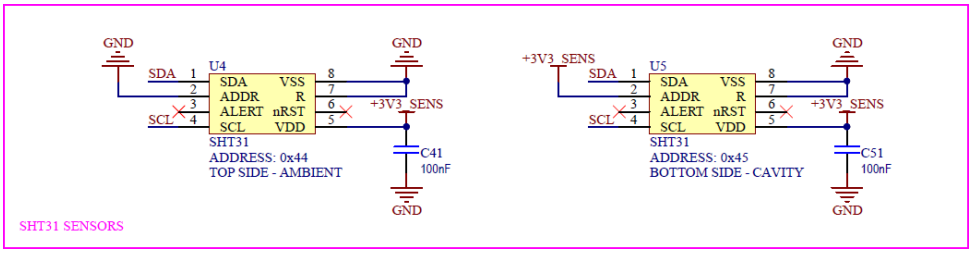

Figure 4.21: Schematic of the SHT31 sensors circuitry, designed in Altium Designer 16

4.1.7 Wood moisture measurement circuitry

Most of the circuitry described bellow was taken from the wired version of the Moisture Guard sensor MHT03485 and wasn't designed by me (just the PCB part was designed by me), but by Aleš Vodička in his diploma thesis and Jan Vyhnánek. Just the voltage inversion part, which needed to by optimized for power consumption, was designed by me. The rest of the circuitry isn't part of this thesis, but it should be described here because it is a part of the device. The block diagram of the measurement hardware can be seen in figure 4.22. The first part of this circuitry is voltage inversion because the second measurement must be taken with an opposite voltage polarity. The next part of the circuitry is excitation circuitry, which is driven by the microcontroller and selects if the excitation voltage is positive or negative. The next part is the integrator circuit, which integrates the current flowing through the measured wood and outputs a voltage ramp. This output enters two comparators, each one with a different threshold voltage. These comparators output logical low or high to the microcontroller GPIOs.

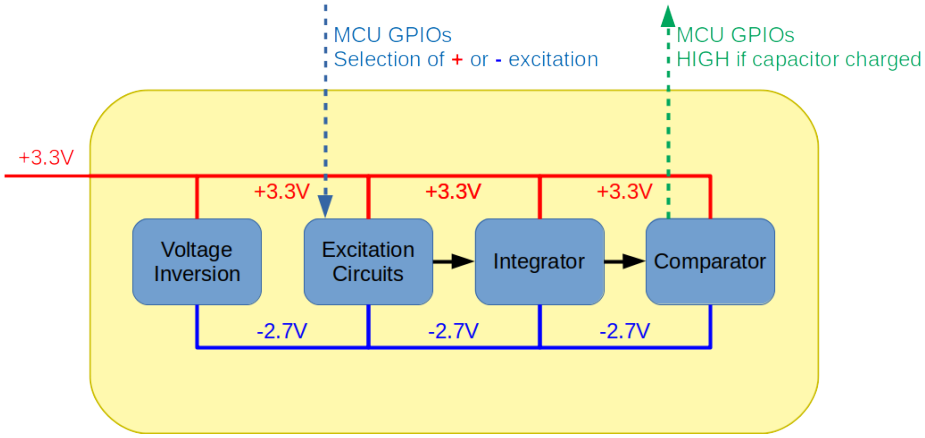

Figure 4.22: Block diagram of the pin-type wood moisture measurement circuitry

Voltage inversion circuits

The inverted voltage needs to be stabilized, so a simple inverting charge pump can not be used. Another integrated circuit to stabilize the voltage would need to be used, and that would increase the total footprint of this circuitry. It was decided to use a DC/DC converter.
To invert the voltage, the inverting DC/DC converter LT1617-1 was used. This DC/DC converter has low quiescent current approximately $I_Q = 20\mu A$, as can be seen in the figure 4.23. The converter will not be under heavy load, so the actual supply current should be similar to the quiescent current.
The converter was set to output the voltage $V_{inv} = -2.7V$, and its layout was designed to take as least space as possible.

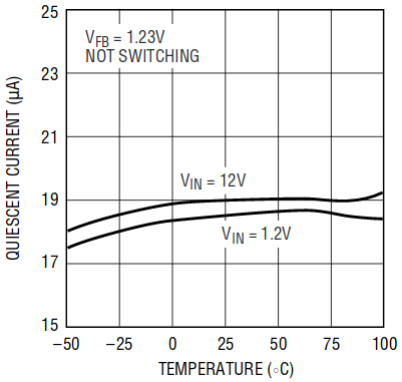

Figure 4.23: Quiescent current of the LT1617-1. Taken from [47]

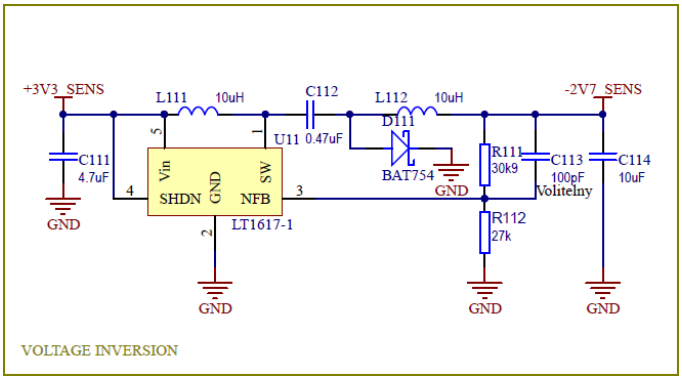

Figure 4.24: Schematic of the voltage inversion circuitry, designed in Altium Designer 16

Excitation Circuitry

The excitation circuitry is used to select whether the excitation voltage will be possitive ($V_{exct} = 3.3V$, or negative $V_{exct} = -2.7V$.
How to drive signals `DRIVE_LO` and `DRIVE_HI` was explained earlier, in the table 4.5.
The supply current of this circuit is negligible.

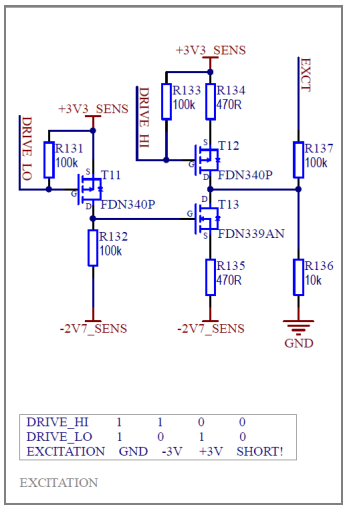

Figure 4.25: Schematic of the excitation circuitry, designed in Altium Designer 16

Measurement circuitry

When the excitation circuitry is set to either positive or negative voltage, the current starts to flow through the measured wood. The JFET `T8` should be closed in order to discharge the `C84` measurement capacitor. By opening the `T8`, the current integration process starts, and the integrator `U8` outputs a voltage slope which is filtered using low pass filter. The input of the comparator is also filtered using a low pass filter. This voltage enters comparators `U9` and `U10`. The comparator `U9` compares the integrated voltage with the positive threshold, the comparator `U10` compares the integrated voltage with the negative threshold. When the integrated voltage reaches the threshold, the relevant comparator drives its output low. This is registered by the microcontroller.
The integrator `U8` IC is MCP6071 high precision rail-to-rail operation amplifier with quiescent current $I_q = 110\mu A$.[48]
The comparators `U9` and `U10` are TL331KDBVR single channel comparators, with the supply current $I_{sup} = 0.7mA$.[49]

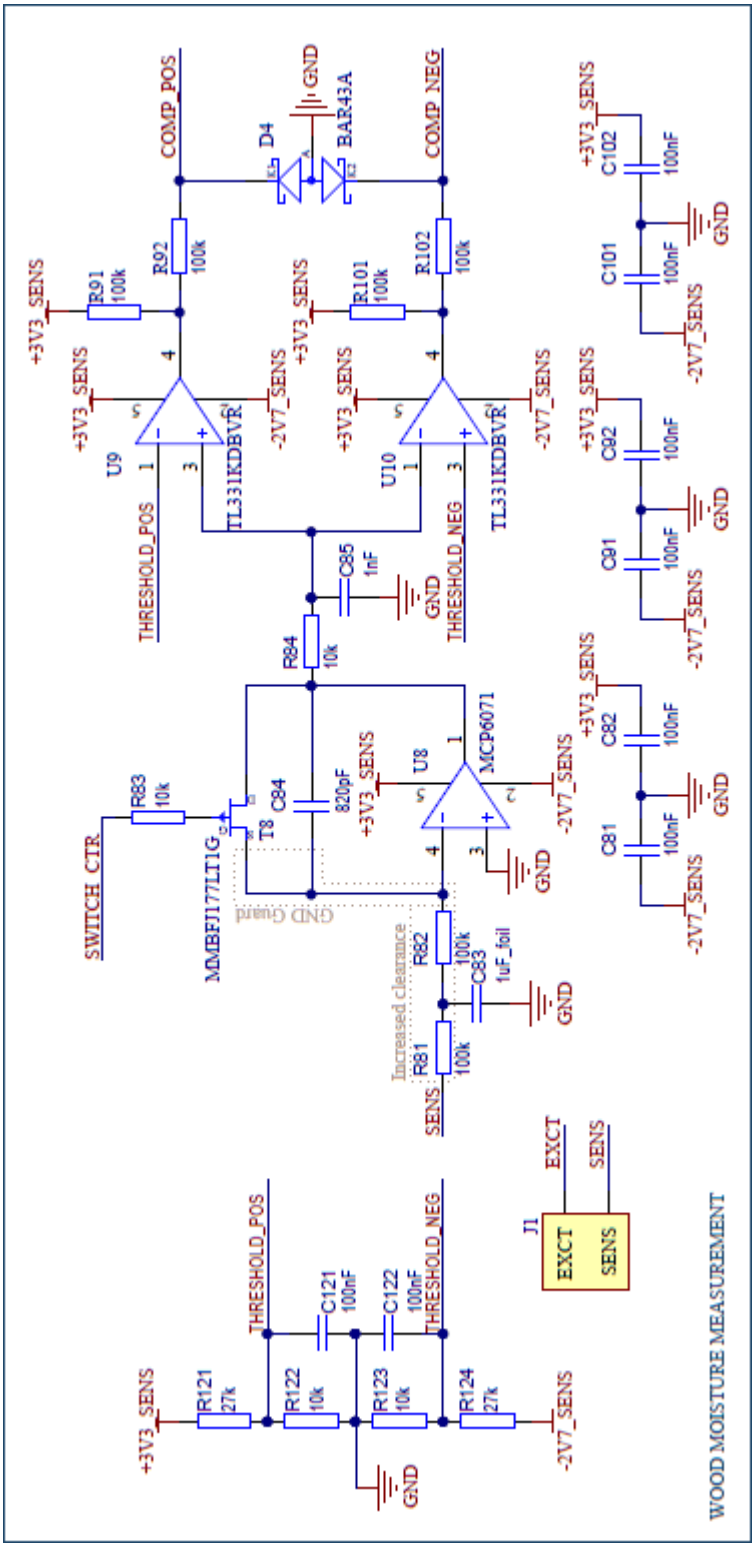

Figure 4.26: Schematic of the measurement circuitry, designed in Altium Designer 16

The measurement circuitry has an issue. The measured output signal for measurement of a $1M\Omega$ resistor can be seen in figure 4.27. The figure contains the output signal for both positive and negative excitation. Both these outputs are different from each other, and moreover, they do not correspond with a reference integrator output, which can be seen in figure 4.28.
The unsuccessful debugging of this issue significantly delayed sensor development and consumed a disproportionate amount of time spent on sensor development.

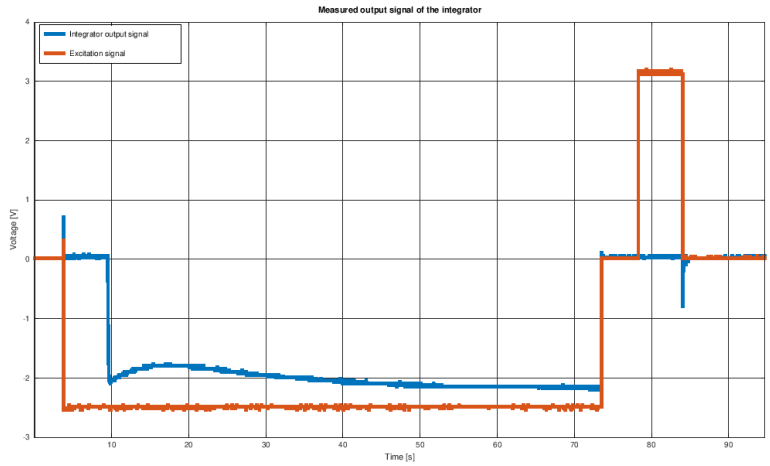

Figure 4.27: Measured output signal of the integrator U8

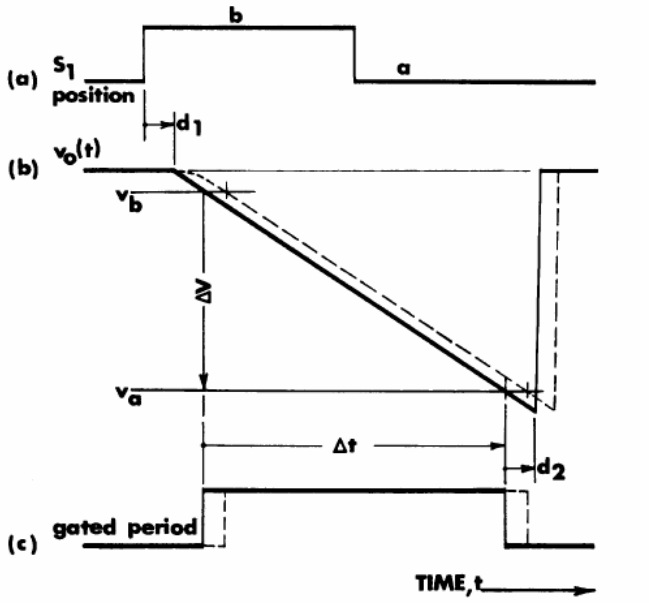

Figure 4.28: An example of the integrator output. Taken from [8].

4.1.8 Power Consumption

Estimated Power Consumption

The power consumption of the sensor is a crucial part of its design. Therefore estimation of the consumption is needed. To process the following data, GNU Octave was used, and the script is provided as an attachment. With minor changes, the script should be MATLAB compatible.
To calculate the electric charge consumed by the sensor and its parts, the running times of these parts in all used modes are required as well as the current consumption during these modes.
The supply currents of the sensor parts can be seen in the table 4.8, the running time of these parts are listed in the table 4.9.

Sensor Part	**Mode**	$\mathbf{I_{sup}}[mA]$
MAX17222	I_Q	0.6
PIC	Sleep	0.0009
PIC	Run	1
TR76	Run	3
TR76	TX	21
SHT31	Measurement	1.5
SHT31	Idle	0.002
LT1617-1	I_Q	0.03
MCP6071	I_Q	0.17
TL331	Run	0.7

Table 4.8: Current consumptions of the sensor parts

The step-up DC/DC convertor MAX17222 datasheet provides only quiescent current I_Q, so this current was multiplied by 10 in the calculation.
The PIC microcontroller has several sleep modes. However, the sleep mode with internal watchdog had to be used, because there is no external circuitry to wake the microcontroller up. The supply current of the PIC microcontroller in running mode varies, depending on the clock speed and used peripherals. In this calculation, 4MHz clock speed was used, but it is likely a lower speed will be used.
The IQRF module TR76D has more RX and TX mode, for this calculation, the standard mode was used, as well as the highest transmission power.
Inverting DC/DC convertor LT1617-1 datasheet provided only the quiescent current I_Q, as well as the operating amplifier MCP6071 datasheet. The load on these circuits will be small, so these currents were multiplied by 10 in the calculation.

The supply current of the TL331 is provided in its datasheet.

Sensor Part	Mode	$\mathbf{t_{run}}[s]$
MAX17222	I_Q	175
PIC	Wakeup	0.0002
PIC	Wait for TX done	5
PIC	Run	175
TR76	Wait for DPA	50
TR76	TX	0.038
TR76	Run	50.038
SHT31	Measurement	0.015
SHT31	Startup	0.001
SHT31	Idle	119.985
LT1617-1	I_Q	120
MCP6071	I_Q	120
TL331	Run	120

Table 4.9: Running times of the sensor parts during a measurement and/or transmission

The total time of SHT31 sensors running was calculated as:

$$T_{SHT31} = T_{SHT31-Startup} + cdotT_{SHT31-Measurement} + T_{SHT31-Idle}[s] \quad (4.4)$$

The total time is largely dependent on the wood resistance measurement since that takes the most time from the measurement. In the worst-case scenario, it is approximately 120 seconds. During this time, all Integrated circuits, but TR76D, are running, so their running times are equal to the time of the moisture resistance:

$$T_{Analog} = T_{SHT31} = T_{LT1617-1} = T_{MCP6071} = T_{TL331}[s] \quad (4.5)$$

The message transmission takes only a fraction of the total running time, the TR76D is waiting for DPA Commands for the most of the time. Running time of the IQRF module TR76D can be calculated using the equation below:

$$T_{TR76-Run} = T_{TR76-WaitforDPA} + T_{TR76-TX}[s] \quad (4.6)$$

The $T_{TR76-TX} = 38ms$ is the transmission time for a message with 64B payload, according to the IQRF OS User's Guide [15]. If a message is sent after each measurement, the payload is smaller, decreasing the transmission time.
The TR76D waiting time is determined by the duty cycle of the 868MHz ISM band, which is 1%, and payload of the DPA commands. Two DPA commands are needed to read the data, both with a payload of 1B, according to the IQRF OS User's Guide [15], the message propagation time is 11 ms. The time between two transmissions should be at least 100 times the message

propagation time. The total waiting time for the transmission is calculated as follows:

$$T_{TR76-WaitforDPA} = N \cdot 100 \cdot 2 \cdot 0.011[s] \tag{4.7}$$

, where N is the number of nodes in the network, which will be circa ten nodes, note that the waiting time $T_{TR76-WaitforDPA}$ is the worst-case scenario waiting time, when the sensor enable TR76D IQRF module just after the coordinator sent a DPA command for this module.

$$T_{PIC-Run} = T_{PIC-wakeup} + T_{Analog} + T_{TR76-Run} + T_{PIC-waitforTXdone}[s] \tag{4.8}$$

, $T_{PIC-waitforTXdone}$ is set to $T_{PIC-waitforTXdone} = 5s$, but can be decreased. Some delay between a message transmission and going back to sleep, because the TR76D module needs few milliseconds to process and transmit the message.
The total sleep time of the PIC microcontroller $T_{PIC-Sleep}$ can be calculated as follows:

$$T_{PIC-Sleep} = 24\ cdot3600 - M \cdot T_{PIC-Run} \tag{4.9}$$

The estimated supply curernt profile of one measurement cycle with a message transmittion can be seen in the figure 4.29.

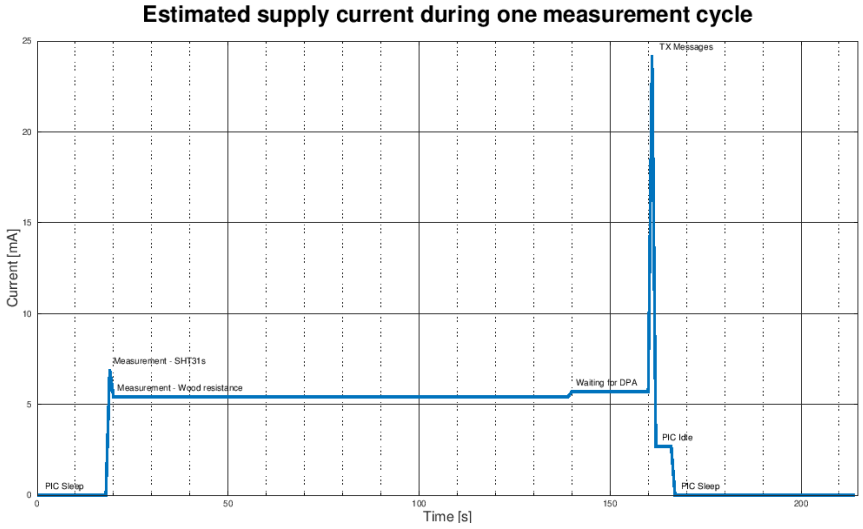

Figure 4.29: Estimated supply current profile during one measurement cycle with a transmission

The consumed electric charge by parts of the sensor can be seen in the table 4.10 bellow.

Sensor Part	$\mathbf{Q_{cycle}}[mAh]$
Total	0.225968
PIC	0.110265
TR76D	0.018453
SHT31s	0.000146
Analog circuitry	0.090241
MAX17222	0.006000

Table 4.10: The electric charge consumed during one measurement cycle with a transmission

The PIC consumption per measurement with a transmission was calculated using the formula below:

$$Q_{PIC} = \frac{I_{PIC-Run} \cdot t_{PIC-Run}}{3600}[mAh] \tag{4.10}$$

The consumptions of other parts were calculated accordingly, in the case only quiescent current I_Q was known, a value five times higher was used. Since any of those components will not be under heavy load, it is safe to use this approximation. The total electric charge consumed is the sum of all electric charges consumed by all sensors parts.
To estimate the battery's lifetime, the following formulas were used:

$$T_{bat} = \frac{Q_{bat}}{Q_year} \tag{4.11}$$

$$Q_{year} = 365 \cdot \frac{((M \cdot \sum Q_{cycle_i}) + T_{PIC-Sleep} \cdot (I_{PIC-Sleep} + I_{MAX17222}))}{3600} + 0.01 \cdot Q_{bat} \tag{4.12}$$

, where M is number of measurements in one day, Q_{cycle_i} are values from the table 4.10, excluding the total value, and $0.01 \cdot Q_{bat}$ is the annual self discharge of the battery. $Q_{bat} = 3600mAh$ is the nominal electrical charge of the battery, the battery has the annual discharge rate 1%.
Daily consumption and battery lifetime for several seting can be seen in the table 4.11.

Measurements a day M	$\mathbf{Q_{day}}[mAh]$	**Battery lifetime** [year]
24	5.423237	1.785
12	2.794419	3.407
6	1.480009	6.243
3	0.822805	10.697
2	0.603736	14.034
1	0.384668	20.397

Table 4.11: The electric charge consumed during one day and predicted battery lifetime with a transmission after every measurement and predicted battery lifetime

One part of the sensor, which can be optimized more is the TR76D IQRF module. From figure 4.29 is visible, that the sensor spends not insignificant time waiting for a DPA Command. This could be optimized by storing the data in the sensor's memory and send them once a day, reducing the total amount of waiting time. This means the electric charge consumed would be lowered not only by the part consumed by the IQRF module TR76D but also by a part consumed by the PIC microcontroller while waiting for an incoming UART command received by the IQRF module via DPA Command.
Since the maximum payload size of an IQRF DPA Response is 56B and the payload of one message sent by the sensor is 16B, the module must send $K = \frac{M}{3}$ messages. For measurement every hour $K = 8$.
The current consumption, in this case, can be seen in figure 4.30.
The electric charge consumptions of the sensor parts per day can be seen in the table 4.12. The coordinator must wait between DPA commands $t_{wait} = 100 \cdot 11ms = 1.1s$, to ensure compliancy with the 868MHz ISM Band. This waiting time is much smaller in comparison with the waiting time for the first DPA command.
Note, that the value of electric charge consumed by TR76D is the total daily value distributed to each measurement cycle, for the case of 24 measurements a day, that means this value represents $\frac{1}{24}$ of the one period when TR76D is active. This was done for illustrative reasons, to represent the difference more easily.
Daily consumption and battery lifetime for several settings can be seen in the table 4.14. Comparison of daily electric charge consumptions can be seen in the figure 4.31.

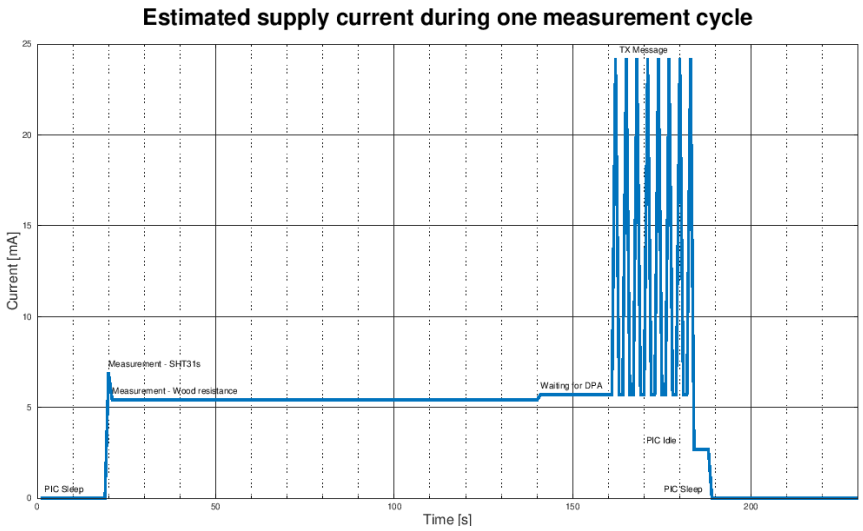

Figure 4.30: Estimated supply current profile during one measurement cycle with a transmission of eight packets

Sensor Part	$\mathbf{Q_{cycle}}[mAh]$
Total	0.198131
PIC	0.099750
TR76D	See the table 4.13
SHT31s	0.000146
Analog circuitry	0.090241
MAX17222	0.006000

Table 4.12: The electric charge consumed during one measurement cycle with a transmission once a day.

Measurements a day M	$\mathbf{Q_{cycle}}[mAh]$	
	TX once a day	TX after every measurement
24	0.027042	0.442867
12	0.022801	0.221433
6	0.020681	0.110717
3	0.019621	0.055358
2	0.019267	0.036906
1	0.018453	0.018453

Table 4.13: Daily consumption of the IQRF Module TR76D

By comparing the tables 4.10 with 4.12 and 4.11 with 4.14, it is clear, that this solution increased battery lifetime mainly in the cases of 3 and 6 and 12 measurements a day, and was not significant in extreme cases of 1 and 24 measurements a day.
This is caused by different reasons for both cases. In the case of 1 measurement a day, the transmitting process is the same. Therefore there is nothing to improve, and the electric charge consumption is the same. The electric charge consumed by TR76D is not significant enough compared to the electric charge consumed by other parts of the sensor, so the difference is smaller.
For optimal performance, a number of measurements per day should be between 3 and 6. The battery lifespan guaranteed by the manufacturer is ten years, so there is no need to try to optimize the sensor to last infinitely.

Measurements a day M	$\mathbf{Q_{day}}[mAh]$	**Battery lifetime** [year]
24	4.755137	2.031
12	2.458248	3.855
6	1.311394	6.990
3	0.738364	11.777
2	0.547413	15.258
1	0.384668	20.397

Table 4.14: The electric charge consumed during one day and predicted battery lifetime with a transmission once a day.

The daily electric charge consumption of the sensor and its parts can be seen in the figures 4.31 and 4.32. It is clearly visible, how the ratio of charge consumed by TR76D while sending a message after each measurement to charge consumed by TR76D while sending the data once a day dropped for six measurements a day in comparison with 24 measurements a day.
It is also visible that the most charge is consumed by the PIC microcontroller, which is the only running component of the sensor, along with step-up DC/DC converter MAX17222, whose consumption is negligible in comparison of the PIC microcontroller.
The analog circuitry for the wood resistance measurement consumes circa 40% of what the PIC microcontroller does.
The charge consumption of SHT31 sensors is negligible.

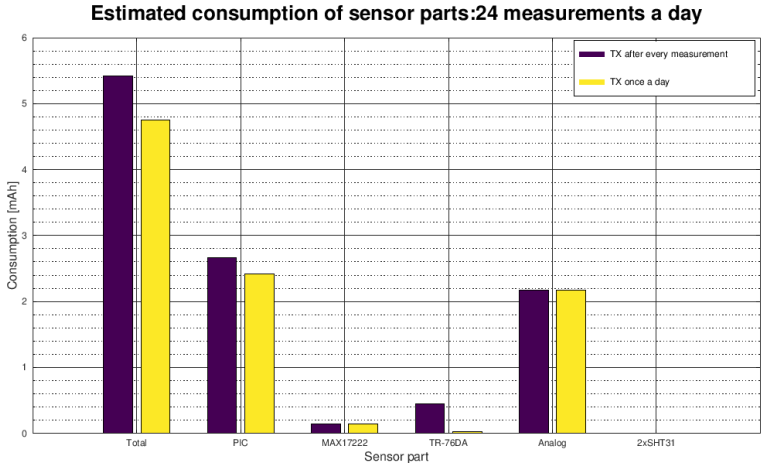

Figure 4.31: Bar graph of total electric charge consumed during one day by the sensor and its parts - comparison of sending a packet after every measurement and as eight packets in a row once a day. 24 measurements a day.

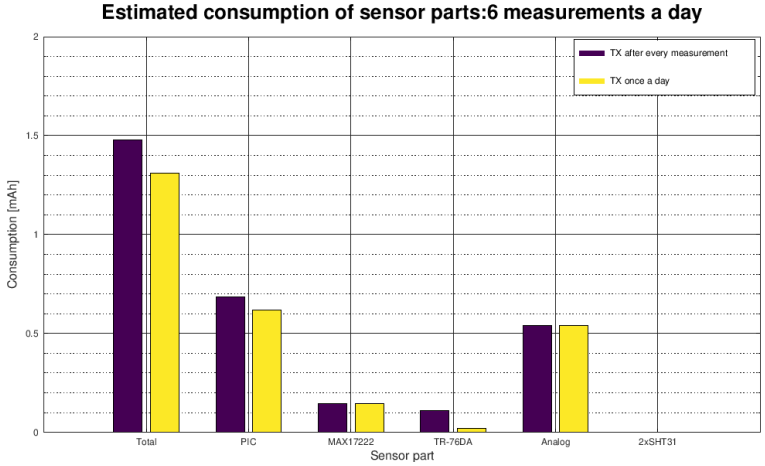

Figure 4.32: Bar graph of total electric charge consumed during one day by the sensor and its parts - comparison of sending a packet after every measurement and as two packets in a row once a day. 6 measurements a day.

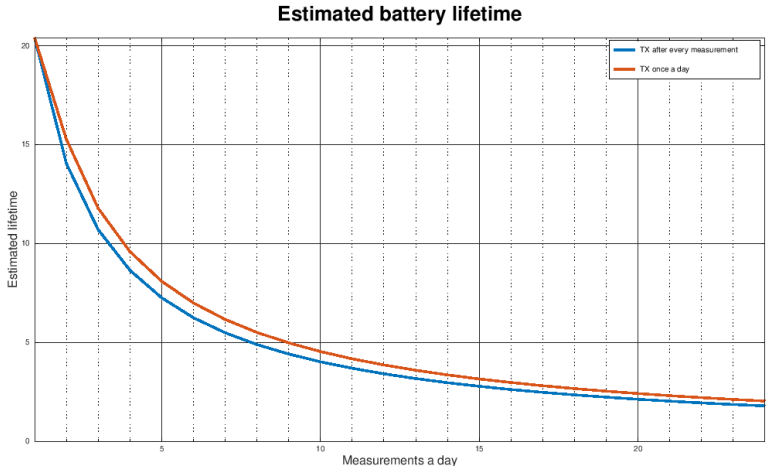

Figure 4.33: The dependence of the battery life on number of measurements a day.

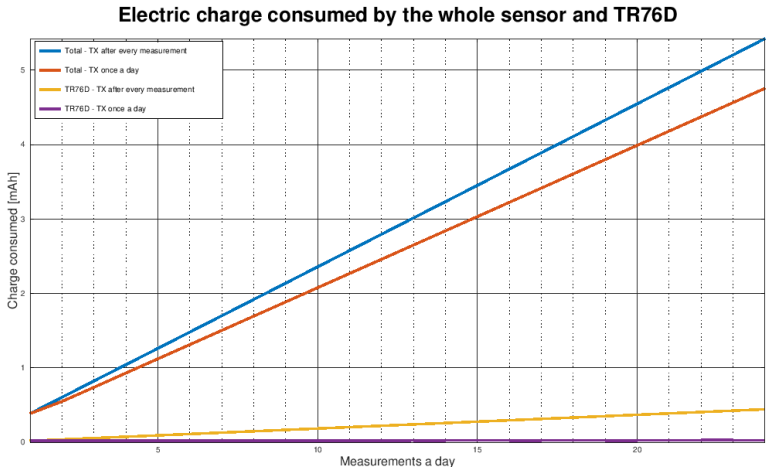

Figure 4.34: Comparison of total electric charge consumption by the whole sensor and just the TR76D IQRF module, dependent on the number of measurements a day

Because the resistance measurement reacts slowly to changes and consumes quite a lot of energy, its operation should be optimized.
The cavity measurement using SHT31 sensor reacts quickly to changes in the wood moisture content changes, and consumes a negligible amount of energy. To take advantage of this knowledge, the resistance moisture measurement can be made less frequently than the cavity humidity measurement.
It can be seen from tables 4.11 and 4.14, that the battery lifetime exceeds ten years in cases of one to three measurements a day, both for transmission after each measurement and transmission once a day.
To ensure the battery lifetime at least ten years, maximally two wood resistance measurement should be taken a day.

The cavity humidity measurement consumes a fraction of the energy. Therefore, it can be taken more often, assuming the transmission will follow only the wood resistance measurement or will be done only in the case of an emergency alert.
The electric charge consumed daily was calculated for resistance measurement once and twice a day, with an additional N cavity humidity measurements a day.
The calculated daily electric charge consumed in a day, and the battery lifetime, can be seen in tables 4.15 and 4.16. Table 4.15 contains the calculated data for two resistive measurements a day in dependence whether a transmission is done once a day, or after every resistive measurement. Table 4.16 contains the calculated data for one resistive measurement a day with a transmission after the measurement.

By comparing the data from these tables with the relevant data from tables 4.11 and 4.14, once can see, that the difference in the battery lifetime is marginal, less than 1%.
It can be assumed, that all configurations presented in tables 4.15 and 4.16 are suitable, and it is feasible to measure the wood moisture often and still achieve the battery lifetime more than ten years.
The consumption of the cavity humidity measurement could be even more optimized by separating its power rail from the power rail of the wood resistance measurement.

Another way how to reduce the current consumption of the sensor could be to terminate the wood resistance measurement after a set time threshold. The main goal of the sensor is to alert the user in case of increased moisture, so there the only point of completing the measurement is to have historical data. Dry wood has a higher resistance than wet wood, and it takes more time to measure dry wood than wet wood, so this could save energy, depending

on how the threshold would be set. The threshold value would need to be determined experimentally.

N	Q_{day} $[mAh]$		Battery Lifetime $[year]$	
	TX once a day	TX twice a day	TX once a day	TX twice a day
4	0.5533	0.6096	15.120	13.917
3	0.5518	0.6082	15.154	13.946
2	0.5504	0.6067	15.189	13.976
1	0.5489	0.6052	15.223	14.005

Table 4.15: Estimated daily charge consumptions and battery lifetimes for wood resistance twice a day and N wood cavity moisture a day with transmission once a day, and twice a day.

N	Q_{day} $[mAh]$	Battery Lifetime $[year]$
4	0.3906	20.151
3	0.3891	20.212
2	0.3876	20.273
1	0.3861	20.335

Table 4.16: Estimated daily charge consumptions and battery lifetimes for wood resistance once a day and N wood cavity moisture a day.

Measured Power Consumption

The current consumption of the sensor was measured using benchtop multimeter UNI-T UT803 connected in series with the sensor, as seen in figure 4.35.
There is also a 100Ω resistor soldered on place of the solderbridge SB1, so the current can be measured as a voltage drop on this resistor. There are test points on both sides of the solderbridge, TP1 and TP2, to attach probes of a voltmeter or an oscilloscope to record the current consumption profile. The schematic can be seen in the figure 4.36.

Because the device is not fully functional yet, the supply current of only a few configurations could have been measured.
The measured idle current consumption of the PIC Microcontroler and MAX17222 step-up inverter is $I_{Idle} \approx 0.5mA$ in total at 31kHz, and $I_{Idle} \approx 1.76mA$ at 4Mhz
The measured sensor current consumption with the measurement parts powered up is $I_{Meas} \approx 5.5mA$.
The measured sensor current consumption with TR76D module powered up is $I_{Meas} \approx 13.25mA$.
The measured sleep current consumption is $I_{Sleep} \approx 85\mu A$. The measured supply current can be seen in table 4.17.

Mode	$I_{sup}\,[mA]$
I_{Idle} at 4MHz	1.76
I_{Idle} at 31kHz	0.5
I_{meas}	5.5
I_{TR76_on}	13.25
I_{sleep}	0.085

Table 4.17: Measured supply current of the device in different modes.

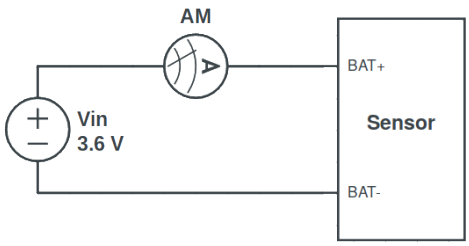

Figure 4.35: The measurement circuit to measure the current consumption of the sensor using an ampermeter.

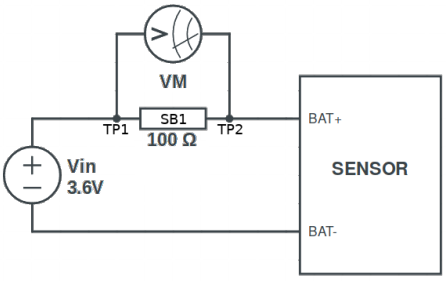

Figure 4.36: The measurement circuit to measure the current consumption of the sensor using an oscilloscope.

4.1.9 PCB Design of the sensor

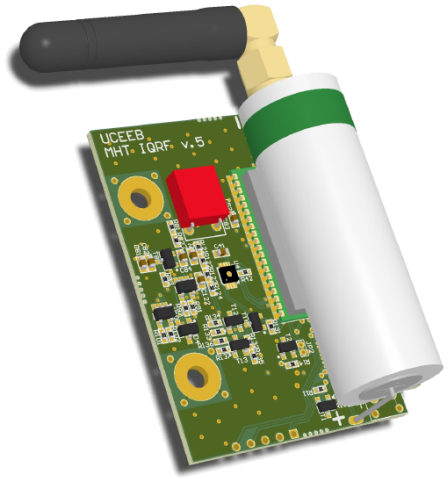

Figure 4.37: The 3D model of the device PCB

The Altium Designer 16 was used to design the device. Multiple footprints and parts libraries were created. In order to make a PCB design and assembly easier, the way how to use mechanical layers while designing a footprint was standardized as follows:

- **Mechanical 1 - 3D Models** : It is preferred each footprint has accurate and nice 3D models. Accurate for mechanical assembly, and nice for 3D preview.
- **Mechanical 3 - Via Keep out** : Some parts, especially communication modules, have areas, where should not be any vias, pads, or other unmasked copper. Mark these areas in this layer, if possible.
- **Mechanical 12 - Connectors Outline** : The outline of the footprint of connectors. This outline should contain the whole footprint, for most footprints a rectangular box is suitable. The outline should be 0.1mm thick. There should be a special string ".Designator" in the center of the outline, in suitable font size. Do not mark pin numbers, just indicate the first pin. Marking of pins should be done manually in the PCB editor, and it should contain the signal name.
- **Mechanical 13 - Assembly Outline** : The outline of the footprint for assembly drawing. This outline should contain the whole footprint, for most footprints a rectangular box is suitable. The outline should be 0.1mm thick. There should be a special string ".Designator" in the center of the outline, in suitable font size. The first pin of parts should

be marked with a circle with the radius of 0.5mm and line width 0.1mm (this can be adjusted accordingly to the size of the footprint). Do not add the outline of connectors to this layer, if one wants to include Connectors into the final Assembly Drawing, one can add Mechanical 12 to the printout, or create the outline manually.

- **Mechanical 14 - Reserved for Assembly Bottom** : In the PCB editor, use this layer as the pair layer for Mechanical 13, so an assembly drawing can be produced for both sides of the PCB.
- **Mechanical 15 - Centers** : This layer should contain the outline of the part, the thickness of the outline should be 0.5mm. More importantly, it should contain the center (of mass) of the part. The center should be a cross 1x1mm and 0.1mm thick.

The PCB itself is a four layer PCB with signal layer on the top and bottom layer. The inner layers serve as ground and supply planes, which not only makes the routing of the PCB easier but more importantly ensures better Electromagnetic Compatibility.

While designing the PCB layout of the voltage regulators, a focus was taken mainly on the MAX17222 step-up DC/DC converter, because it was used in the vast majority of the devices. The general rule to layout its circuitry is to keep traces as short as possible, especially the trace of RSEL pin, in order to avoid producing capacitance. Since this step-up converter uses just five passive components, the PCB design was quite straightforward, this regulator is placed mostly on the top layer of the device, with only the inductor on the bottom layer of the device.

The second voltage regulator, the RT8299A step-down DC/DC converter, has its PCB layout well described in its datasheet[33].These voltage regulators were placed close to each other, in the very top right corner of the PCB, in order to be as far as possible from the analog circuitry.

The PIC microcontroller was placed on the top layer of the device, just opposite of the RT8299A regulator. Now all the major heat sources are in one place, far enough from the analog circuitry.
The communication modules are placed on the top edge of the board too so that they would be far from the analog circuitry.
Unfortunately, these modules can't fit over each other on the same layer, so the LoRa module RN2483 was placed on the top side of the PCB, and the IQRF module TR76-D on the bottom side of the PCB. It is vital to avoid vias, pads or other unmasked copper under these modules because it could cause a short-circuit and ultimately the malfunctioning of the device. These short circuits can be caused by vias and testpoints on the bottom side of the RN2483 LoRa module, which are not described in the datasheet of the module. The

IQRF module TR-76D has pads for a SIM connector. Fortunately, these are precisely described in the module datasheet so that they can be avoided easily.

The antenna trace should not go through the board using via, so each module has its own antenna trace. The antenna will be mounted using edge soldered SMA connector. In order to have the antenna connector on the same place for both variants of the device, a footprint with pads for connecting the antenna pin on both layers of the PCB was created. The one which will not be used should be grounded by soldering this pad to the adjacent pads which are grounded.

The next part of the PCB is the SHT31 sensors. They should be placed in the middle of the x-axis of the PCB, U4 on the top side of the PCB, and U5 on the bottom side of the PCB. The bottom one will be placed in the wood cavity, and it is crucial no vias would be in a 6mm radius, to ensure the cavity to be airtight. Attention should be paid to the parts in the close proximity of this radius, so they would not interfere with the box.

The analog circuitry is sensitive to heat, so these parts were placed as far as possible from the microcontroller, voltage regulators and communication modules. To achieve this, it was decided to place them between holes for measurement electrodes, but this decision demanded to use smaller packages of parts, so resistors in the 0402 package and capacitors in the 0603 package were used. To minimize the number of reels used by a pick-and-place machine, these packages were used in the whole design.

The distance from the heat source is not the only thing to consider while designing sensitive analog operation amplifier circuits, the orientation of the passive components to the heat source also matters. If the junction of a passive component, for example, a resistor, have different temperatures, a thermoelectric voltage is generated. This voltage can affect the measurement. To minimize this thermoelectric voltage, several steps can be taken:

- Adding a heat sink and/or a fan
- Thermal insulation of the sensitive circuitry
- Maximizing the distance between the sensitive circuitry and the heat source(s)

Adding a heat sink or a fan is not an option for this device, because it would increase its dimensions even more, which is undesirable. Simple thermal insulation of the device could be done by creating an area without any copper between the sensitive analog circuitry and the rest of the device, however using a drilled slot between these parts is not acceptable, because this would

weaken the mechanical integrity of the board, therefore the only option is to split up the copper between these parts and join signals in one point. This would be hazardous considering the Electromagnetic Compatibility. The communication modules will be switched off for the most of the time, the microcontroller will be in low-power mode for most of its lifespan and the voltage regulator (only one will be assembled at a time) would not be loaded heavily, so it should not produce so much heat, so it was decided not to cut the copper planes, and I left them in one piece to ensure better Electromagnetic Compatibility.

To minimize a thermoelectric voltage using PCB design all the passive components were placed in parallel to thermal contour lines, as seen in the figure 4.38. Because the analog circuitry is far enough from the heat sources, the thermal contour lines should be straight enough to use this technique.[50]

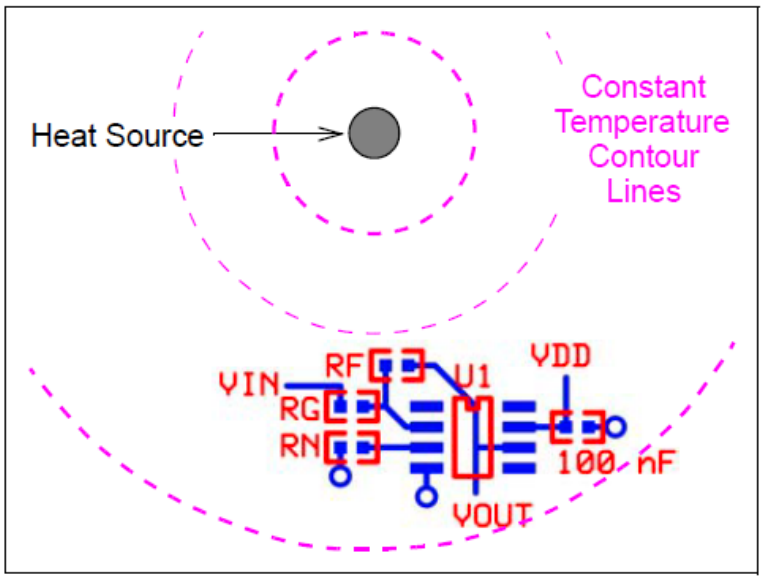

Figure 4.38: Resistors aligned with contour lines. [50]

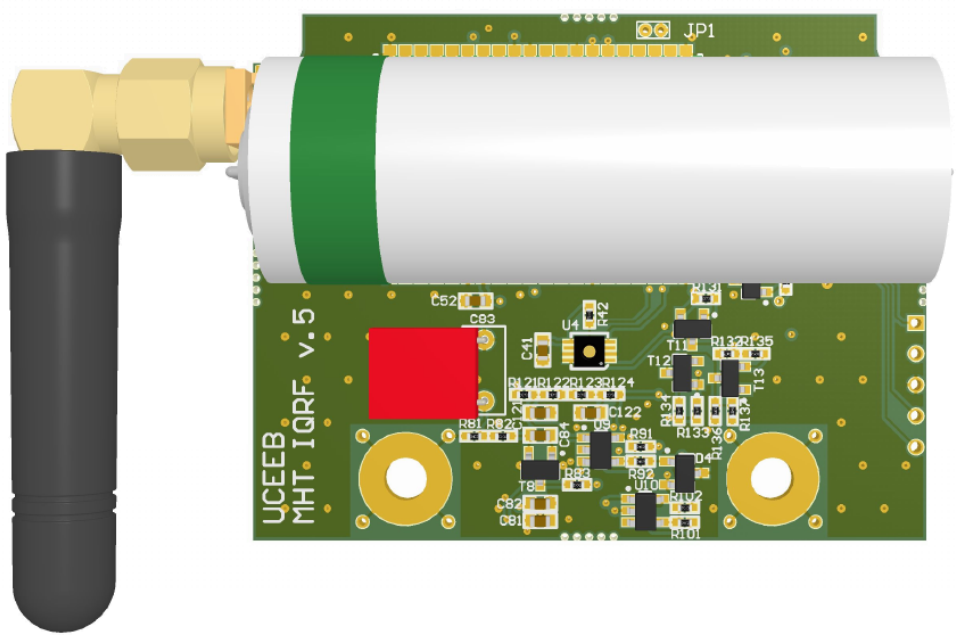

Figure 4.39: 3D Model - Top Side

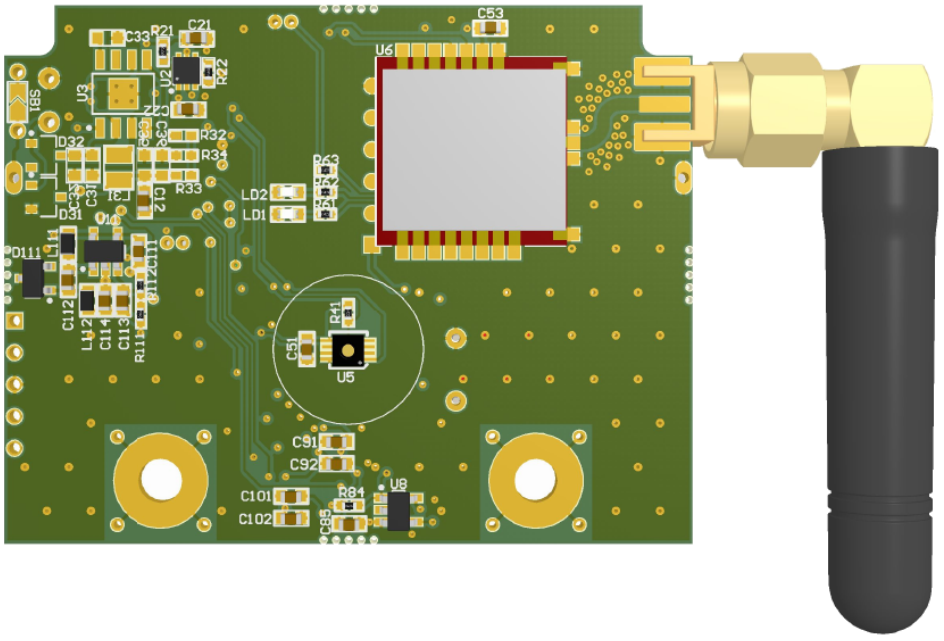

Figure 4.40: 3D Model - Bottom Side

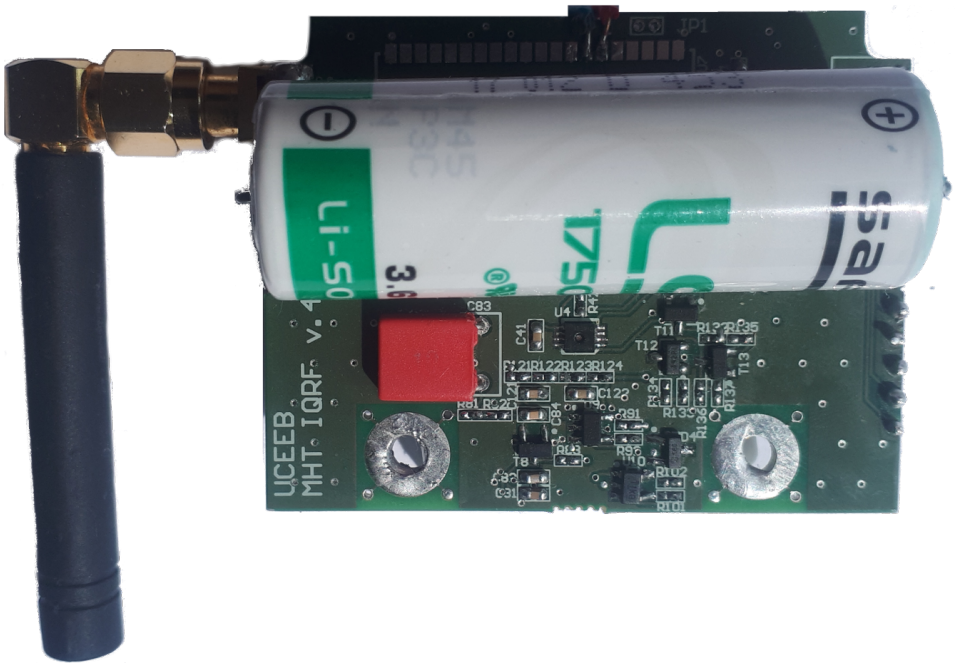

Figure 4.41: Photo of the sensor - Top side

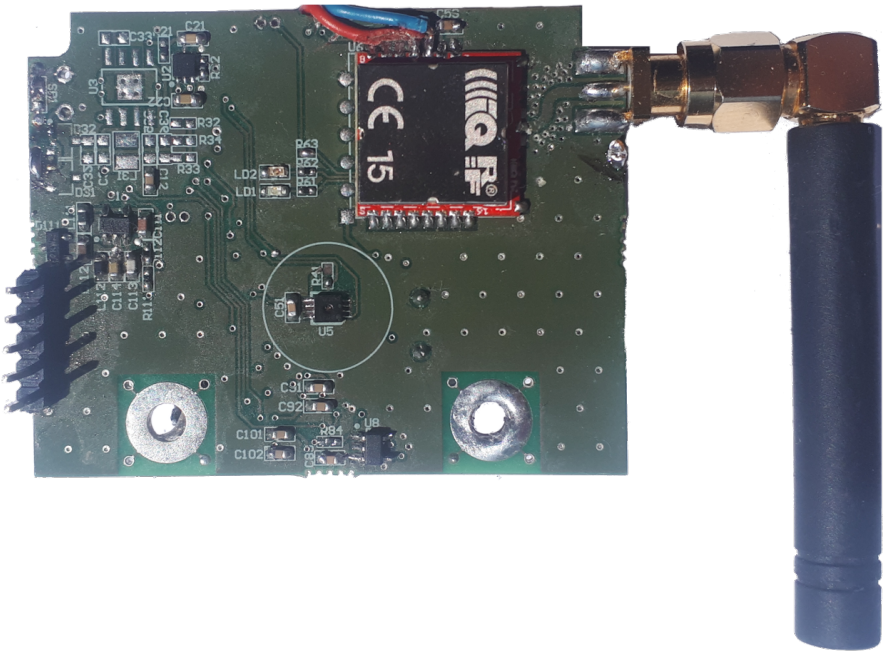

Figure 4.42: Photo of the sensor - Bottom side

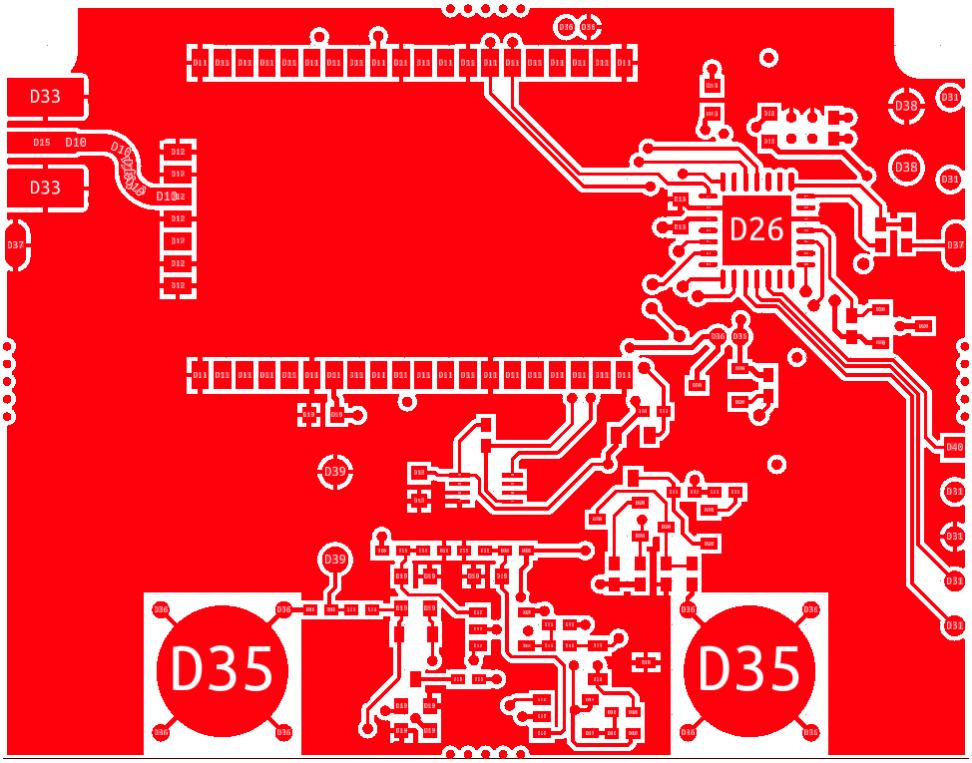

Figure 4.43: Gerbers - Top Layer

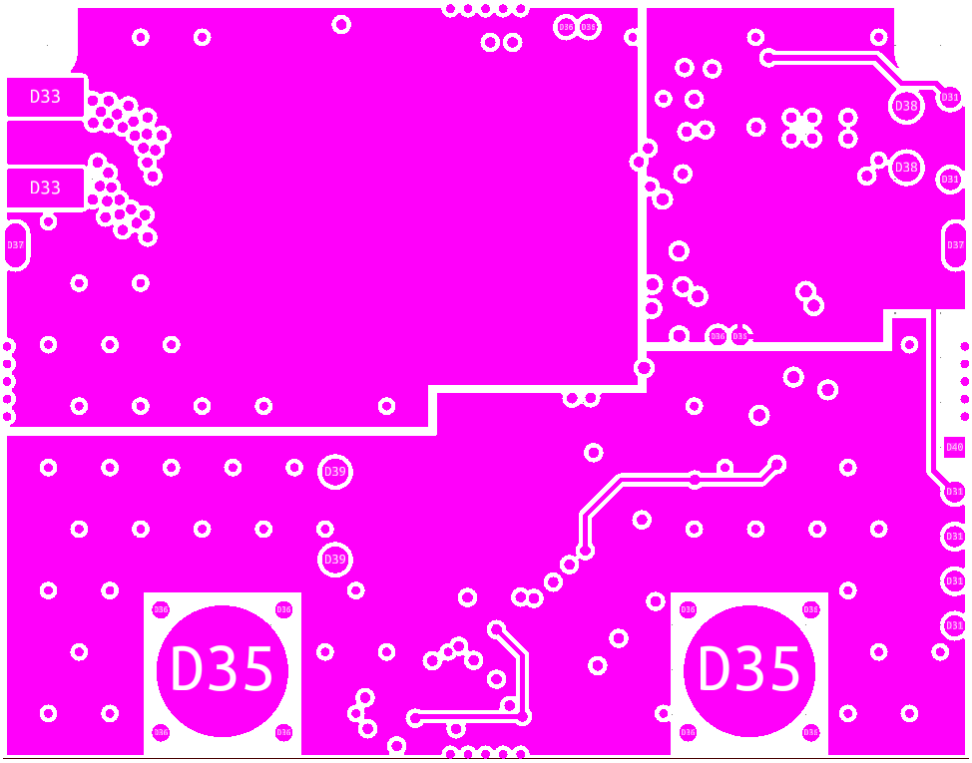

Figure 4.44: Gerbers - VCC Layer

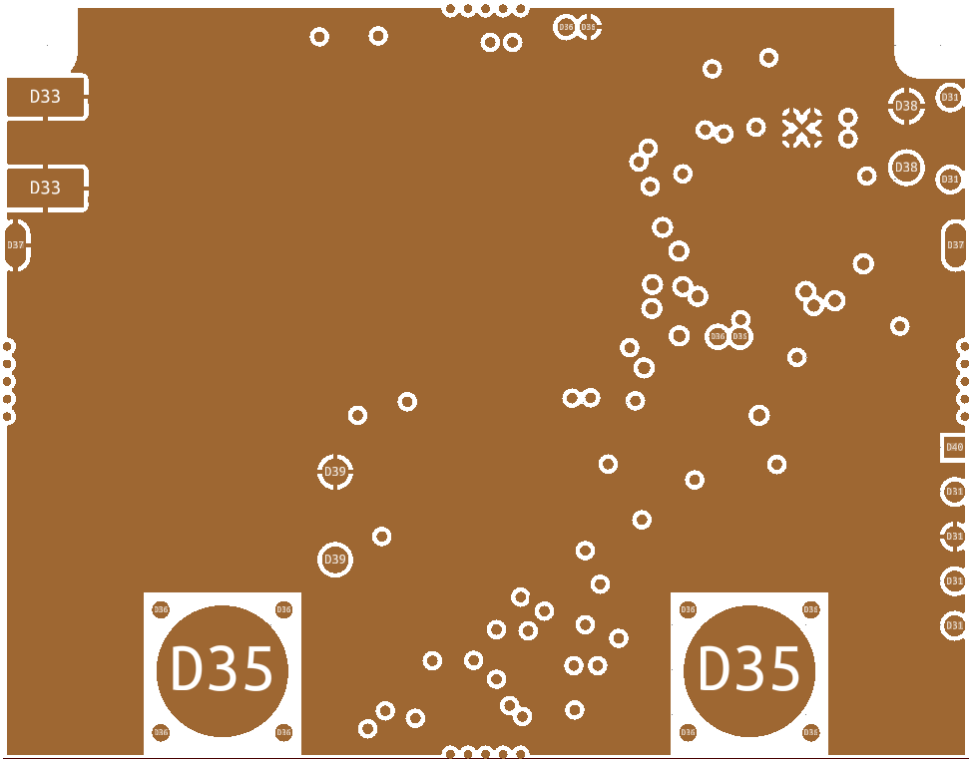

Figure 4.45: Gerbers - GND Layer

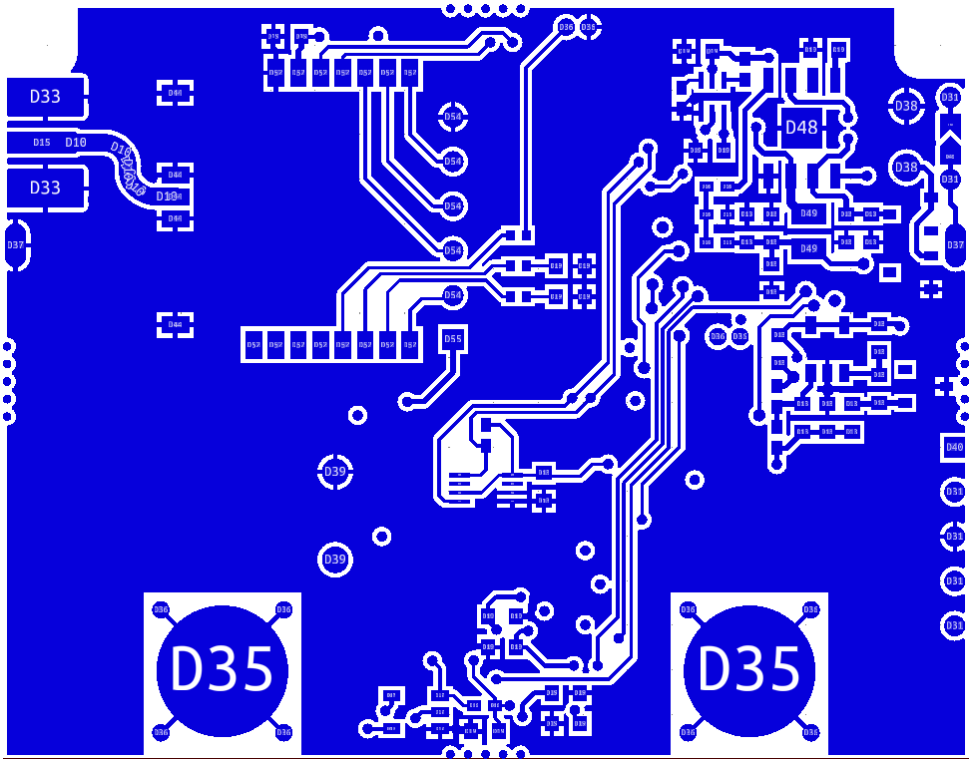

Figure 4.46: Gerbers - Bottom Layer

4.1.10 Sensor Enclosure

The enclosure was designed by Aleš Vodička using SolidWorks software.
The box consists of four parts: The top cover, the inner cover, the bottom cover and a basket for insertion to the cavity.
The main part of the enclosure consists of the top and bottom cover, which are the outer, visible part of the enclosure. The inner cover is inside, and covers the PCB, except for the battery and holes for the screw-type electrodes.
The last part of the enclosure is the basket, which will be inside of the cavity drilled into the wood sample.
The 3D model of the enclosure parts can be seen in figure 4.48. The mounting of the sensor to a wood sample is done using four screws. Two screws go through the PCB and are hidden inside of the box. These screws serve as the electrodes for the wood moisture measurement. Two remaining screws hold the top and the bottom covers together, and are mounted to the wood sample to prevent tilting of the sensor.

The sensor in the enclosure can be seen in figure 4.47.

Figure 4.47: Photo of the sensor in the enclosure

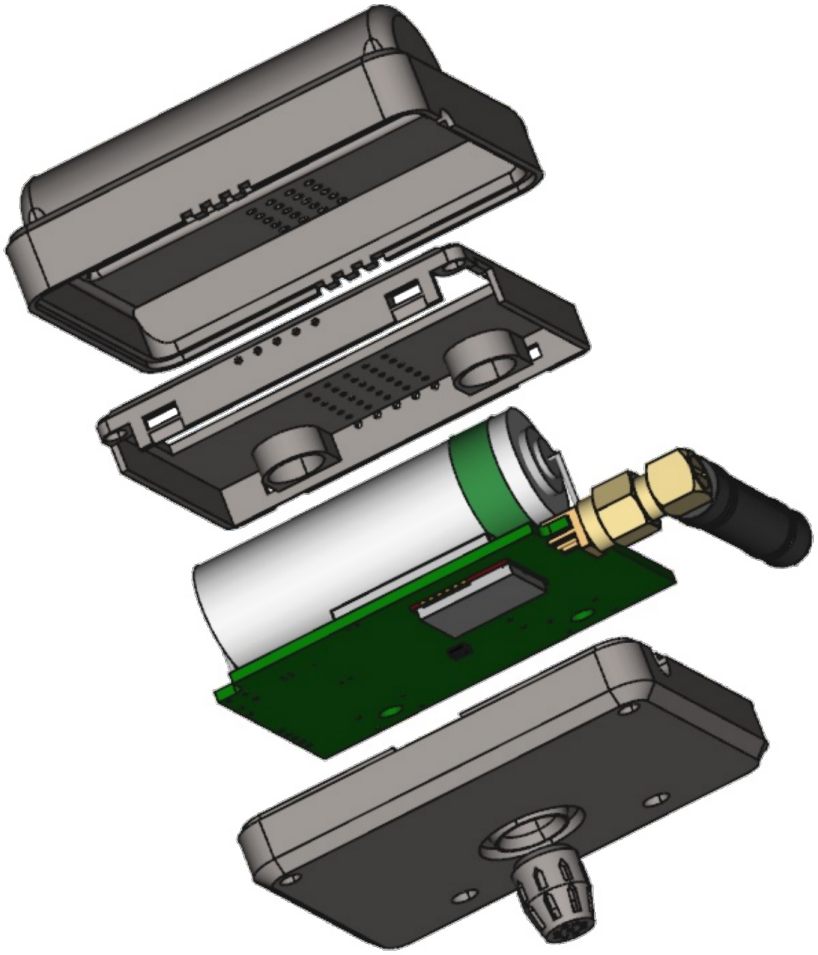

Figure 4.48: 3D Model of the sensor and the enclosure parts

4.2 Software design

The firmware is another important topic of this thesis. The software shall be designed in such a way to minimize the power consumption of the sensor. This can be achieved by disconnecting the power of the measurement and communication circuit.

The simplified block diagram of the sensor is shown in figure 4.49.
Right after the start-up of the device, the peripherals of the microcontroller, such as I^2C bus to communicate with SHT31 temperature and humidity sensors, GPIOs, mainly to control resistive wood moisture measurement, and Analog-to-Digital converter to measure the battery voltage.
After this initialization, the microcontroller checks if it is configured. If not, it goes to the configuration stage.

After configuration, the firmware goes into an endless loop. At the beginning of this loop the power of the rest of the sensor is enabled by using a P-MOSFET transistor. After the sensors are powered up, the wood cavity and ambient humidity and temperature are read using SHT31 sensors connected using I^2C bus. This is done first to avoid reading distorted values by possible heat produced by inverting charge pump on the PCB.

Next step is to read wood moisture using resistance measurement. At last, the battery voltage is read using an ADC. When all of these measurements are finished, the measurement circuitry is powered off. Then the message is constructed, and a communication module is powered on. Then the message can be sent to a communication module via UART. The UART communication itself varies depending on if the sensor is communicating using the IQRF or the LoRa network. After the message is successfully sent, the power for the communication circuitry is switched off and the microcontroller switches itself to a low power mode for a set amount of time. After this time, this process is repeated.

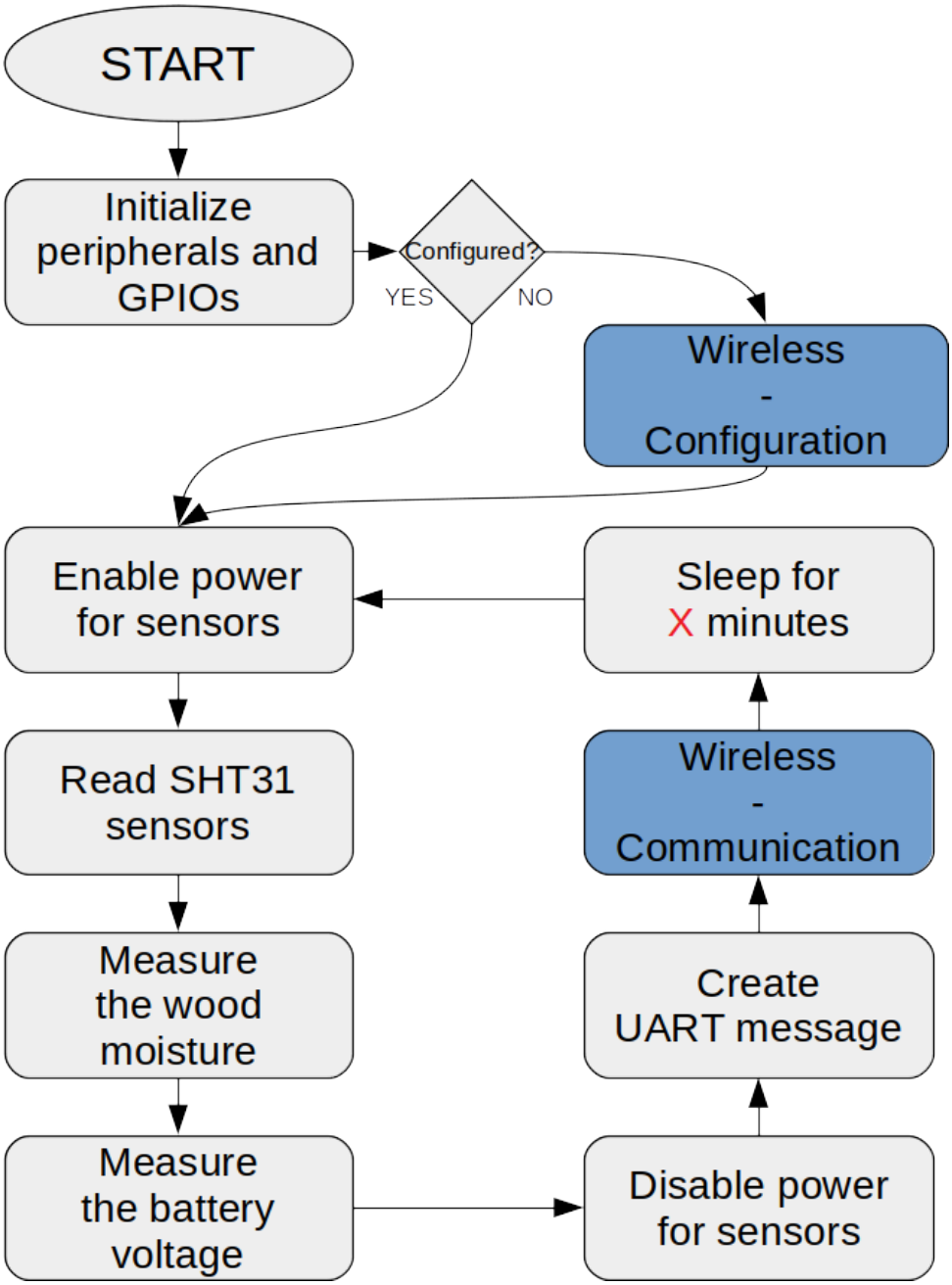

Figure 4.49: Block diagram of the software

4.2.1 SHT31 sensors readout

The SHT31 sensors communicate using I^{2}C bus. The address of the sensor can be set using the ADDR pin. Pulling this pin down sets the address to 0x44, which is the address of the cavity humidity and temperature sensor. Pulling this pin up sets the address to 0x45, which is the address set to the ambient humidity and temperature sensor.
In figure 4.50 can be seen the format of the messages during the communication between the Master (microcontroller) and the Slave (SHT31 sensor).

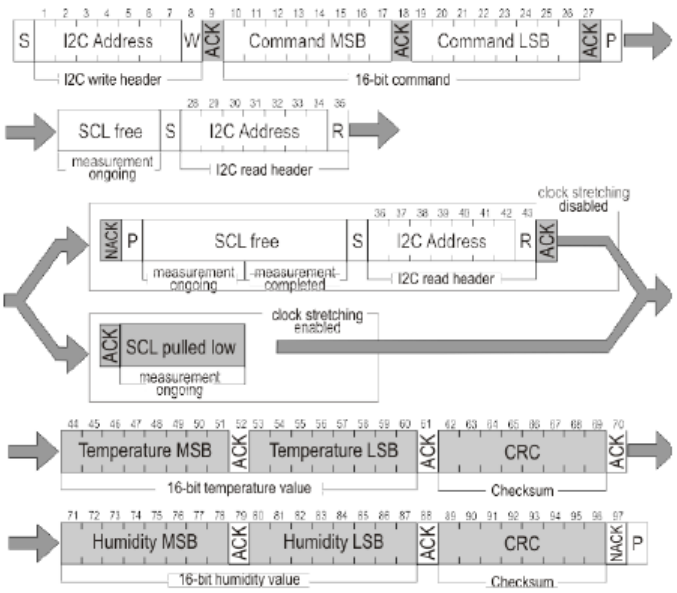

Figure 4.50: The I^{2}C communication format between a microcontroller and a SHT31 sensor

Condition		Hex. code	
Repeatability	Clock stretching	MSB	LSB
High	enabled	0x2C	06
Medium			0D
Low			10
High	disabled	0x24	00
Medium			0B
Low			16

Figure 4.51: I^{2}C commands of the SHT31 sensor

4.2.2 Moisture measurement

The moisture measurement algorithm can be seen in figure 4.52.
Before the measurement itself, the filtering capacitor must be charged.
At the beginning of the measurement, the polarity of the excitation is selected.
The measurement should be done for both positive and negative excitation.
Depending on the excitation, the the `DRIVE_LO` and `DRIVE_HI` are set to the values according to table 4.5.
Then the measurement itself can start. The `SWITCH_CTR` is set to logical high, which enables the measurement capacitor to begin to charge and the time measurement starts.
After the capacitor voltage reaches the threshold set by the voltage dividers, the comparator outputs logical low. The input `COMP_POS`, or `COMP_NEG` depending on the excitation polarity, terminates the time measurement.
The `DRIVE_LO`, `DRIVE_HI`, `SWITCH_CTR`, `COMP_POS` and `COMP_NEG` represent the corresponding GPIO pins.
The measurement should be repeated with the opposite polarity.

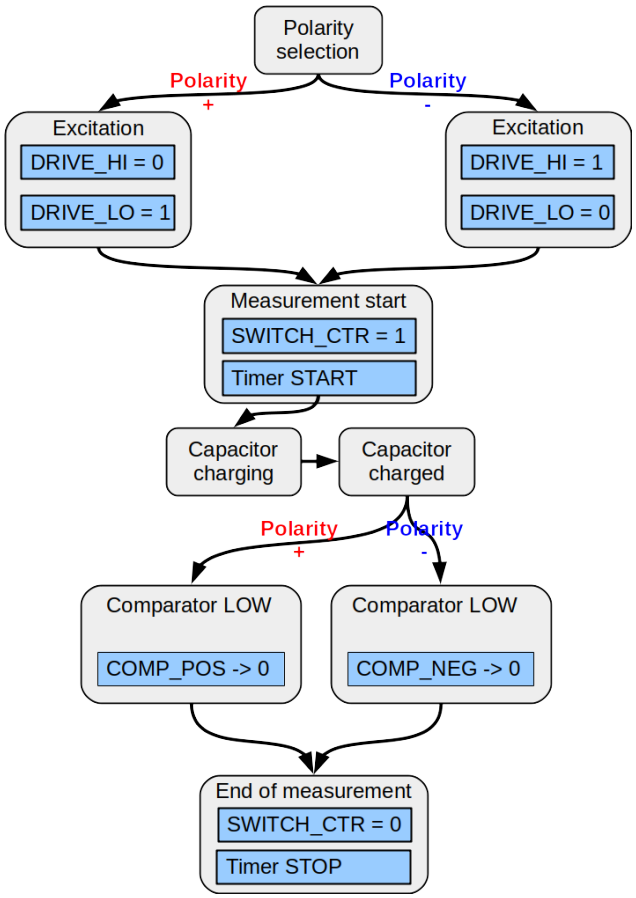

Figure 4.52: The block diagram of the resistive wood moisture measurement software

4.2.3 Battery voltage measurement

The PIC18F26K40 microcontroller is equipped with a 10bit analog-to-digital converter with multiple channels. To measure the battery voltage the `ANC0` ADC channel is used. This ADC measures the output of the switched voltage divider.
Before the start of the ADC conversion, it is necessary to enable the voltage divider. This means pulling the pin `RA6` low.
On the beginning of the ADC conversion, the ADC converter is enabled by setting the `ADON` bit of the `ADCON0` register to 1. Then the `ADGO` bit must be set to 1, which starts the conversion. When the `ADGO` bit changes to 0, the conversion is complete, and the result can be read from `ADRES` register. This register contains 2 bytes, `ADRESL` and `ADRESH`, which are the lower and higher bytes.
After reading these bytes, the `ADON` bit is set to 0, which disables the ADC, and pin `RA6` to 1, which disables the voltage divider.
To convert the measured value N_{ADC} to the battery voltage, the following equation was used:

$$V_{bat} = 2\frac{N_{ADC} \cdot V_{REF} \cdot 1000}{2^{10} - 1}\,[mV] \tag{4.13}$$

, where $V_{REF} = 2.048V$ is the voltage of the internal Fixed Voltage Reference (FVR). The fraction is multiplied by 2 because the voltage divider halves the real battery voltage value.

4.2.4 IQRF communication

Sensor Configuration

Before deploying a sensor, the IQRF Module must be bonded with the coordinator module on UniPi. The initialization of the IQRF module consists of three (optionally four) DPA Commands:

1. Bond Node
2. Set green LED
3. UART Open
4. UART Write

The DPA is described more in detail in section 5.1.

After the start-up of the sensor, the microcontroller reads its EEPROM memory at the address `0xF020` to check, if it contains a valid serial number. If `0xFFFF` value was read, the serial number has not been set, and the sensor enables the IQRF module, and waits for the configuration message.

If the IQRF module is not bonded, the red LED LD1 should begin to blink rapidly for 10 seconds after enabling the IQRF module. Otherwise, the red LED LD1 will blink just once. If the node module is bonded, it is necessary to unbond it to continue in the bonding procedure. To unbond a node, short the jumper JP1 during start-up of the node. The green LED LD2 will turn on for one second, after the green LED LD2 turns on, immediately open the jumper JP1.

To bond the IQRF module with the concentrator, the script on the UniPi must be executed. This script is described in the section 5.2.2. The flow diagram of the configuration stage of the sensor firmware can be seen in figure 4.53.
After the DPA Bond Command is sent, the user has 10 seconds to short the jumper JP1 to bond the node IQRF module. If the bonding was successful, the green LED LD2 will turn on for a few moments.
Then the concentrator opens UART of the bonded node and then writes the configuration UART message, which is shown in the figure 4.54. The sensor receives the UART message, and if the message starts with the byte `0x83`, it reads the next 4 bytes of the message. The first 2 bytes represent the serial

number of the sensor, and the next 2 bytes represent the sleeping period of the sensor in minutes. These values are then stored in the EEPROM at addresses `0xF020` and `0xF060` for the serial number and the sleeping period, respectively.
The user is informed about success or failure of this process within the script. After setting up the sensor, the firmware goes to the infinite measurement loop.

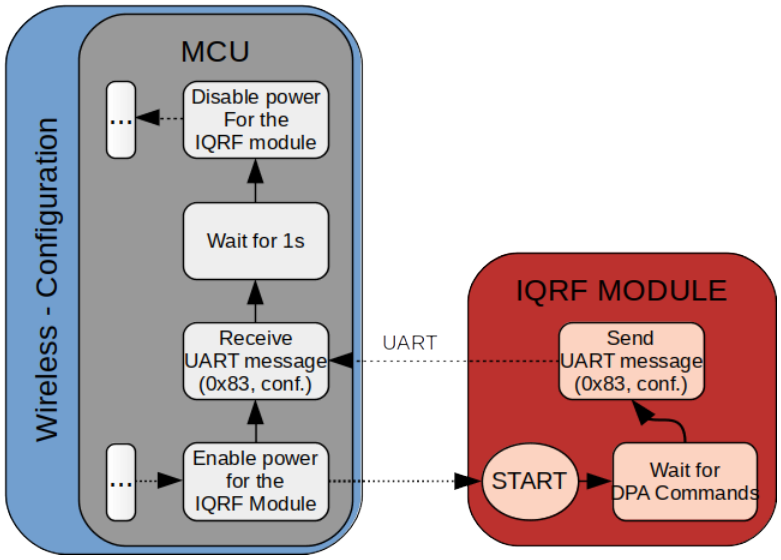

Figure 4.53: Block diagram of the IQRF communication - sensor configuration

1B	2B	2B
0x83	Serial number	Sleep time [min]

Figure 4.54: IQRF Packet - Sensor Configuration

Data sending

After all data are measured, the IQRF module is enabled, and the sensor waits for the UART message received using a DPA command. The flow diagram of the firmware in this stage can be seen in figure 4.55.
Because the IQRF network works on the polling principle, which means the concentrator sends command messages to the nodes, the sensor can not send the data by itself, and it must wait for the DPA command.
In this case, there are two DPA commands - UART Open and UART Write + Read. However, the microcontroller is aware only of UART Write + Read DPA command, because the UART open DPA command concerns only the IQRF module.

The DPA Write + Read DPA command sends UART to command message to the PIC microcontroller and then waits 1 second for the response.
This command message is a simple one byte UART message `0x93`. After the sensor receives this message, it sends a message with the measured data. The format of this message can be seen in figure 4.56.
After the UART message is sent to the IQRF module, the microcontroller waits 1 second to give the IQRF module enough time to send the response, because there is no acknowledgment from the IQRF module if the message was sent or not. Then it disables the IQRF Module and goes to sleep.

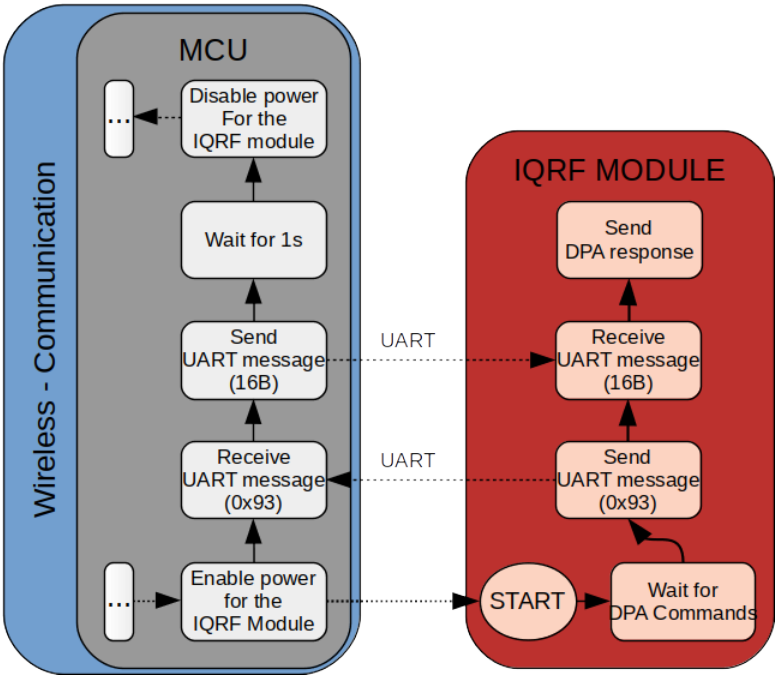

Figure 4.55: Block diagram of the IQRF communication - sending data

2B	2B	4B	2B	2B	2B	2B
Serial number	Battery voltage	Wood Moisture	Cavity humidity	Cavity temp.	Ambient humidity	Ambient temp.

Figure 4.56: IQRF Packet - Data

4.2.5 Sleep and Power Saving mode

To reduce the current consumption to the minimum, the unused modules should be disabled during the normal operation as well as during the sleep mode.
During the normal operation, few modules are used. These modules and their disabling bits and registers are listed in the table 4.18.

Module	Register	Bit
System Clock Network	PMD0	SYSCMD
Fixed Voltage Reference	PMD0	FVRMD
ADC	PMD2	ADCMD
EUSART1	PMD4	UART1MD
I^2C1	PMD4	MSSP1MD

Table 4.18: Used modules and their disabling registers and bits

These modules should be enabled at the beginning of the measurement cycle, and disabled when not needed.
All other modules should be disabled since the beginning of the execution of the programme.
The module is disabled by writing 1 to its bit in the relevant register. To enable the module, the bit should be set to zero.
To disable and enable these modules, functions `disable_used_modules` and `enable_used_modules` were implemented.
Similar functions, `disable_all_modules` to disable and `enable_all_modules` to enable all modules, were also implemented.
The function `disable_all_modules` is during the programme initialization phase, and the function `enable_used_modules` is called right after it.
The function `disable_all_modules` is called before entering the sleep phase of the programme.

The microcontroller wakes up from the sleep mode using Windowed Watchdog Timer (WDT). The period of the WDT can be set using the `WDTCON0` register. By setting its prescaler, using `WDTPS` bites of the register, the timeout of the WDT can be set.
The clock source of the WDT can be set using the bits `WDTCS` of the `WDTCON1` register. By setting `WDTCS` to `000`, the internal low-frequency oscillator, with the frequency 31kHz, is selected.
To enter the low power sleep mode, the `VREGPM1` bit register of the Voltage Regulator Control Register `VREGCON` must be set to 1. Otherwise, the microcontroller enters the regular sleep mode.
The `IDLEN` bit of the `CPUDOZE` register must be set to 0. Otherwise, the microcontroller will not enter the sleep mode.

When the communication and measurement circuitry is powered down, all modules are disabled, and the registers set, the `SLEEP` macro can be called, and the microcontroller enters the sleep mode and is woken up by the timeout of the Windowed Watchdog Timer. The maximal timeout is nominally 256 seconds (by setting the `WDTPS` to `10010`), so in order to stay in the sleep mode for hours, several calls of the `SLEEP` macro must be done.

4.2.6 Software Implementation

The firmware was implemented in the C language for PIC8 microcontrollers. The XC8 v1.45 compiler was used.
The firmware itself contains many sources and header files, providing access to the EEPROM memory, I^{2}C or UART communication, ADC conversion and more.
The logic of the programme is contained in the `main.c` file. The algorithm from figure 4.49 is implemented in this file. The call graph of the `main` function can be seen in figure 4.57.
The files `init.h` and `init.c` contain initialization functions and important configurations of the microcontroller.

The `sensors.c` file contains implementations of the measurement functions, most of them were already implemented, thanks to the compatibility with the wired version of the sensor MHT03485.

The firmware files are included within the thesis attachments.

- `resistance_measure_neg` - Measures the time needed to charge the measurement capacitor using the negative excitation.
- `resistance_measure_pos` - Measures the time needed to charge the measurement capacitor using the positive excitation.
- `resistance_convert` - Converts the time measured by the functions above to the wood resistance.
- `SHT3X_start_data_acquisition` - Starts the data acquisition of the SHT31 sensors in the continuous mode.
- `SHT3X_read_temperature_and_humidity_cs` - Reads the data from the selected SHT31 sensor, I^{2}C clock stretching enabled.
- `SHT3X_read_temperature_and_humidity` - Reads the data from the selected SHT31 sensor, I^{2}C clock stretching disables.
- `sht31_read` - Reads the data from the selected SHT31 sensor in the one-shot mode.
- `SHT3X_convert` - Converts the data sent by an SHT31 sensor to either temperature or relative humidity according to the equation provided by the SHT31 datasheet.

- `battery_voltage_measure` - Measures the ADC connected to the voltage divider to read the battery voltage and converts the measured value to voltage in millivolts. The voltage divider must be enabled before calling this function.

To switch the sensor to the sleep mode, and to save energy, several function were implemented in the `power_management.c` file:

- `power_management_init` - Initializes GPIO pins needed in the following functions.
- `sens_power_enable` - Enables the power for the measurement circuitry by pulling the RA5 GPIO pin low, thus enabling the P-MOSFET T1.
- `sens_power_disable` - Disables the power for the measurement circuitry by pulling the RA5 GPIO pin high, thus disabling the P-MOSFET T1.
- `comm_power_enable` - Enables the power for the communication circuitry by pulling the RA4 GPIO pin low, thus enabling the P-MOSFET T2.
- `comm_power_disable` - Disables the power for the communication circuitry by pulling the RA4 GPIO pin high, thus disabling the P-MOSFET T2.
- `voltage_divider_enable` - Enables the voltage divider by pulling the RA6 GPIO low.
- `voltage_divider_disable` - Disables the voltage divider by pulling the RA6 GPIO high.
- `init_unused` - initializes the unused GPIO pins and pulls them low to save the energy in the sleep mode.
- `enable_all_modules` - Enables all MCU modules by writing to PMDx registers.
- `disable_all_modules` - Disables all MCU modules by writing to PMDx registers.
- `enable_used_modules` - Enables selected MCU modules by writing to PMDx registers.
- `disable_used_modules` - Disables selected MCU modules by writing to PMDx registers.
- `sleep_for_minutes` - Puts the MCU to the sleep mode. This function sets the needed registers, calculates how many calls of `SLEEP` macro are required in order to sleep approximately the required time, and then

clears watchdog and sets the MCU into the sleep mode accordingly. The `WDTPS` bits of `WDTCON0` register must be set in a way the interval is at least 1s.

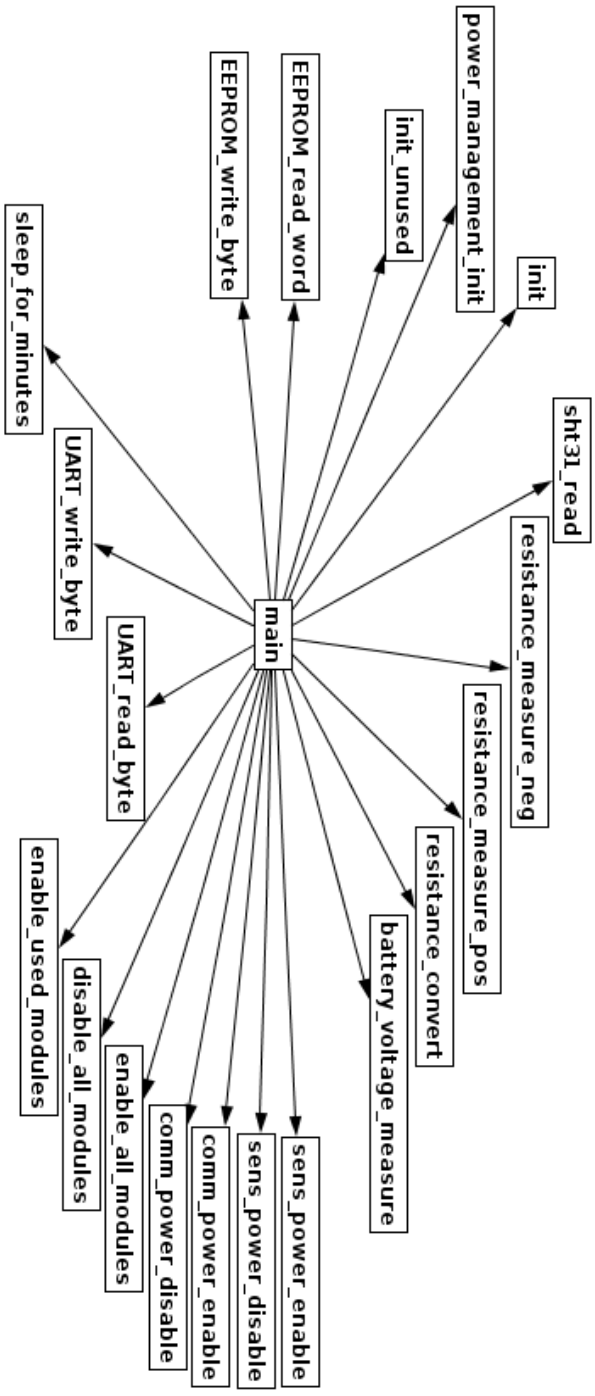

Figure 4.57: Call graph of the main function

Chapter 5

IQRF Concentrator

5.1 UniPi

As the central node of the system, an UniPi PLC was selected in the thesis specification.
UniPi is a Raspberry Pi based PLC developed by the company Faster CZ spol. s r.o.
There are two models of UniPi:

- UniPi Neuron
- UniPi Axon

While UniPi Neuron employs Raspberry Pi 3 as the control unit, UniPi Axon is based on Allwinner H5 ARM processor and the control unit is developed by the Faster CZ company. However, the software, including the operating system, is fully compatible between those two models. The advantage of the Axon model over the Neuron model is better suitability for industrial designs, because of integrated memory, in contrast with an SD Card the Raspberry Pi based Neuron is using. This makes UniPi Axon more stable than UniPi Neuron.
At the beginning of work on this thesis, an UniPi Neuron was chosen, because the UniPi Axon wasn't available on the market. However, UniPi Axon was later introduced, and it was decided to use UniPi Axon as a control unit for

the Moisture Guard system. Because UniPi Axon with an IQRF module is not available, and it is not even developed at this moment, the GW-USB-06 IQRF module must be used, instead of an on-board IQRF module. This is a flaw, not only because an external USB device must be used, but also because the internal antenna of the GW-USB-06 is worse than an external antenna of UniPi Neuron.

(a) : Neuron S103-IQRF. Taken from [53].

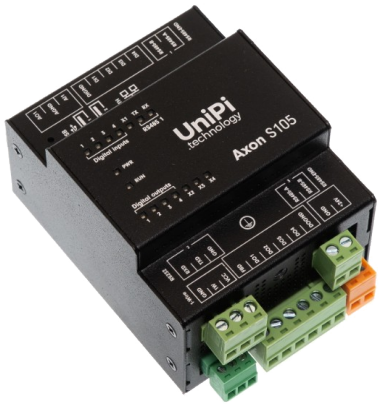

(b) : UniPi Axon S105. Taken from [54].

Figure 5.1: UniPi PLCs

Figure 5.2: GW-USB-06. Taken from [21].

The UniPi Axon PLC is equipped with a Real Time Clock with a backup for seven days.
Because the control unit of the UniPi Neuron is Raspberry Pi 3, it is equipped with Linux operating system Raspbian or its derivative UniPian. The control system is monitored using a watchdog.
UniPi Axon is equipped with 10/100 Ethernet using RJ-45 connector on the board of the Raspberry Pi 3. Four USB ports of the Raspberry Pi 3 can be used too. To communicate with other devices, RS485 and 1Wire can be used.

5.2 Software solution of the concentrator

The software of the concentrator is divided to two parts:

- Network initialization application
- Data Acquisition Application

The IQRF Device GW-USB-06 must be programmed with the Auto Network Coordinator Hardware Profile, provided by the IQRF Tech company.
To use the GW-USB-06 with the UniPi, the IQRF IDE is required to switch it to the IQRF USB CDC Device mode. This process is fairly simple and requires only a few mouse clicks, the start of the process in the IDE can be seen in figure 5.3.
After the device is switched to the IQRF USB CDC Device mode, it can be plugged into a USB port of the UniPi. The GW-USB-06 is mapped to `/dev/ttyACM0` file (assuming it is the first device plugged into the USB), and can be read and written using a serial port. The UniPi can now communicate with the IQRF GW-USB-06 device and create and manage the IQRF network using DPA command.

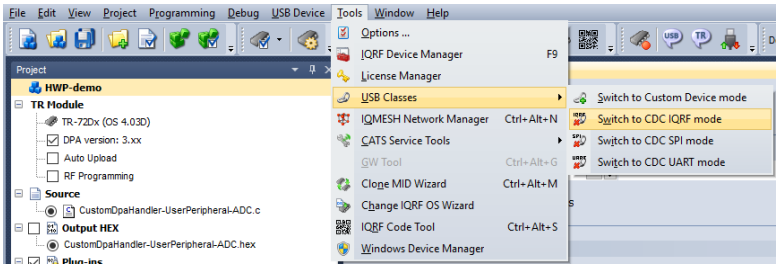

Figure 5.3: Switching the GW-USB-06 to USB CDC IQRF mode

5.2.1 Data Acquisition Application

To acquire data from nodes in the network, a C++ application was developed. This application uses the IQRF SDK [20].

The flowchart of the application can be seen in figure 5.6. Used DPA commands are listed in the table 5.2.
After the start of the application, the DPA command `Get Bonded Nodes` is sent to the IQRF coordinator, which returns a message with addresses of the bonded IQRF nodes. These addresses are contained in the `PData` bytes of the DPA response. Each bit represents one address, and if the bit is set, the particular address is used. By going through these bites, the application creates a list of nodes.

Then the application enters an endless loop, within which it goes through each node and tries to send the DPA command `UART Open` to open the UART interface with the baudrate of 9600 Baud. If a DPA Response is not received, it means the IQRF Module on the polled node is not powered on, and the application carries on the next node.

If a DPA Response was received and opening the UART was successful, the application sends the DPA command `UART Read and Write` is sent to the polled node. If a DPA Response with a data packet, as shown in the figure 5.4, was received, the data are processes and sent to the database using standard output, in following csv format:

```
IQRF Network Address,
Unix Timestamp,
Ambient Temperature ,
Cavity Temperature,
Ambient Relative Humidity,
Cavity Relative Humidity,
Resistance
```

This output is processed by the application handling data and sending them to the UCEEB database.
If the received message was incorrect or the UART reading unsuccessful, the application carries on the next node in the list.

To ensure the compliance with the 868MHz ISM band, the application waits for $T_{wait} = 1100ms$ between each DPA command. This time was calculated as $T_{wait} = \frac{T_{message}}{D} = \frac{11}{0.01}ms$, where $T_{message} = 11ms$ is the RF packet propagation time of a message with a payload of 1 byte, and $D = 0.01$ is the duty cycle of this band. After all the nodes in the list were polled, the process

starts again.

DPA Command	NADR	PNUM	PCMD	HWPID	DATA
Get Bonded Nodes	0x00	0x00		0xFFFF	
UART Open	ADDR	0x0C	0x00	0xFFFF	0x03
UART Read and Write	ADDR	0x0C	0x03	0xFFFF	0x93

Table 5.1: Used DPA commands in the main script

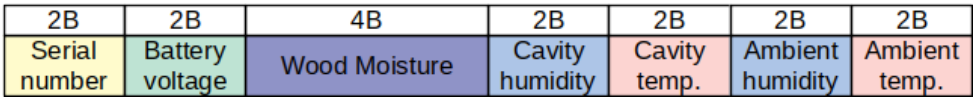

Figure 5.4: IQRF Packet - Data

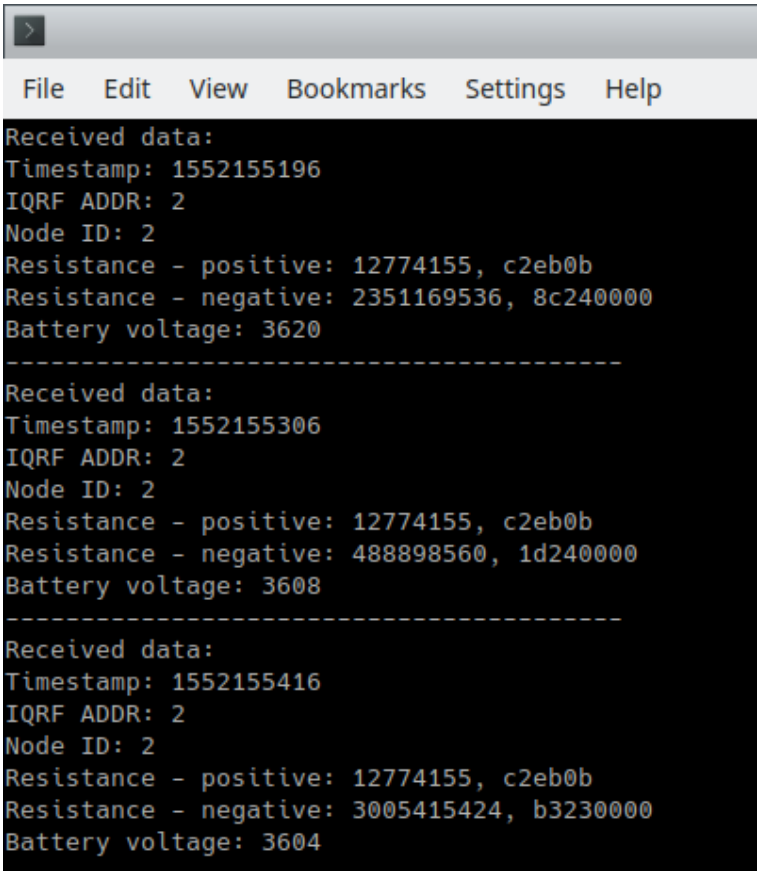

Figure 5.5: Screenshot of the testing version of the application.

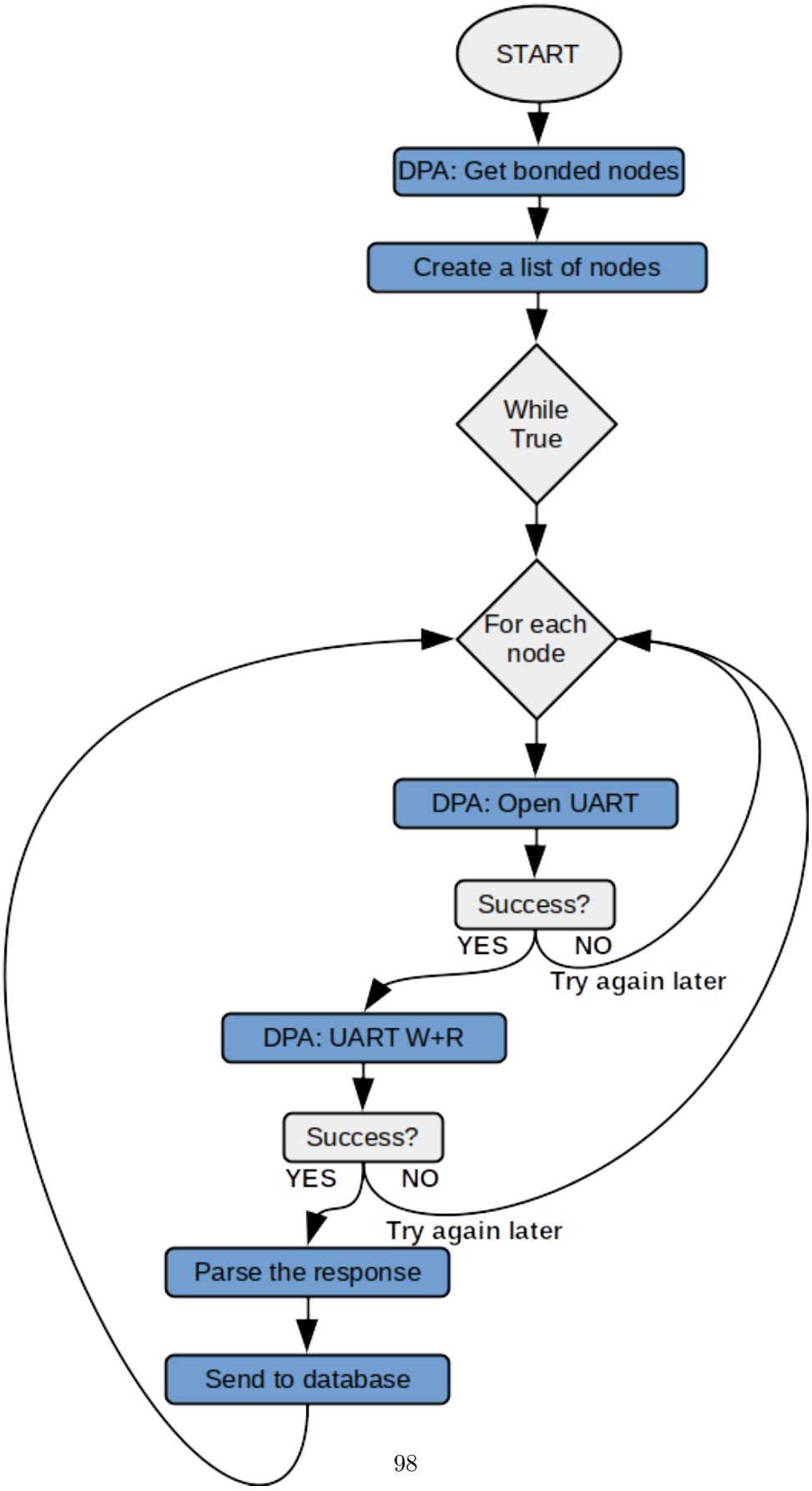

Figure 5.6: The simplified flowchart of the network management application

5.2.2 Network initialization application

Before running the main application, it is necessary to create the network and configure the nodes. To do this, a C++ command line application, described in this section, was implemented using the IQRF SDK [20].
The simplified flowchart of the script can be seen in figure 5.7.
Used DPA commands are listed in the table 5.2.

After the start of the application, the user is asked whether he wishes to clear the network or not.
In the positive case the DPA command `Clear All Bonds` is sent and the bonds in coordinator are cleared. However, the bonds in the existing nodes are not, so rebonding these nodes must be done manually.
To do this, the IQRF Module on the node must be powered up by shorting the jumper JP2 while the jumper JP1 is also shorted. After the green LED LD2 turns on, release the jumper JP1. If the unbonding process was successful, the red LED LD1 will start to rapidly blink for approximately 10 seconds. If not, the process must be repeated.

Then the bonding process begins. To bond a node the DPA command `Bond Node` with ReqAddr bit set to zero, which means the bonded node receives the first free address available. If the bonding was successful, the user can indicate the bonded node by blinking its green LED for 3 seconds. To do this the DPA commands `Green LED On` and `Green LED Off` were used.

Then the user is prompted to enter the node's new ID and sleep time. The new ID and sleep time should be in the range from 1 to 65534 (0xFFFE) because the 65535 (0xFFFF) value is reserved for the uninitialized state. The node receives this configuration using UART. The DPA commands used to do this are `DPA UART Open` to open UART at baudrate 9600 Baud and `DPA UART Write` to write the data packet containing the node configuration.

If configuring the node was successful, the user can bond a new node. After bonding all nodes, the program prints out nodes in the network and ends. The screenshot of this application can be seen in figure 5.8.

DPA Command	NADR	PNUM	PCMD	HWPID	DATA
Clear All Bonds	0x0000	0x00	0x03	0xFFFF	
Bond Node	0x0000	0x00	0x04	0xFFFF	0x00, 0x00
Green LED On	ADDR	0x07	0x01	0xFFFF	
Green LED Off	ADDR	0x07	0x00	0xFFFF	
UART Open	ADDR	0x0C	0x00	0xFFFF	0x03
UART Write	ADDR	0x0C	0x00	0xFFFF	0xFF, 0x83, ID (2B), SLEEP (2B)

Table 5.2: Used DPA commands in the initialization script.[16]

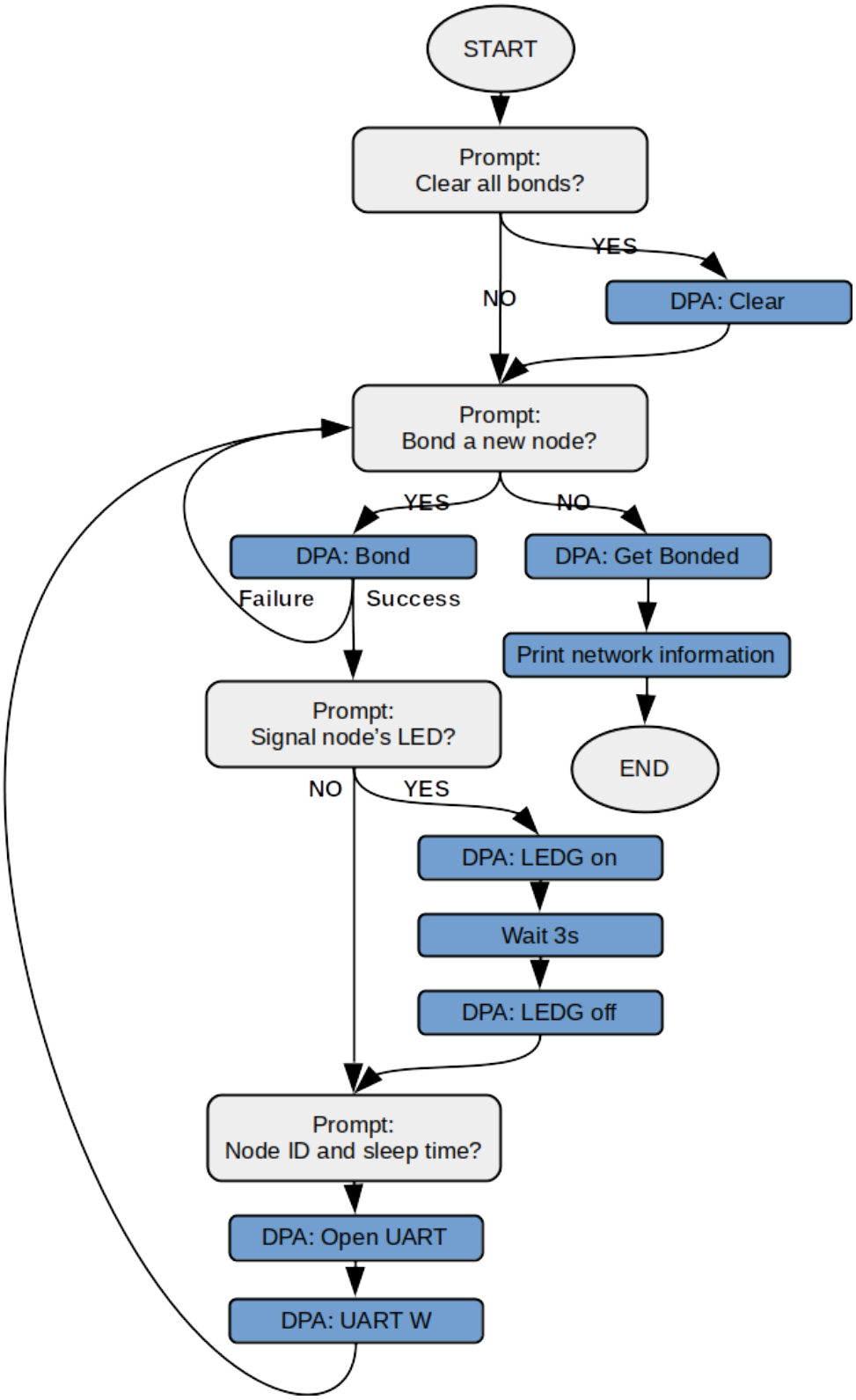

Figure 5.7: The simplified flowchart of the network initialization script

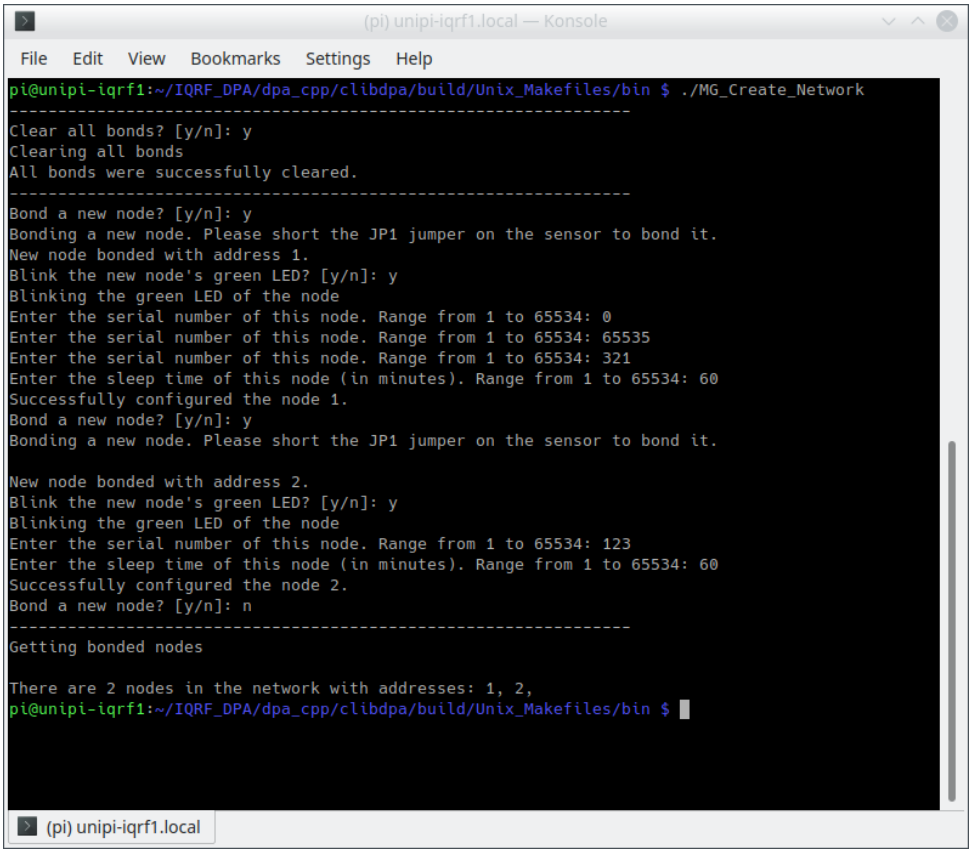

Figure 5.8: The screenshot of the application running on UniPi Neuron.

Chapter 6

Conclusion

In this thesis, a low-power solution of a Moisture Guard wood moisture sensor was designed.
The first version of the sensor was designed with a TR76-D IQRF module as its central unit. However, this solution proved to be not suitable for this application because mainly because of the polling structure of the IQRF network using DPA. This problem can be solved by using the IQRF OS to program the module, but the IQMESH is not available while using this solution, and moreover, the messages are not encrypted so that any IQRF module can receive, or worse, send messages in the network, so this solution was also not suitable.

Then another version of the sensor was developed, with STM32l053 microcontroller as its control unit. However, because of personnel changes at UCEEB CTU, there would be no one with any experience with STM32 microcontrollers, so a decision to change the microcontroller for a PIC18F17K40 was made. The colleagues at UCEEB CTU are familiar with this architecture, and this microcontroller is used in MHT03485 Moisture Guard sensor, so some part of the sensor firmware is compatible.
The development of the sensor was slowed down because of an issue with the resistive method, and its unsuccessful debugging, which proved to be excessively time-consuming.
The development of the rest of the firmware for the PIC microcontroller was slower than expected.

Despite these setbacks, I have created a solid foundation for the future development of the sensor with an emphasis on long-term support and continuation of this project. The low-power and energy efficient components were picked, and a current consumption calculation was made, implying that the sensor could have a lifespan of circa 15 years with a correct software implementation, which was also designed and described, including the setting of registers of the PIC microcontroller.

The concentrator was also designed and consists of an UniPi Neuron PLC and GW-USB-06 IQRF module. An UniPi Axon will be used in the future as the current software is compatible.
Two applications for the UniPi were implemented: one for the network creation and one for the network control and readout of the nodes in the network.
Both of these applications use IQRF SDK to communicate with the GW-USB-06 module which is the coordinator of the IQRF network.
The communication was successfully tested with the UniPi Neuron and three nodes.

Appendix A

Content of the CD

- Root
  - ZAITLIK_DAVID_DP.pdf - This thesis
  - Octave - Folder with GNU Octave scripts to generate used plots
  - Gateway SW - Folder containing software for the gateway
  - Sensor BOX - Folder containing CAD STEP models of the box and FreeCAD preview
  - Sensor FW - Folder containing the code of the sensor firmware
  - Sensor HW - Folder containing Altium Project and its outputs
    - Altium files - Folder containing Altium Designer files
    - Documents - Folder containing the PCB documentation files
    - Fabrication Outputs - Folder containing Gerber and NC-Drill Files
  - Thesis - Folder containing source files of this thesis

Appendix B

Bibliography

[1] Forest Products Laboratory, *Wood Handbook - Wood as an Engineering Material*, Centennial Edition, Madison, WI: U.S. Department of Agriculture, Forest Service, Forest Products Laboratory, 2010, ISBN-13:978-1484859704

[2] William L. James, *Electric Moisture Meters for Wood*, Madison, WI: U.S. Department of Agriculture, Forest Service, Forest Products Laboratory, 1988,

[3] J. Hartley, J. Marchant, *Methods of Determining the Moisture Content of Wood*, Beecroft: Research Division, State Forests of New South Wales, 1995, ISBN1; 0731067215

[4] V. Dashöfer, Montované nosné konstrukce - dřevěné konstrukce, *tzbinfo*, Quoted on 8.5.2019, [online], ISSN 1801-4399, Available at: `https://stavba.tzb-info.cz/drevostavby/5455-montovane-nosne-konstrukce-drevene-konstrukce`

[5] Valdek Tamme, Peeter Muiste, Regino Kask, Allar Padari and Hannes Tamme, Experimental study of electrode effects of resistance type electrodes for monitoring wood drying process above fibre saturation point, **In:** *Forestry Studies*, The Journal of Estonian University of Life Sciences, Tartu:DE GRUYTER OPEN, 2012, Vol. 56, Pages 42-55, ISSN: 1736-8723

[6] Valdek Tamme,Peeter Muiste, Hannes Tamme, Experimental study of resistance type wood moisture sensors for monitoring wood drying process above fibre saturation point, **In:** *Forestry Studies*, The Journal of Estonian University of Life Sciences, Tartu:DE GRUYTER OPEN, 2013, Vol. 59, Pages 28-44, ISSN: 1736-8723

[7] Valdek Tamme, *Development of Resistance-Type Control Methods for Wood Drying*, Tartu, 2016, Doctoral Thesis, Estonian University of Life Sciences

[8] S. Hoi Tsao, An Accurate, Semiautomatic Technique of Measuring High Resistances, **In:** *IEEE Transactions on Instrumentation and Measurement*, 1967, Pages 220-225, ISSN: 0018-9456

[9] Gert Rietveld, Dean Jarrett, and Beat Jeckelmann, Accurate High-Ohmic Resistance Measurement Techniques up to 1 PΩ, **In:** *CPEM Digest (Conference on Precision Electromagnetic Measurements)*, 2014, ISSN: 0589-1485

[10] Maria Fredriksson, Lars Wadso, Peter Johansson, Small resistive wood moisture sensors: a method for moisture content determination in wood structures, **In:** *European Journal of Wood and Wood Products*, 2013, Pages 515-524, ISSN: 0018-3768

[11] Christian Brischke, Andreas Otto Rapp, Rolf Bayerbach, Measurement system for long-term recording of wood moisture contentwith internal conductively glued electrodes, **In:** *Building and Environment*, 2007, Pages 1566-1574, ISSN: 0360-1323

[12] Philipp Dietsch, Steffen Franke, Bettina Franke, Andreas Gamper, Stefan Winter Methods to determine wood moisture content and their applicability in monitoring concepts, **In:** *Journal of Civil Structural Health Monitoring*, 2014, Pages 115-127, ISSN: 2190-5452

[13] Comarch Technologies, *Conectivity Protocols Landscape*, [image], In: *Comarch BLE & LoRa devices*, [online], [23.4.2019], available at: `https://www.slideshare.net/Comarch_Benelux/comarch-ble-lora-devices`

[14] IQRF Tech, *IQRF Technical Guide*, 2016, Quoted 13.3.2018, [online], available at: `https://www.iqrf.org/support/download&kat=51&ids=79`

[15] IQRF Tech, "IQRF OS Operating System Version 4.02D for (DC)TR-7xD User's Guide", 2018, Quoted 24.3.2018, [online], available at: `https://www.iqrf.org/support/download&kat=35&ids=155`

[16] IQRF Tech, "IQRF DPA Framework Technical Guide Version v4.0 IQRF OS v4.03D", 20. 1. 2019, Quoted 10.2.2019, [online], available at: `https://www.iqrf.org/support/download&kat=54&ids=565`

[17] IQRF Tech, *2 Application Approaches*, [image], In: *2 Application Approaches*, [online], [10.2.2019], available at: `https://iqrf.org/technology/2-application-approaches`

[18] IQRF Tech, emphFRC, [image], In: *FRC*, [online], [10.2.2019], available at:`https://www.iqrf.org/technology/miscellaneous/frc`

[19] IQRF Tech, emphDPA Command, [image], In: *DPA*, [online], [10.2.2019], available at: `https://iqrf.org/technology/dpa`

[20] IQRF Tech, IQRF SDK GitHub [online], available at: `https://github.com/iqrfsdk`

[21] IQRF Tech, *GW-USB-06*, [image], In: *GW-USB-06* [online], [23.11.2018], available at: `https://www.iqrf.org/products/gateways/gw-usb-06`

[22] LoRa Aliance, "LoRaWAN TM 101 A Technical Introduction", Quoted 10.12.2018, [online], available at: `https://eleven-x.com/wp-content/uploads/2018/04/LoRaWAN-101-A-Technical-Introduction.pdf`

[23] K. Mekki, E. Bajic, F. Chaxel, and F. Meyer, *A comparative study of LPWAN technologies for large-scale IoT deployment*, **In:** *ICT Express*, 2018, Pages 1-7, ISSN: 2405-9595

[24] L. Bao, L. Wei, C. Jiang, W. Miao, B. Guo, W. Li, X. Cheng, R. Liu, and J. Zou, *Coverage Analysis on NB-IoT and LoRa in Power Wireless Private Network*, **In:** *Procedia Computer Science*, 2018, vol. 131, Pages 1032–1038, ISSN: 1877-0509

[25] České Radiokomunikace a.s, *Mapa pokrytí ČR LoRaWAN*, [image], In: *Služby CRA IoT*, [online], [23.4.2019],available at: `https://www.cra.cz/sluzby-iot`

[26] Silicon Labs, "An Introduction to Wireless M-Bus", Quoted 13.3.2018, [online], available at: `http://pages.silabs.com/rs/634-SLU-379/images/introduction-to-wireless-mbus.pdf`

[27] Maarten Weyn, Glenn Ergeerts, Rafael Berkvens, Bartosz Wojciechowski, Yordan Tabakov "DASH7 Alliance Protocol 1.0: Low-Power, Mid-Range Sensor and Actuator Communication", DOI: 10.1109/C-SCN.2015.7390420, 2015, Quoted 13.3.2018, [online], available at: `https://www.researchgate.net/publication/283278341_DASH7_Alliance_Protocol_10_Low-Power_Mid-Range_Sensor_and_Actuator_Communication`

[28] DASH7 Alliance, "Wireless Sensor and Actuator Network Protocol VERSION 1.1", 2016, Quoted 13.3.2018, [online], available at: `http://www.dash7-alliance.org/product/d7ap1-1/`

[29] SAFT, "LS 17500 Primary Li-SOCl2 cell", Datasheet, 2016, Quoted 12.4.2019, [online], available at: `https://www.saftbatteries.com/products-solutions/products/ls-lsh`

[30] SAFT, "Battery Information Sheet", Datasheet, 2016, Quoted 12.4.2019, [online], available at: `https://www.saftbatteries.com/products-solutions/products/ls-lsh`

[31] Texas Instruments, "TPS61098x Ultra-Low Quiescent Current Synchronous Boost with Integrated LDO/Load Switch", TPS61098x, Datasheet, 2016, Quoted 13.3.2018, [online], available at: http://www.ti.com/lit/ds/symlink/tps610987.pdf

[32] Maxim Integrated, "MAX17220–MAX17225, 400mV to 5.5V Input, nanoPower Synchronous Boost Converter with True Shutdown", MAX17222, Datasheet, 2017, Quoted 13.3.2018, [online], available at: https://datasheets.maximintegrated.com/en/ds/MAX17220-MAX17225.pdf

[33] Richtek, "RT8299A, 3A, 24V, 500kHz Synchronous Step-Down Converter", RT8299A, Datasheet, 2014, Quoted 13.3.2018, [online], available at: http://www.richtek.com/assets/product_file/RT8299A/DS8299A-03.pdf

[34] Microchip Technology Inc. , "STM32L053C6 STM32L053C8 STM32L053R6 STM32L053R8 , Ultra-low-power 32-bit MCU Arm®-based Cortex®-M0+, up to 64KB Flash, 8KB SRAM, 2KB EEPROM, LCD, USB, ADC, DAC", September 2017, Quoted 19.4.2019, [online], available at: https://www.st.com/content/st_com/en/products/microcontrollers-microprocessors/stm32-32-bit-arm-cortex-mcus/stm32-ultra-low-power-mcus/stm32l0-series/stm32l0x3/stm32l053c8.html

[35] Microchip Technology Inc. , "PIC18(L)F27/47K40 - 28/40/44-Pin, Low-Power, High-PerformanceMicrocontrollers with XLP Technology", 2018, Quoted 11.3.2019, [online], available at: http://ww1.microchip.com/downloads/en/DeviceDoc/PIC18LF27_47K40-Data-Sheet-40001844E.pdf

[36] Microchip Technology Inc. , "TB3123 - Windowed Watchdog Timer on PIC® Microcontrollers", 2018, Quoted 11.3.2019, [online], available at: http://ww1.microchip.com/downloads/en/DeviceDoc/PIC18LF27_47K40-Data-Sheet-40001844E.pdf

[37] Microchip Technology Inc. , "PIC18(L)F2X/4XK40 - PIC18(L)F2X/4XK40 Memory Programming Specification", 2017, Quoted 11.3.2019, [online], available at: http://ww1.microchip.com/downloads/en/DeviceDoc/40001772C.pdf

[38] IQRF Tech, "TR-76D, RF Transceiver Module Series", TR-76D, Datasheet, 2018, Quoted 13.3.2018, [online], available at: iqrf.org/weben/downloads.php?id=441

[39] IQRF Tech, "Low Power", IQRF Low power leaflet, 2017, Quoted 13.4.2018, [online], available at: https://www.iqrf.org/support/download&kat=51&ids=535

[40] IQRF Tech, "RF Range At (DC)TR-7xDx transceivers Application Note AN014", 2017, Quoted 13.4.2018, [online], available at: https://www.iqrf.org/support/download&kat=43&ids=500

[41] Microchip Technology Inc., "RN2483 - Low-Power Long Range LoRa® TechnologyTransceiver Module", 2019, Quoted 9.1.2019, [online], available at: http://ww1.microchip.com/downloads/en/DeviceDoc/RN2483-Low-Power-Long-Range-LoRa-Technology-Transceiver-Module-Data-Sheet-DS50002346pdf

[42] Nemeus, "MM002-xx-EU - Datasheet", 2016, Quoted 9.1.2019, [online], available at: https://wiki.nemeus.fr/images/4/4f/MM002-xx-EU_datasheet_v1.1.pdf

[43] Sensirion, "Datasheet SHT3x-DIS", May 2018, Quoted 11.11.2018, [online], available at: https://www.sensirion.com/fileadmin/user_upload/customers/sensirion/Dokumente/0_Datasheets/Humidity/Sensirion_Humidity_Sensors_SHT3x_Datasheet_digital.pdf

[44] Sensirion, "Overview of SHT3x Versions", January 2018, Quoted 11.11.2018, [online], available at: https://www.sensirion.com/fileadmin/user_upload/customers/sensirion/Dokumente/2_Humidity_Sensors/Sensirion_Humidity_Sensor_SHT3x_Table_Overview.pdf

[45] Sensirion, "Datasheet Membrane Option", January 2017, Quoted 11.11.2018, [online], available at: https://www.sensirion.com/fileadmin/user_upload/customers/sensirion/Dokumente/0_Datasheets/Humidity/Sensirion_Humidity_Sensors_SHT3x_Datasheet_Filter_Membran.pdf

[46] Sensirion, "Datasheet Protective Cover Option", February 2016, Quoted 11.11.2018, [online], available at: https://www.sensirion.com/fileadmin/user_upload/customers/sensirion/Dokumente/0_Datasheets/Humidity/Sensirion_Humidity_Sensors_SHT3x_Datasheet_Protective_Cover.pdf

[47] Linear Technology, "LT1617/LT1617-1 Micropower Inverting DC/DC Converters in SOT-23", February 2016, Quoted 11.11.2018, [online], available at: https://www.analog.com/media/en/technical-documentation/data-sheets/16171f.pdf

[48] Microchip Technology, "MCP6071/2/4 110 μA, High Precision Op Amps", 2010, Quoted 11.11.2018, [online], available at: http://ww1.microchip.com/downloads/en/DeviceDoc/22142_B_MCP6071.pdf

[49] Texas Instruments, "TL331 Single Differential Comparator", 2015, Quoted 11.11.2018, [online], available at: http://www.ti.com/lit/ds/symlink/tl331.pdf

[50] Microchip, "AN1258 Application note - Op Amp Precision Design: PCB Layout Techniques", 2009, Quoted 18.11.2018, [online], available at: http://ww1.microchip.com/downloads/en/AppNotes/01258B.pdf

[51] Faster CZ spol. s r.o., "UniPi Neuron M10x", Quoted 23.11.2018, [online], available at: https://kb.unipi.technology/_media/files:products:neuron:datasheets:neuron_m10x_datasheet_en.pdf

[52] Faster CZ spol. s r.o., "Product line of programmable controllers and extension modules UniPi Neuron", Quoted 23.11.2018, [online], available at: https://kb.unipi.technology/_media/files:products:neuron:neuron_technical_documentation_en.pdf

[53] Faster CZ spol. s r.o., *UniPi Neuron S1O3-IQRF Picture*, [image], In: *Neuron S103-IQRF*, [online], [23.11.2018], available at: https://www.unipi.technology/neuron-s103-iqrf-p152

[54] Faster CZ spol. s r.o., *UniPi Axon S105 Picture*, [image], In: *UniPi Axon S105*, [online], [23.11.2018], available at: https://www.unipi.technology/unipi-axon-s105-p171

ZADÁNÍ DIPLOMOVÉ PRÁCE

I. OSOBNÍ A STUDIJNÍ ÚDAJE

Příjmení: **Žaitlík** Jméno: **David** Osobní číslo: **420352**

Fakulta/ústav: **Fakulta elektrotechnická**

Zadávající katedra/ústav: **Katedra řídicí techniky**

Studijní program: **Kybernetika a robotika**

Studijní obor: **Kybernetika a robotika**

II. ÚDAJE K DIPLOMOVÉ PRÁCI

Název diplomové práce:

Návrh bezdrátového senzoru pro měření vlhkosti dřevěných konstrukcí

Název diplomové práce anglicky:

Wireless Wooden Structure Sensor Design

Pokyny pro vypracování:

1. Navrhněte a realizujte bezdrátový senzor vlhkosti vázané ve dřevě, vhodný pro trvalou zástavbu do konstrukce, který bude měřit několik parametrů (teplota, vzdušná vlhkost uvnitř konstrukce, rovnovážná vzdušná vlhkost v kavitě materiálu, hmotnostní vlhkost materiálu pomocí odporové metody).
2. Senzor navrhněte s ohledem na bateriové napájení, a dlouhou dobu životnosti (min 10 let).
3. Pro přenos dat mezi senzorem a gateway využijte bezdrátovou technologii IQRF.
4. Při návrhu HW i komunikace se zaměřte na nízkou spotřebu zařízení a aplikaci systému v konstrukcích rezidenčních budov.
5. Funkčnost senzoru ověřte na demonstraci systému s několika senzory a IQRF gateway (např. PLC UniPI), pro kterou navrhněte knihovní funkce pro komunikaci se senzory a SW, který bude tuto knihovnu využívat pro poskytování přijatých dat pomocí API. Vše vytvořte pomocí běžně používaných standardů a řádně zdokumentujte.

Seznam doporučené literatury:

[1] J. Hartley, J.Marchant, Methods of determining the moisture content of wood, State Forests - Research Devision ISSN 1324-4345, 1995
[2] IQRF Alliance, IQRF technology for wireless, www.iqrf.org/technology
[3] UniPi.technology, UniPi Neuron S103 Datasheet - Technological specification of the product, www.unipi.technology/unipi-neuron-s103-p93

Jméno a pracoviště vedoucí(ho) diplomové práce:

Ing. Jan Včelák, Ph.D., UCEEB

Jméno a pracoviště druhé(ho) vedoucí(ho) nebo konzultanta(ky) diplomové práce:

Datum zadání diplomové práce: **19.02.2018** Termín odevzdání diplomové práce: **25.05.2018**

Platnost zadání diplomové práce: **30.09.2019**

Ing. Jan Včelák, Ph.D. podpis vedoucí(ho) práce	prof. Ing. Michael Šebek, DrSc. podpis vedoucí(ho) ústavu/katedry	prof. Ing. Pavel Ripka, CSc. podpis děkana(ky)

III. PŘEVZETÍ ZADÁNÍ

Diplomant bere na vědomí, že je povinen vypracovat diplomovou práci samostatně, bez cizí pomoci, s výjimkou poskytnutých konzultací.
Seznam použité literatury, jiných pramenů a jmen konzultantů je třeba uvést v diplomové práci.

. _____
Datum převzetí zadání

_____
Podpis studenta